ISSN 1984-6428

Orbital

The Electronic Journal of Chemistry

APRIL - JUNE
2009
VOLUME 1
NUMBER 2

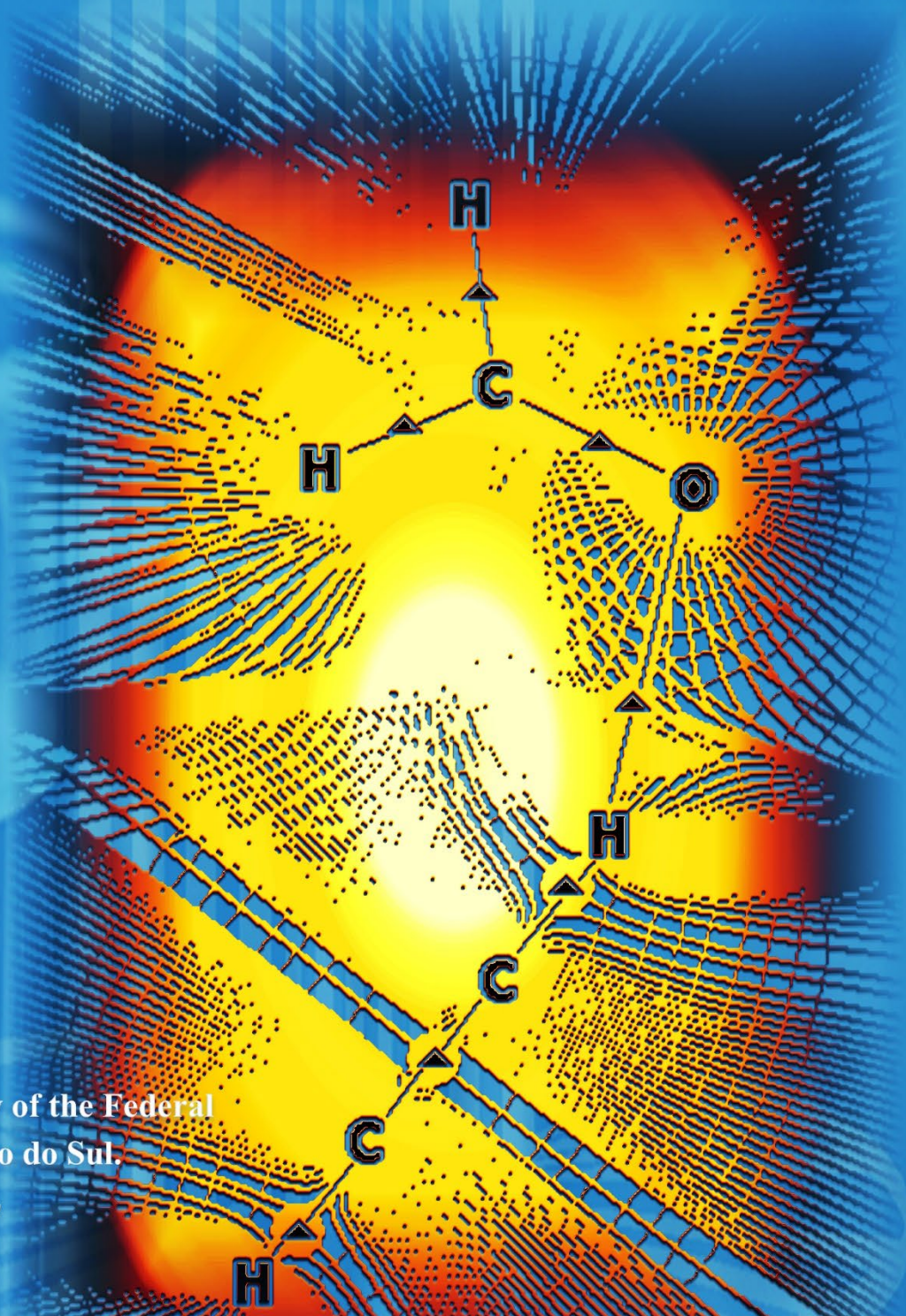

Published by the
Department of Chemistry of the Federal
University of Mato Grosso do Sul.
Campo Grande, BRAZIL

UFMS

www.orbital.ufms.br

Orbital - Vol. 1 No. 2 - April-June 2009

Table of Contents

EDITORIAL

FULL PAPERS

Orbital
The Electronic Journal of Chemistry

Editorial

Orbital Journal – The Electronic Journal of Chemistry – was conceived of as an *Open Access Journal*: it allows free access to the articles without the need to sign in, and publishes material exclusively on the Internet.

Now both the brazilian and international scientific communities have this new communication channel which provides free access to information in the areas of Chemistry and its correlated areas making it possible to add scientific contributions produced both in Brazil and other countries to other specialized publications. It is worth highlighting that we have some scientific articles in this issue that came from collaborators in India and Morocco, besides Brazil.

Another important aspect we would like to emphasize is that all editorial activities have been and will always be performed like any other kind of contribution, despite the fact that Orbital is a new communication channel for scientific contributions from researchers at the Department of Chemistry at the Federal University of the State of Mato Grosso do Sul in Brazil. Although its origin is in Brazil, Orbital Journal has goals that go beyond our borders, as you can verify in the articles that have already been published.

Bearing this in mind and on behalf of the Editorial Board, I would like to thank all referees, who seek not only original manuscripts with technical-scientific merit, but also papers that offer a clear theoretical explanation to our readers.

Best regards,

Marcos Serrou do Amaral (UFMS)

Editor Orbital (Theoretical Chemistry)

A revista Orbital – *The Electronic Journal of Chemistry* – foi idealizada pela linha de *Open Access Journal*, permitindo livre acesso aos seus artigos, sem necessidade de qualquer cadastro e apresentando publicações exclusivamente pela internet.

Com isso, a comunidade científica brasileira e internacional ganha este canal de divulgação com livre acesso nas áreas de química e correlatas. Possibilitando somar com outras revistas as diversas contribuições científicas produzidas no Brasil e em outros países. Vale ressaltar que nesta edição, temos artigos científicos de colaboradores da Índia e Marrocos, além do Brasil.

Outro aspecto importante de se mencionar é que, apesar de ser um novo canal de divulgação de contribuições científicas de pesquisadores do Departamento de Química da Universidade Federal de Mato Grosso do Sul, todos os trâmites editoriais vêm sendo e serão sempre realizados como qualquer outra contribuição. Apesar de sua origem no Mato Grosso do Sul, a Orbital tem metas além de nossas fronteiras, como pode ser vistos nos artigos já publicados.

Tendo isso em vista, gostaria de agradecer, em nome do Corpo Editorial, a todos os avaliadores que buscam não só aceitar manuscritos originais com mérito técnico-científico, mas também trabalhos que apresentam clareza de exposição teórica para nossos leitores.

Saudações,

Marcos Serrou do Amaral (UFMS)

Editor Orbital (Química Teórica)

La revista Orbital – *The Electronic Journal of Chemistry* – fue idealizada en el contexto de *Open Access Journal*, permitiendo el libre acceso de sus artículos, sin necesidad de cadastro, y presentando publicaciones exclusivamente por Internet.

Con esto, la comunidad científica brasilera e internacional ganan este canal de divulgación con libre acceso al área de química y áreas correlacionadas. Posibilitando sumar con otras revistas las diversas contribuciones científicas producidas en el Brasil y en otros países. Vale resaltar que en esta edición, tenemos artículos científicos de colaboradores de la India y Marruecos, además de Brasil.

Otro aspecto importante de mencionarse, es el hecho de que la revista, a pesar de ser un nuevo canal de divulgación de contribuciones científicas de investigadores del Departamento de Química de la Universidad Federal de Mato Grosso do Sul, todos los tramites editoriales vienen siendo y serán siempre realizados como cualquier otra contribución. A pesar de su origen en Mato Grosso do Sul, Orbital tiene metas más allá de nuestras fronteras, como puede apreciarse en los artículos ya publicados.

Considerando todo esto, gustaría de agradecer, en nombre del cuerpo editorial, a todos los evaluadores que buscan no solo aceptar manuscritos técnicos con meritos técnico-científico, si no también trabajos que presentan clareza de exposición teórica para nuestros lectores.

Cordialmente,

Marcos Serrou do Amaral (UFMS)

Editor Orbital (Química Teórica)

ISSN 1984-6428
ONLINE
www.orbital.ufms.br

Orbital 2009, *1* (2), 138-155

Full Paper

Adsorption of rhodamine B by acid activated carbon-kinetic, thermodynamic and equilibrium studies

Shanmugam Arivoli[a], M. Thenkuzhali[b] and P. Martin Deva Prasath[b]*

[a]Department of Chemistry, H H The Rajah's Government College, Pudukkottai- 622 001, India.
[b]Department of Chemistry, T. B. M. L.College, Porayar 609 307, India.

Received: 20 November 2008; revised: 24 January 2009; accepted: 10 February 2009. Available online: 26 April 2009

***ABSTRACT**: A carbonaceous adsorbent prepared from an indigenous waste by acid treatment was tested for its efficiency in removing Rhodamine B (RDB). The parameters studied include agitation time, initial dye concentration, carbon dose, pH and temperature. The adsorption followed first order kinetics and the rate is mainly controlled by intra-particle diffusion. Freundlich and Langmuir isotherm models were applied to the equilibrium data. The adsorption capacity (Q_m) obtained from the Langmuir isotherm plots were 40.161, 35.700, 38.462 and 37.979 mg/g respectively at an initial pH of 7.0 at 30, 40, 50 and 60 ^{0}C. The temperature variation study showed that the RDB adsorption is endothermic and spontaneous with increased randomness at the solid solution interface. Significant effect on adsorption was observed on varying the pH of the RDB solutions. Almost 85% removal of RDB was observed at 60 ^{0}C. The Langmuir and Freundlich isotherms obtained, positive ΔH^0 value, pH dependent results and desorption of dye in mineral acid suggest that the adsorption of RDB by Banana bark carbon involves physisorption mechanism.*

***Keywords:** activated carbon (BC), rhodamine B (RDB), adsorption isotherm, kinetic and thermodynamic parameters*

**Corresponding author: arivu3636@yahoo.com*

Introduction

The discharge of highly coloured effluents into natural water bodies is not only aesthetically displeasing, but it also impedes light penetration, thus upsetting biological processes within a stream. In addition, many dyes are toxic to some organisms causing direct destruction of aquatic communities. Some dyes can cause allergic dermatitis, skin irritation, cancer and mutation in man. Wastewaters from dyeing industries released into nearby land or rivers without any treatment because the conventional treatment methods are not cost effective in the Indian context. Adsorption is one of the most effective methods and activated carbon is the preferred adsorbent widely employed to treat wastewater containing different classes of dyes, recognizing the economic drawback of commercial activated carbon [1-3].

Many investigators have studied the feasibility of using inexpensive alternative materials like pearl millet husk, date pits, saw dust, buffing dust of leather industry, coir pith, crude oil residue, tropical grass, olive stone, almond shells, pine bark, wool waste, coconut shell etc., as carbonaceous precursors for the removal of dyes from water and wastewater [1-3].

The present study undertaken to evaluate the efficiency of a carbon adsorbent prepared from acid activated Banana bark carbon for the removal of dye in aqueous solution. In order to design adsorption treatment systems, knowledge of kinetic and mass transfer processes is essential. In this paper, the applicability of kinetic and mass-transfer models for the adsorption of Rhodamine B onto acid activated carbon was reported.

Material and Methods

Adsorbent Materials

The dried Banana bark was carbonized with concentrated sulphuric acid in the weight ratio of 1:1 (w/v). Heating for twelve hours in a furnace at 600 °C has completed the carbonization and activation. The resulting carbon was washed with distilled water until a constant pH of the slurry was reached. Then the carbon was dried for four hours at 100 °C in a hot air oven. The dried material was ground well to a fine powder and sieved to 0.05 mm by using a standard mesh.

Adsorption dynamic experiments

Batch equilibration method

The adsorption experiments were carried out in a batch process at 30, 40, 50 and 60° C temperatures. The known weight of adsorbent material was added to 50 mL of the dye solutions with an initial concentration of 10 mg/L to 60 mg/L. The contents were shaken thoroughly using a mechanical shaker (Remi Model) rotating with a speed of 120 rpm. The solution was then filtered at preset time intervals and the residual dye concentration was measured by double beam UV-Visible spectrophotometer using 548 nm filters.

Effect of variable parameters

Dosage of adsorbents

The various doses of the adsorbent were mixed with the dye solutions and the mixture was agitated in a mechanical shaker. The adsorption capacities for different doses were determined at definite time intervals by keeping all other factors constant.

Initial concentration of dye

In order to determine the rate of adsorption, experiments were conducted with different initial concentrations of dyes ranging from 10 to 60 mg/L. All other factors were kept constant.

Contact time

The effect of contact time on the removal of dye by the adsorbent in a single cycle was determined by keeping particle size, initial concentration, dosage, pH and concentration of other ions as constant.

pH

Adsorption experiments were carried out at pH 3, 4, 5, 6, 7, 8, 9 and 10. The acidic and alkaline pH of the media was maintained by adding the required amounts of 0.1 mol/L hydrochloric acid and sodium hydroxide solutions. The parameters like particle size of the adsorbents, dye concentration, dosage of the adsorbent and concentration of other ions are kept constant while carrying out the experiments. The pH of the samples was determined using a portable pH meter (Systronics Model). The pH meter was calibrated with 4.0 and 9.2 buffers.

Chloride

The experiments were done in the presence of varying chloride environments using sodium chloride solutions. While doing the experiments, the absence of other anions was ensured.

Temperature

The adsorption experiments were performed at 30, 40, 50 and 60 ^{o}C in a thermostat attached water bath shaker (Remi Model). The constancy of the temperature was maintained with an accuracy of ± 0.5 ^{o}C.

Zero point charge

The zero point charge of the carbon (pHzpc) was measured using the pH drift method [4]. The pH of the solution was adjusted by using 0.01 mol/L sodium hydroxide or hydrochloric acid. Nitrogen was bubbled through the solution at 25 ^{0}C to remove the dissolved carbon dioxide. 50 mg of the activated carbon was added to 50 mL of the solution. After stabilization, the final pH was recorded. The graph of final pH versus initial pH was used to determine the zero point charge of the activated carbon.

Titration studies

According to Boehm [4] only strong acidic carboxylic acid groups are neutralized by sodium bicarbonate, where as those neutralized by sodium carbonate are thought to be lactones, lactol and carboxyl group. The weakly acidic phenolic groups only react with strong alkali, sodium hydroxide. Therefore, by selective neutralization using bases of different strength, the surface acidic functional group in carbon can be characterized both quantitatively and qualitatively. Neutralization with hydrochloric acid characterizes the amount of surface basic groups that are, for example, pyrones and chromenes. The basic properties have described to surface basic groups and the pi electron system of carbon basal planes. The results indicate that the activated carbon used may possess acidic oxygen functional group on their surface and this is supported well by their respective zeropoint charge values. The results obtained from the above characterization studies are given in the Table.1.

Desorption studies

Desorption study was used to elucidate the nature of adsorption and recycling of the spent adsorbent. The effect of various reagents used for desorption were studied.

Results and Discussion

Characterization of the adsorbent

Activated carbons are widely used as an adsorbent due to the high adsorption capacity, high surface area, micro porous structure and high degree of surface respectively. The wide usefulness of carbon is a result of their high chemical and mechanical stability. The chemical nature and pore structure usually determines the sorption activity. The physico chemical properties of the adsorbent were measured by

various standard procedures including Drift method and Boehm titration studies are listed in the Table 1.

Effect of contact time and initial dye concentration

The experimental results of adsorptions of at various concentrations (10, 20, 30, 40, 50 and 60 mg/L) with contact time are shown in representative Figure 1. The equilibrium data were collected in Table 2 reveals that, percent adsorption decreased with increase in initial dye concentration, but the actual amount of dye adsorbed per unit mass of carbon increased with increase in dye concentration. It means that the adsorption is highly dependent on initial concentration of dye. It is because of that at lower concentration, the ratio of the initial number of dye molecules to the available surface area is low subsequently the fractional adsorption becomes independent of initial concentration. However, at high concentration the available sites of adsorption becomes fewer and hence the percentage removal of dye is dependent upon initial concentration [5, 6]. The adsorption attains equilibrium at 40 minutes for all concentrations. Figure 1 reveals that the curve is single, smooth and continuous, leading to saturation, suggesting the possible monolayer coverage of the dyes on the carbon surface.

Table 1. Characteristics of the adsorbent

Properties	Banana bark carbon
Particle size (mm)	0.05
Density (g/cc)	0.3986
Moisture content (%)	1.85
Loss on ignition (%)	83.5
Acid soluble matter (%)	4.00
Water soluble matter (%)	0.75
pH of aqueous solution	6.85
pH_{zpc}	6.5
Surface groups (m equiv/g)	
i) Carboxylic acid	0.352
ii) Lactone, lactol	0.056
iii) Phenolic	0.068
iv) Basic (pyrones and chromenes)	0.047

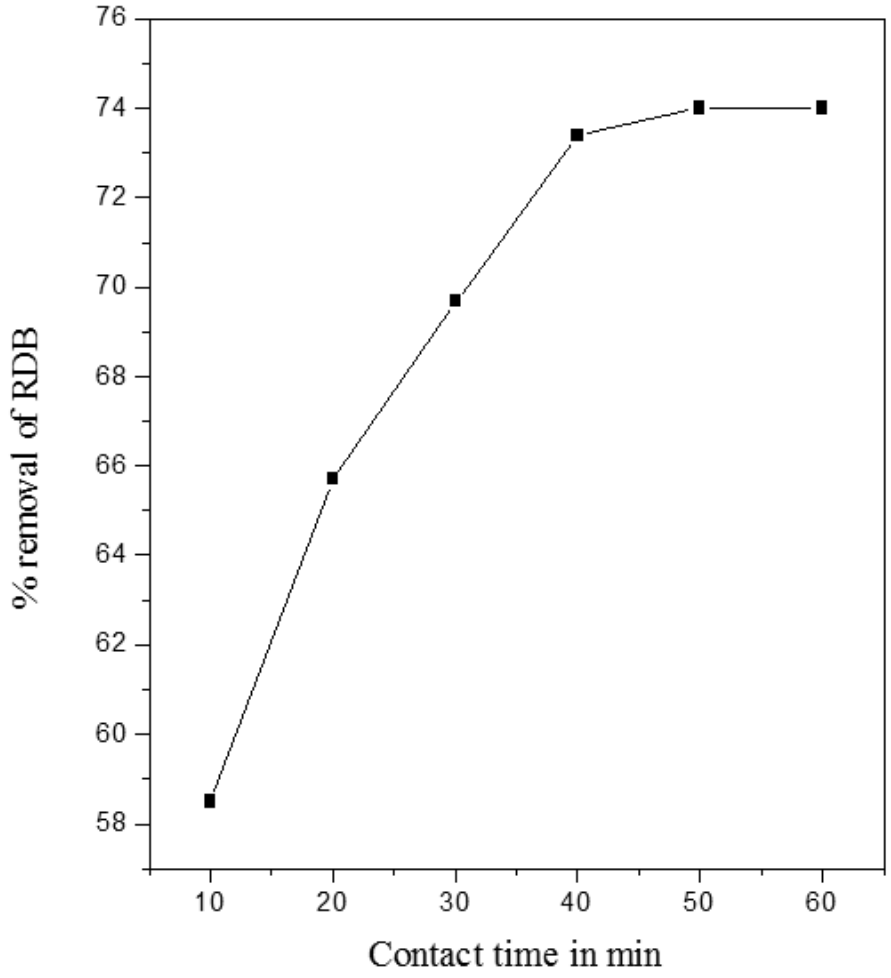

Figure 1. Effect of contact time on the removal of RDB. [RDB] = 30 mg/L; pH = 7; adsorbent dose = 50 mg/50 mL

Effect of adsorbent dosage

The adsorption of the dyes onto the adsorbent was studied by varying the adsorbent dose (25-250 mg/50mL) for 30 mg/L of dye concentration. The percentage of adsorption increased with increase in the dosage of the adsorbent (Figure 2). This was attributed to increased surface area and availability of more adsorption sites [5, 6]. Hence the remaining parts of the experiments were carried out with the adsorbent dose of 50 mg/50 mL.

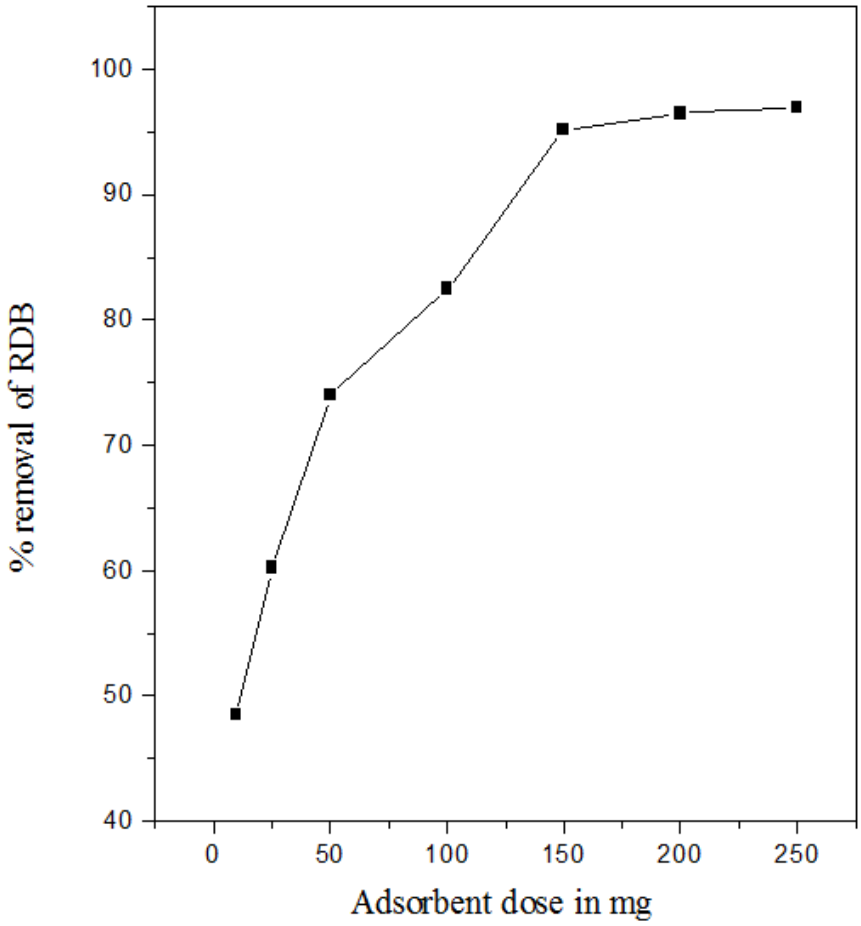

Figure 2. Effect os adsorbent dose on the removal of RDB. [RDB] = 30 mg/L; Contact time = 60 min; pH = 7.

Adsorption isotherm

The experimental data are analyzed by the linear form of the Langmuir and Freundlich isotherms [7, 8]. The Langmuir isotherm was represented by the following equation

$$C_e/Q_e = 1/Q_m b + C_e/Q_m$$

Where C_e is the equilibrium concentration (mg/L), Q_e is the amount adsorbed at equilibrium (mg/g) and Q_m and b is Langmuir constants related to adsorption efficiency and energy of adsorption, respectively. The linear plots of C_e/Q_e versus C_e suggest the applicability of the Langmuir isotherms (Figure 3). The values of Q_m and b were determined from slope and intercepts of the plots and are presented in Table 3. The results of adsorption efficiency Q_m and adsorption energy b of the adsorbent conclude that the maximum adsorption corresponds to a saturated monolayer of adsorbate molecules on adsorbent surface with constant energy and no transmission of adsorbate in the plane of the adsorbent surface. The observed b values shows that the adsorbent

prefers to bind acidic ions and that speciation predominates on sorbent characteristics, when ion exchange is the predominant mechanism takes place on the adsorption of RDB and it confirms the endothermic nature of the process involved in the system [8-10]. To confirm the favourability of the adsorption process, the separation factor (R_L) was calculated and presented in Table 4. The values were found between 0 and 1 confirms the ongoing adsorption process is much more favorable [1, 10, 11].

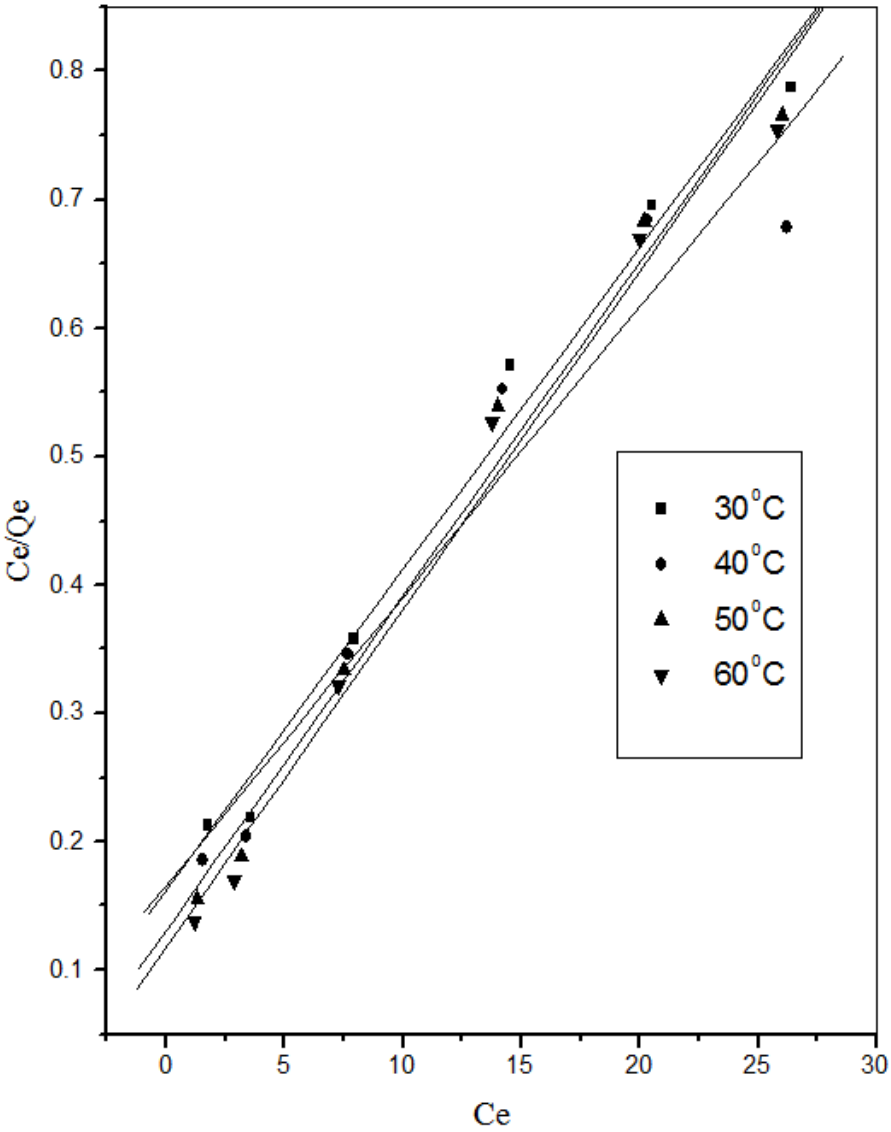

Figure 3. Langmuir adsorption isotherm for the removal of RDB

The Freundlich equation was employed for the adsorption of RDB dye onto the adsorbent. The Freundlich isotherm was represented by

$$\log Q_e = \log K_f + 1/n \log C_e$$

Where Q_e is the amount of Rhodamine B dye adsorbed (mg/g), C_e is the equilibrium concentration of dye in solution (mg/L) and K_f and n are constants incorporating the

factors affecting the adsorption capacity and intensity of adsorption, respectively. Linear plots of log Q_e versus log C_e shows that the adsorption of Rhodamine B dye obeys the Freundlich adsorption isotherm (Figure 4). The values of K_f and n given in the Table 5 show that the increase in negative charges on the adsorbent surface that makes electrostatic forces like van der Waals between the adsorbent surface and dye ion. The molecular weight, size and radii either limit or increase the possibility of the adsorption of the dye onto adsorbent. However, the values clearly show the dominance in adsorption capacity. The intensity of adsorption is an indicative of the bond energies between dye and adsorbent and the possibility of slight chemisorptions rather than physisorption [10-12]. However, the multilayer adsorption of RDB through the percolation process may be possible. The values of n are greater than one indicating the adsorption is much more favorable [12-14].

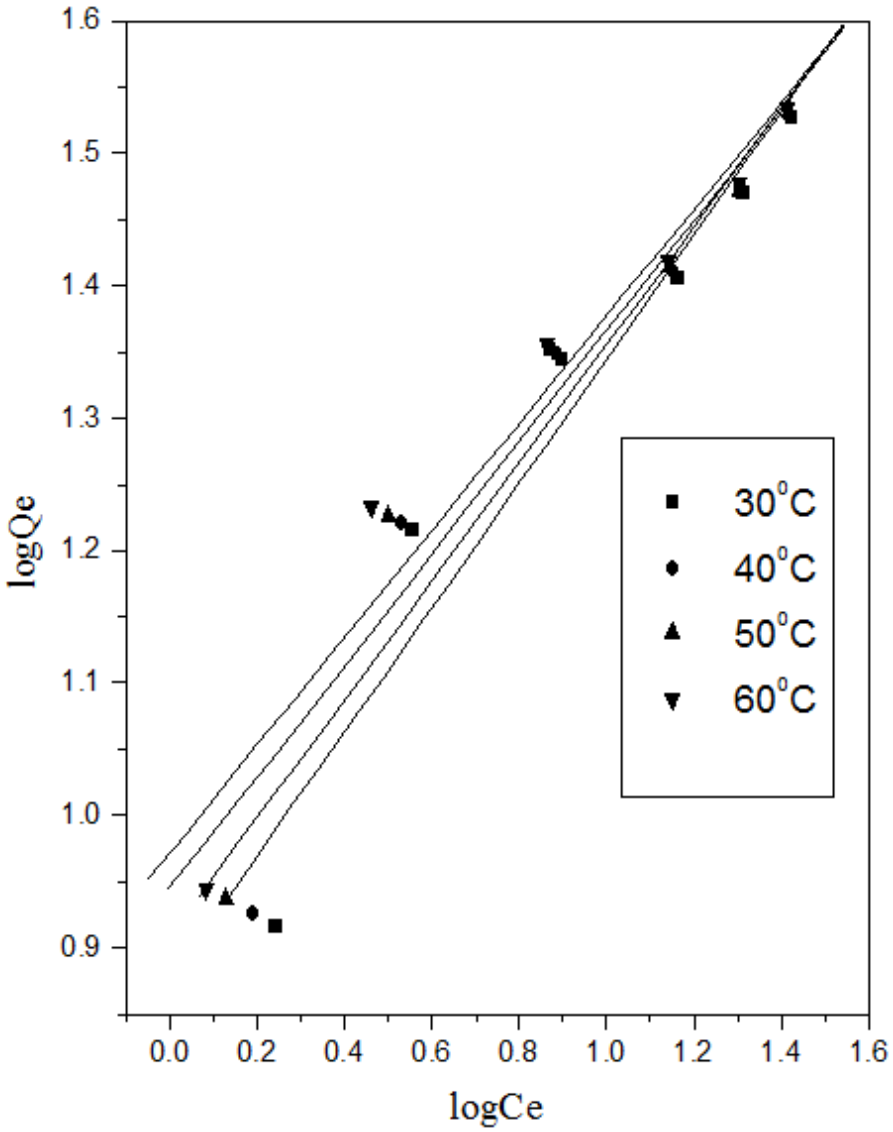

Figure 4. Freundlich isotherm for the adsorption of RDB

Table 2. Equilibrium parameters for the adsorption of RDB Dye onto activated Carbon

$[D]_0$	Ce (mg/L)				Qe (mg/g)				Dye removed (%)			
	Temperature (C)											
	30 °	40 °	50 °	60 °	30 °	40 °	50 °	60 °	30 °	40 °	50 °	60 °
10	1.7534	1.5588	1.3427	1.2124	8.2466	8.4412	8.6573	8.7876	82.6	84.4	86.5	87.8
20	3.5897	3.3799	3.1659	2.9025	16.4103	16.6201	16.8341	17.0975	82.0	83.1	84.1	85.4
30	7.9112	7.7098	7.5014	7.2941	22.0888	22.2922	22.4986	22.7039	73.6	74.3	74.9	75.6
40	14.5328	14.2257	14.0132	13.8012	25.4672	25.7746	25.9868	26.1988	63.6	64.4	64.9	65.4
50	20.5126	20.3099	20.2042	20.0017	29.4874	29.6921	29.5800	9.9983	258.9	59.3	59.5	59.9
60	26.4254	26.2194	26.0141	25.8029	33.5746	33.7806	33.9858	34.1971	55.9	56.3	56.6	56.9

Table 3. Langmuir isotherm results

Dye RDB	Temp (^{0}C)	Statistical parameters/constants		
		r^2	Q_m	b
	30	0.9919	40.161	0.1531
	40	0.9920	38.462	0.1995
	50	0.9646	35.700	0.2164
	60	0.9234	37.979	0.2224

Table 4. Dimensionless Separation factor (R_L)

	Temperature (^{0}C)			
$[D]_0$ (mg/L)	30	40	50	60
10	0.395	0.333	0.316	0.310
20	0.246	0.200	0.185	0.183
30	0.178	0.143	0.133	0.130
40	0.140	0.111	0.104	0.101
50	0.115	0.091	0.085	0.082
60	0.098	0.077	0.071	0.069

Table 5. Freundlich isotherm results

Dye RDB	Temp (^{0}C)	Statistical parameters/constants		
		r^2	K_f	n
	30	0.9693	1.5977	2.1335
	40	0.9725	1.5645	2.2338
	50	0.9758	1.5233	2.3758
	60	0.9862	1.4988	2.4709

Effect of temperature

The adsorption capacity of the adsorbent increased with increase in the temperature of the system from 30°-60°C. Thermodynamic parameters such as change in free energy were determined using the following equations (ΔG°) (kJ/mol), enthalpy (ΔH°)(kJ/mol) and entropy (ΔS°)(J/K/mol) were determined using the following equations

$$K_0 = C_{solid}/C_{liquid}$$

$$\Delta G° = -RT \ln K_O$$

$$\Delta G° = \Delta H° - T\Delta S°$$

$$\ln Ko = \Delta G°/(RT) = \Delta S°/(R) - \Delta H°/(RT)$$

$$\log K_0 = \Delta S°/(2.303R) - \Delta H°/(2.303RT)$$

Where Ko is the equilibrium constant, C_{solid} is the solid phase concentration at equilibrium (mg/ L), C_{liquid} is the liquid phase concentration at equilibrium (mg/L), T is the temperature in Kelvin and R is the gas constant. The ΔH° and ΔS° values obtained from the slope and intercept of Van't Hoff plots have presented in Table 6. The values ΔH° is with in the range of 1 to 93 KJ/mol indicates the physisorption. The result points out physisorption are much more favorable for the adsorption of RDB and the endothermic nature of adsorption [12-14]. Because in the case of physical adsorption, while increasing the temperature of the system, the extent of dye adsorption increases, this rules out the possibility of chemisorption [1, 12, 14, 15]. The low ΔH° value depicts dye is physisorbed onto the adsorbent.

The negative values of ΔG° (Table 6) shows the adsorption is highly favorable and spontaneous. The positive values of ΔS° (Table 6) shows the increased disorder and randomness at the solid solution interface of RDB with the adsorbent, while the adsorption there are some structural changes in the dye and the adsorbent occur. The adsorbed water molecules, which were displaced by the adsorbate species, gain more translational entropy than is lost by the adsorbate molecules, thus allowing the prevalence of randomness in the system. The enhancement of adsorption capacity of the adsorbent at higher temperatures was attributed to the enlargement of pore size and activation of the adsorbent surface [1, 13-15].

Kinetics of adsorption

In the present study, the kinetics of the dye removal was carried out to understand the behaviour of the low cost carbon adsorbent. The adsorption of dye from an aqueous solution follows reversible first order kinetics, when a single species are considered on a heterogeneous surface. The heterogeneous equilibrium between the dye solutions and the activated carbon are expressed as

$$A \underset{k_2}{\overset{k_1}{\rightleftharpoons}} B$$

Where k_1 is the forward rate constant and k_2 is the backward rate constant. A represents dye remaining in the aqueous solution and B represent dye adsorbed on the surface of activated carbon. The equilibrium constant (K_0) is the ratio of the concentration of dye in adsorbent and in aqueous solution ($K_0=k_1/k_2$).

In order to study the kinetics of the adsorption process under consideration the

following kinetic equation was proposed by Natarajan and Khalaf as cited in literature has been employed [1,13,14].

$$\log C_0/C_t=(K_{ad}/2.303)t$$

Where C_0 and C_t are the concentrations of the dye in (in mg/L) at the time zero and time t. The rate constants (K_{ad}) for the adsorption processes were calculated from the slope of the linear plots of log C_0/C_t versus t for different concentrations and temperatures. The rate constants are determined by the following equation.

$$K_{ad}=k_1+k_2=k1+(k_1/K_0)=k_1[1+1/K_0]$$

The overall rate constant k_{ad} for the adsorption of dye at different temperatures are calculated from the slopes of the linear Natarajan-Khalaf plots. The rate constant values are collected in Table 7 shows that the rate constant (k_{ad}) increases with increase in temperature suggesting that the adsorption process in endothermic in nature. The over all rate of adsorption is separated into the rate of forward and reverse reactions using the above equation. The rate constants for the forward and reverse processes are also collected in Table 7 indicate that, at all initial concentrations and temperatures, the forward rate constant is much higher than the reverse rate constant suggesting that the rate of adsorption is clearly dominant [13-15].

Intraparticle diffusion

The most commonly used technique for identifying the mechanism involved in the sorption process is by fitting the experimental data in an intraparticle diffusion plot. Previous studies by various researchers [15-17] showed that the plot of Qt versus $t^{0.5}$ represents multi linearity, which characterizes the two or more steps involved in the sorption process. According to Weber [16], an intraparticle diffusion coefficient K_p is defined by the equation:

$$K_p=Qt/t^{0.5}+C$$

Thus the K_p(mg/g $min^{0.5}$) value can be obtained from the slope of the plot of Qt(mg/g) versus $t^{0.5}$ for Rhodamine B. From Figure 5, it was noted that the sorption process tends to be followed by two phases. The two phases in the intraparticle diffusion plot suggest that the sorption process proceeds by surface sorption and intraparticle diffusion [15-17]. The initial curved portion of the plot indicates a boundary layer effect while the second linear portion is due to intraparticle or pore diffusion. The slope of the second linear portion of the plot has been defined as the intraparticle diffusion parameter K_p(mg/g $min^{0.5}$). On the other hand, the intercept of the plot reflects the boundary layer effect. The larger the intercept, the greater is the contribution of surface sorption in the rate limiting step. The calculated intraparticle diffusion coefficient K_p value was given by 0.307, 0.310, 0.318, 0.322 and 0.328 mg/g $min^{0.5}$ for initial dye concentration of 10, 20, 30, 40, 50 and 60 mg/L at 30^0C.

Table 6. Equilibrium constant and thermodynamic parameters for the adsorption of dyes onto carbon

$[D]_0$	K_0				ΔG^o					
	Temperature (°C)									
	30	**40**	**50**	**60**	**30**	**40**	**50**	**60**	**ΔH^o**	**ΔS^o**
10	4.7032	5.4151	6.4476	7.2480	-3.90	-4.39	-5.00	-5.48	12.23	53.19
20	4.5714	4.9170	5.3173	5.8906	-3.83	-4.14	-4.48	-4.91	6.93	35.43
30	2.7920	2.8910	2.9992	3.1129	-2.58	-2.76	-2.95	-3.14	3.00	18.44
40	1.7523	1.8118	1.8544	1.8982	-1.41	-1.54	-1.66	-1.77	2.19	11.91
50	1.4375	1.4620	1.4742	1.4997	-0.94	-0.98	-1.04	-1.12	1.12	6.72
60	1.2705	1.2880	1.3064	1.3253	-0.60	-0.66	-0.72	-0.80	1.16	5.83

Table 7. Rate constants for the adsorption of Rhodamine B dye (10^3 k_{ad}, min^{-1}) and the constants for forward (10^3 k_1, min^{-1}) and reverse (10^3 k_2, min^{-1}) process

Temperature (°C)												
$[D]_0$	**k_{ad}**				**30**		**40**		**50**		**60**	
	30°	**40°**	**50°**	**60°**	**k_1**	**k_2**	**k_1**	**k_2**	**k_1**	**k_2**	**k_1**	**k_2**
10	13.4	14.83	17.08	18.74	11.05	2.35	12.52	12.31	14.78	2.30	16.47	0.93
20	6.47	7.13	7.59	8.88	5.31	1.16	5.92	1.21	6.39	1.20	7.59	1.29
30	3.56	3.17	3.27	3.36	2.62	0.94	2.36	0.82	2.45	0.82	2.54	0.82
40	1.70	1.72	1.77	1.79	1.09	0.61	1.11	0.62	1.15	0.62	1.17	0.62
50	1.24	1.24	1.24	1.24	0.73	0.51	0.74	0.50	0.74	0.50	0.75	0.49
60	0.94	0.92	0.96	0.97	0.52	0.42	0.52	0.40	0.55	0.42	0.56	0.41

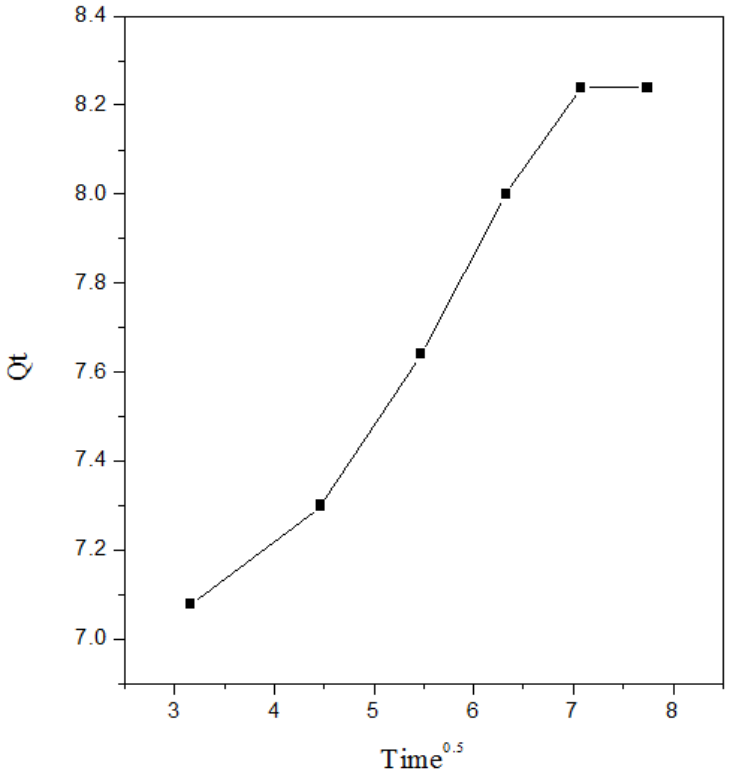

Figure 5. Intraparticle diffusion effect for the removal of RDB.

Effect of pH

The effect of pH on the adsorption of RDB onto the adsorbent was studied in wide range of pH. The results are shown in Figure 6 shows that the uptake of RDB ions at pH 8 was the minimum and maximum at pH 6.5. However, when the pH of the solution was increased (beyond pH 8.5), the uptake of RDB ions was increased. It appears that a change in pH of the solution results in the formation of different ionic species and different surface charge. At pH values lower than 7.5, the RDB ions can enter into the pore structure. At a pH value higher than 7.5, the zwitterions form of RDB in water may increase the aggregation of RDB to form a bigger molecular form (dimer) and become unable to enter into the pore structure of the adsorbent surface. The greater aggregation of the zwitterionic form is due to the attractive electrostatic interaction between the carboxyl and xanthane groups of the monomer.

At a pH value higher than 8.5, the existence of OH^- creates a competition between $-N^+$ and COO^- and it will decrease the aggregation of RDB, which causes an increase in the adsorption of RDB ions on the adsorbent surface. The effect of the charge on the surface and the electrostatic force of attraction/repulsion between the adsorbent surface and the RDB ions cannot explain the result [1, 17].

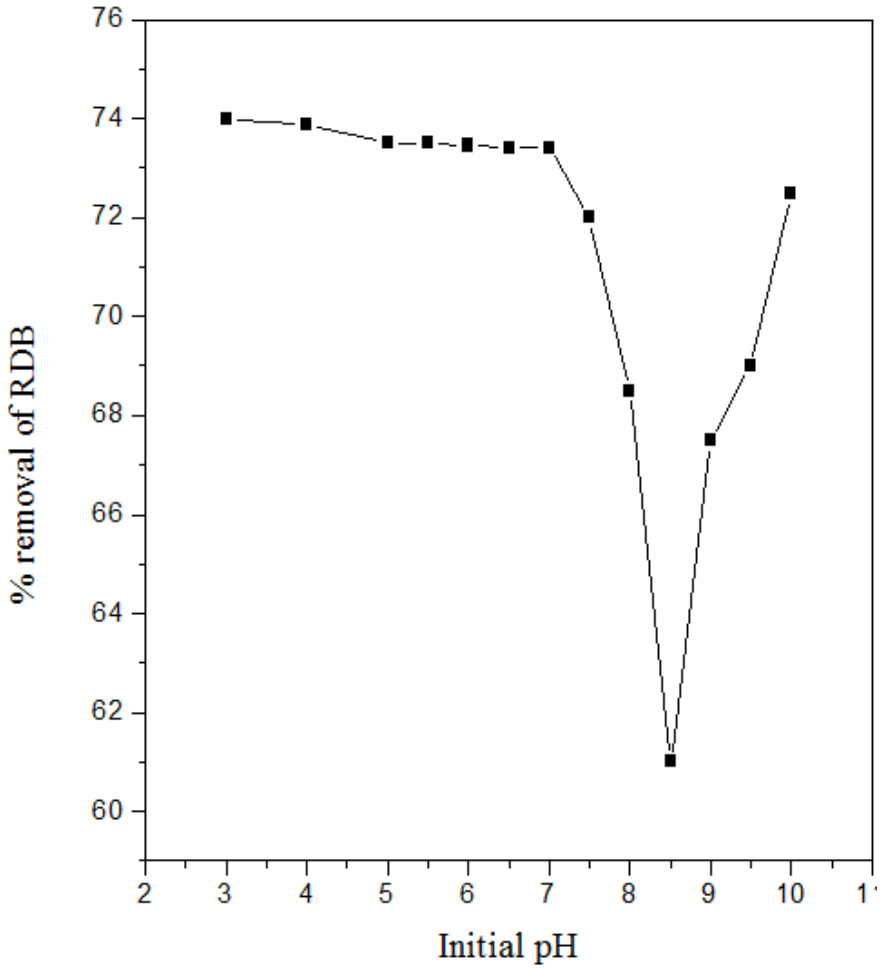

Figure 6. Effect of initial pH on the removal of RDB. [RDB] = 30 mg/L; Adsorbent dose = 50 mg/50 mL; pH = 7

Effect of the ionic strength on the adsorption of RDB

The effect of sodium chloride on the adsorption of RDB by the adsorbent is shown in Figure 7 shows that low concentrated solution of NaCl had little influence on the adsorption capacity. At higher ionic strength the adsorption RDB will be increased due to the partial neutralization of the positive charge on the adsorbent surface and a consequent compression of the electrical double layer by the Cl^- anion. The chloride ion can also enhances adsorption of RDB ion onto the adsorbent by pairing of their charges and hence reducing the repulsion between the RDB ion and adsorbent surface. This initiates the adsorbent to adsorb more positive RDB ions on its surface [1, 15, 17, 18].

Desorption studies

Desorption studies help to elucidate the nature of adsorption and recycling of the spent adsorbent and the dye. If the adsorbed dyes can be desorbed using neutral pH water, then the attachment of the dye by the adsorbent is through the weak bonds. If sulphuric acid or alkaline water desorp the dye then the adsorption is by ion exchange. If organic acids, like acetic acid can desorb the dye, then the dye was held by the

adsorbent through chemisorption. The effect of various reagents used for desorption studies indicate that hydrochloric acid is a better reagent for desorption, because more than 85% of the adsorbed dye were removed. The desorption of dye by mineral acids indicate that the dyes were adsorbed onto the adsorbent through by physisorption mechanisms [1, 15, 17, 18].

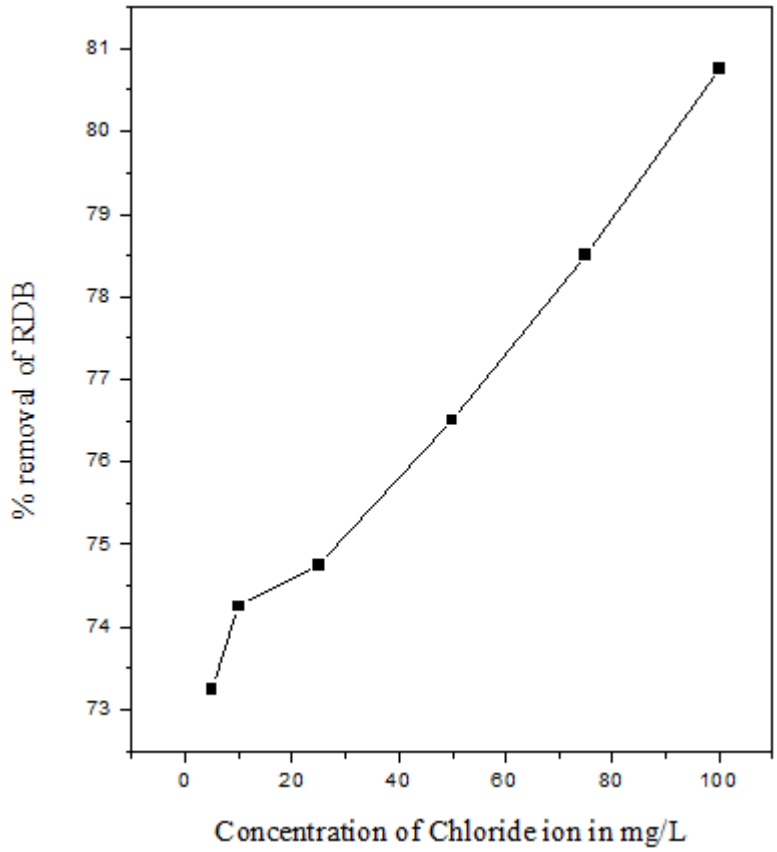

Figure 7. Effect of chloride ion on the removal of RDB. [RDB] = 30 mg/L; Adsorbent dose = 50 mg/50 mL; pH = 7

Conclusion

The experimental data are correlated reasonably well by the Langmuir and Freundlich adsorption isotherms. The low as well high pH value shows the optimum amount of adsorption of RDB by the adsorbent. The amount of RDB adsorbed by the adsorbent was increased with increasing ionic strength and temperature. The dimensionless separation factor (R_L) shows that the chosen activated carbon can be used for the removal of RDB from aqueous solution. The values of ΔH°, ΔS° and ΔG° results

shows that the activated carbon employed has a considerable potential as an adsorbent for the removal of RDB.

Acknowledgement

The authors acknowledge sincere thanks to Mrs. Mala Arivoli, The Principal, M.R.Government Arts College, Mannargudi and The Director of Collegiate Education, Chennai for carrying out this research work successfully.

References and Notes

[1] Arivoli S. Kinetic and thermodynamic studies on the adsorption of some metal ions and dyes onto low cost activated carbons. **[**Ph.D. Thesis.] Gandhigram Rural University, Gandhigram, 2007.
[2] Sekaran G.; Shanmugasundaram K. A.; Mariappan M. and Raghavan K. V. *Indian J. Chem. Technol.* **1995**, *2*, 311**.**
[3] Selvarani K. Studies on Low cost Adsorbents for the removal of organic and Inorganics from Water. **[**Ph.D. Thesis.] Regional Engineering College, Thiruchirapalli**,** 2000.
[4] Jia Y. F. and Thomas K. K. *Langmuir* **2002**, *18*, 470.
[5] Namasivayam C.; Muniasamy N.; Gayathri K.; Rani M. and Renganathan K. *Biores. Technol*. **1996**, *57*, 37.
[6] Namasivayam C. and Yamuna R. T**.** *Environ. Pollut.* **1995**, *89*, 1.
[7] Langmuir I**.** *J. Am. Chem. Soc*. **1918**, *40*, 1361.
[8] Reundlich H. *Phys. Chemie* **1906**, *57*, 384.
[9] Krishna D. G. and Bhattacharyya G**.** *Appl. Clay Sci*. **2002**, *20*, 295.
[10] Arivoli S.; Viji J. M. and Rajachandrasekar T. *Mat. Sci. Res. India* **2006**, *3*, 241.
[11] Arivoli S. and Hema M. *Intern. J. Phys. Sci*. **2007**, *2*, 10.
[12] Arivoli S.; Venkatraman B. R.; Rajachandrasekar T. and Hema M. *Res. J. Chem. Environ*. **2007**, *17*, 70.
[13] Arivoli S.; Kalpana K.; Sudha R. and Rajachandrasekar T. *E. J. Chem.* **2007**, *4*, 238.
[14] Renmin G.; Yingzhi, S.;, Jian, C.; Huijun, L.; Chao, Y. *Dyes and Pigments*, **2005**, *67*, 179.
[15] Vadivelan V.; Vasanthkumar K. *J. Colloid Inter. Sci.* **2005**, *286*, 91.
[16] Weber W. J. Principle and Application of Water Chemistry, edited by Faust S. D. and Hunter J. V. Wiley, New York, 1967.
[17] Yupeng, G.; Jingzhu, Z.; Hui, Z.; Shaofeng, Y.; Zichen, W.; Hongding, X. *Dyes and Pigments* **2005**, *66*, 123.
[18] Sreedhar M. K. and Anirudhan, T. S. *Indian J. Environ. Protect* **1999**, *19*, 8.

ISSN 1984-6428
ONLINE
www.orbital.ufms.br

Orbital 2009, *1* (2), 156-166

Full Paper

A PBE hybrid functional study of blue-shifting and red-shifting hydrogen bonds in π hydrocarbons

Boaz G. Oliveira[a*], *Regiane C. M. U. de Araújo*[a], *Mozart N. Ramos*[b]

[a]Departamento de Química – Universidade Federal da Paraíba. CEP 58036-300, João Pessoa – PB, Brazil.
[b]Departamento de Química Fundamental – Universidade Federal de Pernambuco. CEP 50739-901, Recife – PE, Brazil.

Received: 24 November 2008; revised: 25 January 2009; accepted: 16 February 2009. Available online: 26 April 2009

ABSTRACT: *This study examines a selected group of π hydrocarbon complexes, represented by $C_2H_4\cdots HCF_3$, $C_2H_2\cdots HCF_3$, $C_2H_4\cdots HCF_3$ and $C_2H_2\cdots HCF_3$, from a theoretical point of view. From BPBE/6-311++G(d,p) calculations, the geometrical results of these complexes revealed an elongation and shortening of the H—C bond lengths of chloroform ($HCCl_3$) and fluoroform (HCF_3), respectively. In terms of the infrared spectrum, the analysis of stretch frequencies revealed that the variations in the H—C modes are essentially recognized as red and blue-shifting modes. For the purposes of understanding the two vibrational phenomena of the π hydrocarbon complexes studied here, PBE/6-311++G(d,p) calculations were carried out and partitioning of atomic charges derived from the ChelpG algorithm were also used. A theoretical justification of red- and blue-shift effects was drawn up using charge-transfer analysis, which is manifested in the π bonds of acetylene and ethylene to chloroform ($H—CCl_3$) and fluoroform ($H—CF_3$), respectively. Finally, a further debate regarding the distinct polarizability power of chloroform and fluoroform is presented, concluding that, in comparison with fluoroform, chloroform possesses the requisite features for conventional proton donors and a red-shift is therefore observed in the $C_2H_4\cdots HCCl_3$ and $C_2H_2\cdots HCCl_3$ complexes.*

Keywords*: red-shifting, blue-shifting, Hydrogen bonds*

*Corresponding author: boazgaldino@gmail.com

Introduction

For many years, the numerous molecular systems formed by non-covalent interactions have been a focus for research in the chemical, physical and biological sciences [1]. In conceptual terms, although van der Waals's or London's dispersion forces are important, the hydrogen bonds (Y···H) are considered to be one of the most important interactions because there are an enormous number of phenomena inherent in the contact between proton donors (H) and acceptors (Y = F, O, N, S and π centers) [2-4]. In practice, the importance of hydrogen bonding is essential in almost all branches of chemistry, such as, for example, the activation of biomolecules [5], the formation of transition state structures in organic reactions [6] and the development of pharmacological substances [7].

In terms of physical chemistry, hydrogen bonding can be interpreted using the theory of electronic partition, which includes the electrostatic potential term (U), the polarizability effect (P), the exchange spin terms (EX), and charge transfer quantities (Q). The relative contributions of these parameters in quantifying the total energy have been clearly defined, although the electrostatic potential is often the most important [8]. A theoretical study carried out by King and Weinhold [9] revealed the special importance of charge transfer in determining the stabilization energy of HCN linear chains. In traditional hydrogen-bonded complexes, however, the accumulation of charge density on proton donors (HX = Cl, F and CN groups) leads to drastic changes in their structures. One of these changes is the bond length enhancement [10-13], according to which the HX infrared stretch frequencies are shifted downwards and a strong increase in the absorption intensity occurs [14]. In spectroscopy, this phenomenon is known as red-shift, although it should also be remembered that such an effect is commonly observed, not only in van der Waals intermolecular systems, but also in hydrogen-bonded complexes formed by π electron donors [15-16].

However, Hobza *et al.* [17] have recently found a new kind of intermolecular interaction known as antihydrogen bond. Owing to inverse and unusual spectroscopic behavior on the part of the proton donors, a blue- rather than red-shift effect is observed on their bonds [18]. In contrast to the traditional appearance of red-shifts in hydrogen-bonded systems, in antihydrogen-bonded complexes there is a strengthening of the HX bond, which leads to its stretch frequency being shifted to higher wave numbers [19-21]. The anti-hydrogen bonds have thus been designated blue-shifting hydrogen bonds. It is agreed that the blue-shifting hydrogen-bonded systems routinely studied are related to aromatic [22], halogen hydrocarbons [23] and heterocyclic compounds [24], but not to aliphatic hydrocarbons. Although there are still many outstanding questions regarding the

characterization of blue-shifting hydrogen bonds [25], it is of great importance that an investigation and debate be conducted as to whether there are red-shift and blue-shift modes on the C—H bonds in both HCF_3 and $HCCl_3$ molecules upon the formation of π hydrocarbon complexes formed by acetylene and ethylene, for example. In other words, besides the capacity of acetylene and ethylene to form traditional hydrogen-bonded complexes with monoprotic halogen acids, i.e., hydrochloric acid and hydrofluoric acid [15-16], the formation of blue-shifting hydrogen bonds in $C_2H_2\cdots HCF_3$ and $C_2H_4\cdots HCF_3$ π hydrocarbon complexes requires more thorough examination.

For the purposes of examining the properties of blue-shifting hydrogen bonds in $C_2H_2\cdots HCF_3$, $C_2H_4\cdots HCF_3$, $C_2H_4\cdots HCCl_3$ and $C_2H_2\cdots HCCl_3$ π-complexes, it is theoretically necessary to use an efficient set of methodologies which efficiently describe the red- and blue-shift effects. The specialized literature reveals a large number of studies of hydrogen-bonded complexes which point to the efficiency of Density Functional Theory (DFT) [26]. Thus, analysis of structural, electronic and, principally vibrational parameters, using DFT hybrid functionals, may produce satisfactory results, not only for red-shift interactions, but also for the blue-shift hydrogen-bond type. Furthermore, the quantification of electronic density is a useful parameter for explaining the formation of intermolecular interactions [27]. In practice, the charge transfer in hydrogen-bonded complexes has been used to characterize the formation of red-shift effects on proton donors [28-29]. This study will thus also include an analysis of the charge transfer on the $C_2H_2\cdots HCF_3$, $C_2H_4\cdots HCF_3$, $C_2H_4\cdots HCCl_3$ and $C_2H_2\cdots HCCl_3$ π systems. This investigation will be performed using the ChelpG algorithm [30], whose efficiency is well-known among the theoreticians [31]. Among many other applications, a number of important studies of the formation of hydrogen-bonded complexes have been published using ChelpG calculations [32-33].

Computational Details

The optimized geometries of the $C_2H_2\cdots HCF_3$, $C_2H_4\cdots HCF_3$, $C_2H_4\cdots HCCl_3$ and $C_2H_2\cdots HCCl_3$ π complexes were obtained using the Perdew-Burke-Ernzerhof (PBE) density functional formulation and combined with the 6-311++G(d,p) basis set, with all calculations carried out using the GAUSSIAN 98W program [34]. The PBE hybrid was chosen due to its competence to describe hydrogen bonds [35] and intermolecular interactions [36]. The intermolecular energies were determined using the supermolecule approach [37], and the energy corrections were obtained by means of Zero Point Energy (ZPE) [38] and Basis Sets Superposition Error (BSSE) [39] calculations. The ChelpG method was used to calculate the atomic charges. All the calculations were performed using the GAUSSIAN 98W program.

Results and Discussion

Geometry and infrared harmonic spectrum

The optimized geometries of the $C_2H_2\cdots HCF_3$ (**I**), $C_2H_4\cdots HCF_3$ (**II**), $C_2H_2\cdots HCCl_3$ (**III**) and $C_2H_4\cdots HCCl_3$ (**IV**) π complexes are depicted in Figure 1, and their main structural results are listed in Table 1.

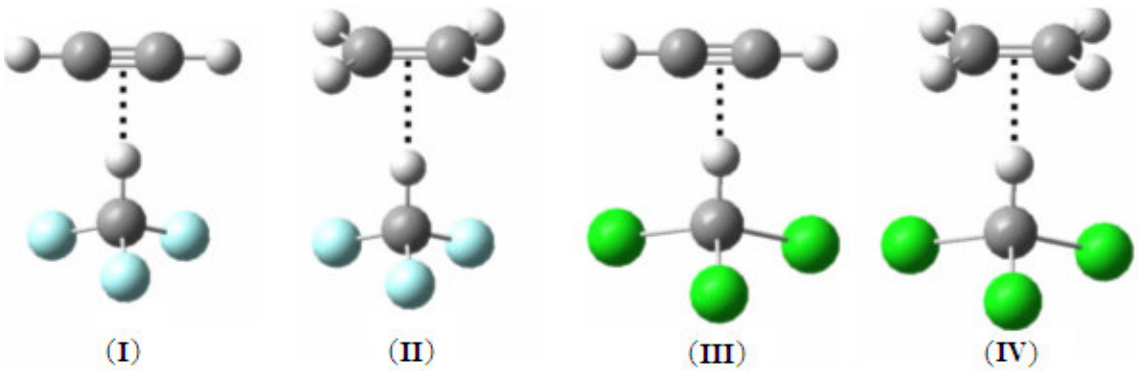

Figure 1. Optimized geometries of the $C_2H_2\cdots HCF_3$ (**I**), $C_2H_4\cdots HCF_3$ (**II**), $C_2H_2\cdots HCCl_3$ (**III**) and $C_2H_4\cdots HCCl_3$ (**IV**) π complexes using BPBE/6-311++G(d,p) calculations.

Table 1. Structural parameters and infrared modes of HCF_3 and $HCCl_3$ monomers, as well as of $C_2H_2\cdots HCF_3$ (**I**), $C_2H_4\cdots HCF_3$ (**II**), $C_2H_2\cdots HCCl_3$ (**III**) and $C_2H_4\cdots HCCl_3$ (**IV**) π complexes using the PBE/6-311++G(d,p) calculations.

Parameters	Molecular systems					
	HCF_3	**$HCCl_3$**	**(I)**	**(II)**	**(III)**	**(IV)**
R(H···π)	—	—	2.9304	2.9898	2.8298	2.8338
r(C—H)	1.0987	1.0913	1.0983	1.0984	1.0925	1.0928
Δr(C—H)	—	—	-0.0004	-0.0003	0.0012	0.0015
υ(H···π)	—	—	35.9	37.3	41.10	40.00
I(H···π)	—	—	0.2	0.15	0.30	0.25
υ(C—H)	3057.1	3104.2	3059.8	3058.4	3088.4	3084.6
I(C—H)	36.6	0.04	7.3	6.3	32.0	36.8
Δυ(C—H)	—	—	2.8	1.3	-15.8	-19.6
I(C—H),c/I(C—H),m	—	—	0.2	0.17	800.0	920.0

* Values of R and r are given in Å;
* Values of υ and I are given in cm^{-1} and km mol^{-1}, respectively.

Initially, one important structural observation in (**I**) and (**II**) is the contraction of -0.0004 Å and -0.0003 Å for the r(C—H) bond of the fluoroform, as well as the changes on its υ(C—H) frequencies which are shifted upward to values of 2.8 cm^{-1} and 1.3 cm^{-1} followed by a substantial diminution in absorption intensities, e.g., ratios of 0.2 and 0.17.

As it is widely known that these infrared changes are blue-shifting, it can be presumed that (**I**) and (**II**) are blue-shifting hydrogen complexes. On the other hand, the r(C—H) bond length of chloroform increases by 0.0012 Å and 0.0015 Å on the formation of the (**III**) and (**IV**) systems, respectively. The $\Delta\upsilon$(C—H) results of -15.8 cm^{-1} and -19.6 cm^{-1} as well as absorption ratios I(C—H),c/I(C—H),m of 800 and 920 indicate behavior opposite to that observed for (**I**) and (**II**). In fact, π systems formed by chloroform present typical red-shifts on their C—H bonds. Therefore, both (**III**) and (**IV**) can be called conventional hydrogen-bonded complexes. In terms of interaction strength, the (**III**) and (**IV**) complexes present shorter R(H···π) distance values, which, in comparison with the C=C bond of ethylene, shows that the higher electronic density on C≡C bond of acetylene is not responsible for stronger hydrogen-bonded complexes. The π systems formed by chloroform, specifically (**III**) and (**IV**), are thus the most strongly bonded systems. In fact, regardless of whether vibrational or structural parameters are considered, it can be observed that more strongly (I(C—H),c/I(C—H),m ≥ 1) and more weakly (I(C—H),c/I(C—H),m < 1) bonded systems are connected with red- (**I-II**) and blue-shift (**III-IV**) π hydrocarbons, respectively. According to Barnes [40], analysis of infrared intensity provides an argument for interpreting the formation of red- and blue-shift hydrogen bonds, which are identified by a drastic increase or decrease, respectively, in their absorption intensities.

Intermolecular energies and charge transfer

Recent studies of hydrogen-bonded complexes have established intermolecular energy as a parameter widely used to explain the interaction strength [29] and, in some cases, the hydrogen bond stretch frequencies also corroborate this. Therefore, in strong agreement with findings reported by van der Veken *et al.* [41], the results of this study also indicated that blue- and red-shifts are related to weak (C_2H_2···HCF_3 and C_2H_4···HCF_3) and strong (C_2H_2···$HCCl_3$ and C_2H_4···$HCCl_3$) bonded systems, respectively. According to Table 2, note that, the interaction energy values ΔE^C for (**I**) and (**II**) lie in the range of 2.30-2.35 kJ mol^{-1}, whereas the (**III**) and (**IV**) complexes are bonded by energy values varying from 2.56 kJ mol^{-1} to 2.65 kJ mol^{-1}. Even though the energy difference between the complexes formed by fluoroform and chloroform are in the range of 0.3 kJ mol^{-1}, it should be noted that these interaction energy levels are lower than those documented for model blue-shifting complexes formed by halogen hydrocarbons and water [42], for instance. Taking into account important studies of π hydrogen-bonded complexes [11, 15], which report that the quantification of charge transfer can help to interpret the variation in the stretch frequencies of proton donors, in particular their red-shifts, for the intermolecular systems under study here the Figure 2 illustrates the relationship between the values of infrared changes on C—H bonds and ΔQ^{ChelpG} intermolecular charge transfer

values.

Table 2. Electronic parameters of the $C_2H_2\cdots HCF_3$ (**I**), $C_2H_4\cdots HCF_3$ (**II**), $C_2H_2\cdots HCCl_3$ (**III**) and $C_2H_4\cdots HCCl_3$ (**V**) complexes using PBE/6-311++G(d,p) calculations.

Parameters	Complexes			
	(I)	**(II)**	**(III)**	**(IV)**
ΔE	2.9	3.0	4.1	4.3
BSSE	0.54	0.69	1.45	1.74
ΔE^C	2.35	2.30	2.65	2.56
ΔQ^{ChelpG}	-0.031	-0.030	-0.025	-0.023
Δμ	0.31	0.36	0.40	0.45

* Values of ΔE, BSSE and ΔE^C are given in kJ mol^{-1};
* Values of ΔQ^{ChelpG} are given in electronic units (e.u.);
* Values of μ for HCF_3 and $HCCl_3$ monomers are 1.68 D and 1.15 D, respectively.

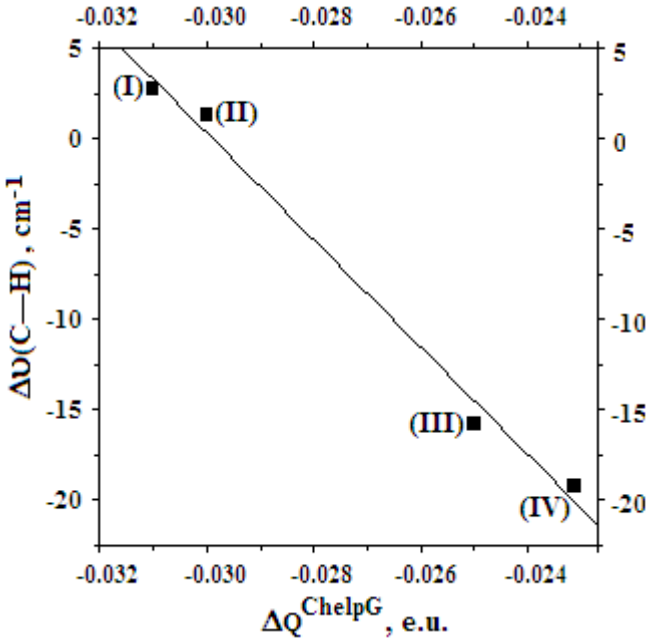

Figure 2. Relationship between the infrared changes in C—H bonds and ΔQ^{ChelpG} intermolecular charge transfer in $C_2H_2\cdots HCF_3$ (**I**), $C_2H_4\cdots HCF_3$ (**II**), $C_2H_2\cdots HCCl_3$ (**III**) and $C_2H_4\cdots HCCl_3$ (**IV**) π complexes using BPBE/6-311++G(d,p) calculations.

Not surprisingly, the R^2 linear coefficient yielded by equation (1) is a strong indicator of the formation of blue-shifting and red-shifting hydrogen bonds on the (**I**), (**II**), (**III**) and (**IV**) π systems, respectively.

$$\Delta u(C—H) = -88.7 - 2970\ \Delta Q^{ChelpG}\ ;\ R^2 = -0.99. \qquad (1)$$

In terms of notation, although several methods are routinely used to calculate atomic charges [43], the ChelpG calculations have provided excellent results for charge transfer [29, 32]. In fact, this is a decisive point because the electronic transfer between

the HOMO and LUMO orbital of proton acceptor and donor need to be accurately evaluated. Thus, according to the ΔQ^{ChelpG} values for -0.031 e.u. and -0.030 e.u. of the (**I**) and (**II**) complexes, their blue-shifting effects are directly correlated with larger charge transfers, while the (**III**) and (**IV**) have smaller results for -0.025 e.u. and -0.023 e.u., respectively.

Influence of the polarizability of the proton donors

It should also be mentioned that the polarizabilities of HCF_3 and $HCCl_3$ proton donors must affect their interactions with π molecules, such as acetylene and ethylene. However, the nature of blue-shift hydrogen bonds has been debated by Hobza and Havlas [44], who have demonstrated that the C—H bond length of fluoroform is drastically affected by variation in its dipole moment. It has been pointed out that, in case of HCF_3, the shortening its bond length leads to larger dipole moments [45], as demonstrated in Figure 3. Similar conclusions have also been reported by Barnes [40], who also discusses whether negative dipole moment derivatives ($\delta\mu^0/\delta\mu rHX$) also reveal the propensity of proton donors to bind with high density centers of red and blue-shift systems. In other words, as also demonstrated by Hobza and Havlas [44], as presented above, this study confirms the trend towards reduction and increase in the dipole moment of fluoroform and chloroform, respectively. In fact, the shortening of the C—H bonds of (**I**) and (**II**) reinforces the idea that these π systems are blue-shifting hydrogen-bonded complexes.

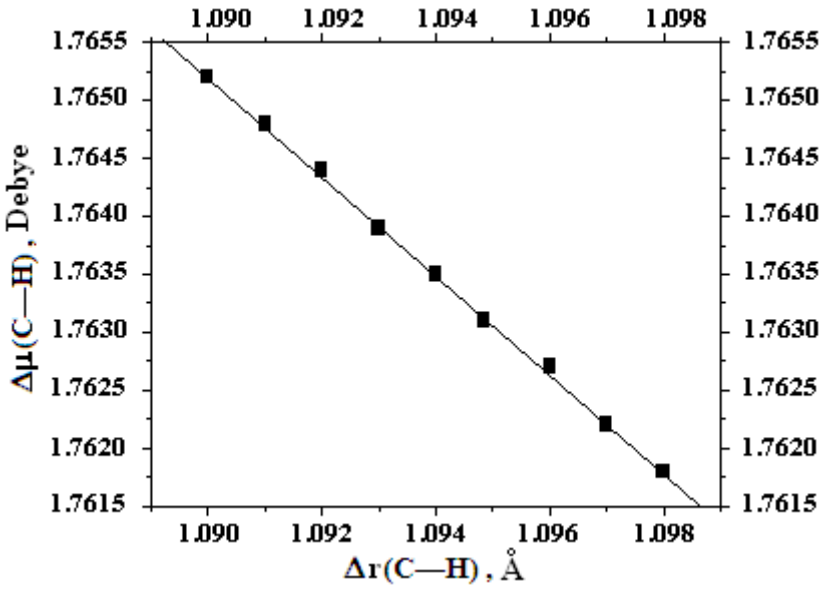

Figure 3. Variation of dipole moment ($\vec{\mu}$) and changes of C—H bond length of the HCF_3 molecule using PBE/6-311++G(d,p) calculations.

However, analysis of Figure 4 shows that $HCCl_3$ behaves in a similar fashion with polar molecules, such as water, where the elongation of C—H leads to an increase in the

dipole moment value. Therefore, this study casts no doubt on the efficiency of the PBE functional to detect the dispersion energy and attractions forces and the results presented here are in satisfactory agreement with the explanations put forward by Hobza and Havlas [44]. With regard to this, even though many works have demonstrated that $HCCl_3$ has the property of forming blue-shifting hydrogen bond complexes [46], our results revealed an intriguing feature of HCF_3 and $HCCl_3$, which provide the formation of blue-shifting hydrogen bonds in (**I**) and (**II**), as well as red-shifting hydrogen bonds in (**III**) and (**IV**) π complexes, respectively. Nevertheless, some studies have demonstrated that chloroform has the property of forming conventional hydrogen-bonded complexes [41] or those whose stretch frequency of C—H bond is set to red wave numbers [47]. Finally, the red-shift behavior of chloroform is not surprising because such a phenomenon has already been detected experimentally in solution [48, 49] or in gaseous phase [50].

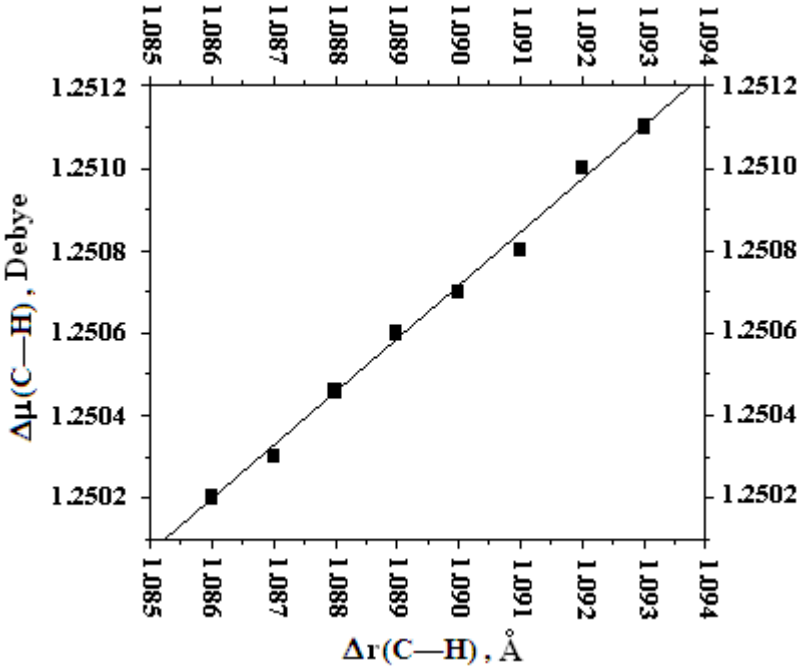

Figure 4. Variation of dipole moment ($\vec{\mu}$) and changes of C—H bond length of the $HCCl_3$ molecule using BPBE/6-311++G(d,p) calculations.

Conclusions

A theoretical study of the molecular properties and infrared spectrum of the $C_2H_2\cdots HCF_3$, $C_2H_4\cdots HCF_3$, $C_2H_2\cdots HCCl_3$ and $C_2H_4\cdots HCCl_3$ π complexes has been presented in this paper. According to PBE/6-311++G(d,p) calculations, structural evidence has been adduced to show that the blue-shifting hydrogen bonds and red-shifting hydrogen bonds

result from the shortening and lengthening of the C—H of fluoroform and chloroform, respectively. Using spectroscopy, the deformations in C—H bonds can be shown to lead to changes in their stretch frequencies, which are shifted to blue and red regions of the infrared spectrum when the respective $C_2H_2\cdots HCF_3$, $C_2H_4\cdots HCF_3$, $C_2H_2\cdots HCCl_3$ and $C_2H_4\cdots HCCl_3$ π complexes are formed. In terms of electronic parameters, the intermolecular energy corroborates the blue- and red-shift effects, with the quantification of higher and lower ΔQ^{ChelpG} charge transfers fully explaining these vibrational phenomena. Finally, analysis of the dipole moment leads to the conclusion that chloroform has a similar behavior to polar molecules; namely, an increase in C—H bond lengths as well as dipole moment. On the other hand, fluoroform causes contraction of the C—H bond lengths and hence, diminishes its dipole moment.

Acknowledgements

The authors gratefully acknowledge partial financial support from CAPES and CNPq Scientific Brazilian Funding agencies.

References and Notes

[1] Grabowski, S.J. in: *Hydrogen Bonding – New insights*, Berlin: Springer, 2006.

[2] Marechal, Y. *The Hydrogen Bond and the Water Molecule: The Physics and Chemistry of Water, Aqueous and Bio Media*, Paris, Elsevier, 2007.

[3] R. Desiraju, G.R.; Steiner, T. *The Weak Hydrogen Bond: In Structural Chemistry and Biology*, Oxford, Oxford University Press, 2001.

[4] Meot-Ner (Michael) M. *Chem. Rev.* **2005**, *105*, 213.

[5] Banks, H. D. *J. Org. Chem.* **2003**, *68*, 2639.

[6] Teberekidis, V. I.; Sigalas, M. P. *J. Mol. Struct. (THEOCHEM)* **2007**, *803*, 29.

[7] Koch, U.; Popelier, P. L. A. *J. Phys. Chem.* **1995**, *99*, 9747.

[8] Umeyama, H.; Morokuma, K. *J. Am. Chem. Soc.* **1977**, *99*, 1316.

[9] King, B. F.; Weinhold, F. *J. Chem. Phys.* **1995**, *103*, 333.

[10] Araújo, R. C. M. U.; da Silva, J. B. P.; Ramos, M. N. *Spectrochim. Acta A* **1995**, *51*, 821.

[11] Araújo, R. C. M. U.; Ramos, M. N. *J. Mol. Struct. (THEOCHEM)* **1996**, *366*, 233.

[12] Oliveira, B. G.; Araújo, R. C. M. U.; Carvalho, A. B.; Ramos, M. N. *J. Mol. Model.* **2009**, *15*, 123.

[13] Oliveira, B. G.; Araújo, R. C. M. U.; Chagas, F. F.; Carvalho, A. B.; Ramos, M. N. *J. Mol. Model.* **2008**, *14*, 949.

[14] Nesbitt, D. J. *Chem. Rev.* **1988**, *88*, 843.
[15] Araújo, R. C. M. U.; Ramos, M. N. *J. Braz. Chem. Soc.* **1998**, *9*, 499.
[16] Oliveira, B. G.; Araújo, R. C. M. U.; Pereira, F. S.; Lima, E. F.; Silva, W. L. V.; Carvalho, A. B.; Ramos, M. N. *Quim. Nova* **2008**, *31*, 1673.
[17] Hobza, P.; Špirko, V.; Havlas, Z.; Buckhold, K.; Reiman, B.; Barth, H.D.; Brutschy, B. *Chem. Phys. Lett.* **1999**, *299*, 180.
[18] Hobza, P.; Havlas, Z. *Chem. Rev.* **2000**, *100*, 4253.
[19] Oliveira, B. G.; Santos, E. C. S.; Duarte, E. M.; Araújo, R. C. M. U.; Ramos, M. N.; Carvalho, A. B. *Spectrochim. Acta A* **2004**, *60*, 1883.
[20] Oliveira, B. G.; Duarte, E. M.; Araújo, R. C. M. U.; Ramos, M. N.; Carvalho, A. B. *Spectrochim. Acta A* **2005**, *61*, 491.
[21] Oliveira, B. G.; Araújo, R. C. M. U.; Carvalho, A. B.; Ramos, M. N. *Spetrochim. Acta A* **2007**, *68*, 626.
[22] Hermida-Ramón, J. M.; Graña, A. M.; *J. Comp. Chem.* **2006**, *28*, 540.
[23] Domagała, M.; Grabowski, S. J. *J. Phys. Chem. A* **2005**, *109*, 5683.
[24] Oliveira, B. G. *J. Arg. Chem. Soc.* **2007**, *95*, 59.
[25] Hobza, P.; Špirko, V.; Selzle, H.L.; Schlag, E.W. *J. Phys. Chem.* **1998**, *102*, 2501.
[26] Hohenberg, P.; Kohn, W. *Phys. Rev. B* **1964**, *136*, 864.
[27] Oliveira, B. G.; Araújo, R. C. M. U.; Ramos, M. N. *Struc. Chem.* **2008**, *19*, 185.
[28] Oliveira, B. G.; Araújo, R. C. M. U.; Ramos, M. N. *Struc. Chem.* **2008**, *19*, 665.
[29] Oliveira, B.G.; Araújo, R.C.M.U. *Quim. Nova* **2007**, *30*, 791.
[30] Breneman, C. M.; Wiberg, K. B. *J. Comp. Chem.* **1990**, *11*, 361.
[31] Wiberg, K. B.; Rablen, P. R. *J. Comp. Chem.* **1993**, *14*, 1504.
[32] Oliveira, B. G.; Vasconcellos, M. L. A. A. *J. Mol. Struct. (THEOCHEM)* **2006**, *774*, 83.
[33] Oliveira, B. G.; Araújo, R. C. M. U.; Pereira, F. S.; Lima, E. F.; Silva, W. L. V.; Carvalho, A. B.; Ramos, M. N. *Quim. Nova* **2008**, *7*, 1673.
[34] Frisch, M. J.; *et al*, Gaussian, Inc., Pittsburgh PA, 2001 Gaussian 98W (Revision A.1), Gaussian, Inc., Pittsburgh PA, 1998.
[35] Rao, L.; Ke, H.; Fu, G.; Xu, X.; Yan, Y. *J. Chem. Theo. Comp.* **2009**, *5*, 86.
[36] Jacobsen, H.; *Chem. Phys.* **2008**, *345*, 95.
[37] van Duijneveldt, F. B.; Murrell, J. N. *J. Chem. Phys.* **1967**, *46*, 1759.
[38] McQuarrie, D. A. in: *Statistical Thermodynamics*, New York: Harper and Row, 1973.
[39] Boys, S. B.; Bernardi, F. *Mol. Phys.* **1970**, *19*, 553.
[40] Barnes, A. J.; *J. Mol. Struct.* **2004**, *704*, 3.
[41] Delanoye, S. N.; Herrebout, W. A.; van der Veken, B.J. *J. Am. Chem. Soc.* **2004**, *124*, 11854.
[42] Kryachko, E. S.; Zeegers-Huyskens, T. *J. Phys. Chem.* **2001**, *105*, 7118.

[43] Mulliken, R. S. *J. Chem. Phys.* **1995**, *23*, 1833.

[44] Hobza, P.; Havlas, Z. *Chem. Phys. Lett.* **1999**, *303*, 447.

[45] Solimannejad, M.; Amlashi, L. M.; Alkorta, I.; Elguero, J. *Chem. Phys. Lett.* **2006**, *422*, 226.

[46] Cubero, E.; Orozco, M.; Hobza, P.; Luque, F. J. *J. Phys. Chem. A* **1999**, *103*, 6394.

[47] Allerhand, A.; von Ragué Schleyer, P. *J. Am. Chem. Soc.* **1963**, *85*, 1715.

[48] Devaure, J.; Turrell, G.; van Houng, P.; Lacombe, J. *J. Phys. Chem.* **1968**, *65*, 1064.

[49] Oszczapowicz, J.; Jaroszewska-Manaj, J.; Golimowska, K. *J. Chem. Soc., Perkin Trans.* **2000**, *2*, 2343.

[50] Hussein, M.A.; Millen, D.J. *Chem. Soc., Faraday Trans.* **1976**, *272*, 693.

ISSN 1984-6428
ONLINE
www.orbital.ufms.br

Orbital 2009, *1* (2), 167-182

Full Paper

Uma comprovação químico-quântica sobre a formação de ligações de hidrogênio e interações secundárias em sistemas heterocíclicos intermoleculares

Boaz Galdino de Oliveira[a], Regiane de Cássia Maritan Ugulino de Araújo[a], Antônio Bezerra de Carvalho[a], Mozart Neves Ramos[b]*

[a]Departamento de Química – Universidade Federal da Paraíba. CEP 58036-300, João Pessoa – PB, Brasil.
[b]Departamento de Química Fundamental – Universidade Federal de Pernambuco. CEP 50739-901, Recife – PE, Brasil.

Recebido em 02/02/2009; revisado em 09/03/2009; aceito em 23/03/2009; publicado na internet em 27/04/2009

***RESUMO**: Realizamos um estudo teórico sobre a topologia da densidade de carga dos complexos $C_2H_4O\cdots C_2H_2$ e $C_2H_4S\cdots C_2H_2$. Através de cálculos da Teoria Quântica de Átomos em Moléculas (QTAIM – Quantum Theory of Atoms in Molecules), foi observada a formação de ligações de hidrogênio e interações secundárias nestes complexos. Tal análise foi executada mediante determinação das geometrias otimizadas destes complexos no nível de cálculo B3LYP/6-31G(d,p), pelo qual os operadores topológicos QTAIM foram computados, tais como a densidade eletrônica ρ(r), o Laplaciano $\nabla^2\rho(r)$, e a elipicidade ε. A caracterização das ligações de hidrogênio (O···H—C) e (S···H—C) foi feita baseada nos cálculos destes operadores, embora também tenha sido detectada a existência de uma interação secundária entre os átomos de hidrogênio axiais H_a e o carbono do acetileno. Nesta visão, esta interação secundária foi verificada apenas no complexo $C_2H_4S\cdots C_2H_2$ devido ao fato de sua estrutura ser propícia a formar múltiplas interações.*

***Palavras-chave**: QTAIM, ligação de hidrogênio, interação secundária*

* *Autor de correspondência: e-mail: boazgaldino@gmail.com*

Introdução

Muitos dos métodos cristalográficos e espectroscópicos são utilizados no estudo de sistemas formados através da formação de ligações de hidrogênio [1]. A aplicação destes procedimentos experimentais tem por objetivo caracterizar fenômenos físico-químicos decorrentes do contato entre um hidrogênio (H—X) e dois centros contendo alta densidade eletrônica (Y ou X = F, O, N, S, ligações π e pseudo-π) [2-5]. A técnica espectroscópica experimental de microondas com transformada de Fourier [6] é considerada uma das ferramentas mais eficientes na caracterização estrutural de sistemas intermoleculares, dentre os quais, alguns são formados e estabilizados através de ligações de hidrogênio do tipo (Y···H—X) [7-9]. Foi nesta visão que Legon e colaboradores elucidaram dentre muitas outras estruturas moleculares, a geometria do complexo de hidrogênio $C_2H_4O\cdots C_2H_2$ [10]. Neste sistema, além da determinação das distâncias e ângulos de ligação, foi observado um intrigante fenômeno estrutural: a não linearidade (θ) na ligação de hidrogênio (O···H—C) [11]. Considerando a possibilidade dos átomos de hidrogênio axiais H_α dos grupos CH_2 da oxirana (C_2H_4O) interagirem com a densidade eletrônica da ligação π, admiti-se que esta interação secundária ($H_\alpha\cdots\pi$) além de provocar a não linearidade na ligação de hidrogênio (O···H—C), também causa uma distorção no eixo internuclear H-C-C-H do acetileno.

Através das determinações experimentais FTMS [12-13], sabe-se que por meio destas são identificadas transições roto-vibracionais e seus respectivos acoplamentos, os quais são utilizados na determinação dos momentos de inércia moleculares [14]. Dessa maneira são calculadas as distâncias entre os átomos e conseqüentemente a geometria do sistema estudado pode ser estimada. Embora a técnica FTMS tenha sido usada para caracterizar a geometria de equilíbrio do complexo $C_2H_4O\cdots C_2H_2$, como também sua ligação de hidrogênio (O···H—C) e a não linearidade θ, devemos ressaltar que nenhuma análise de natureza experimental foi realizada com o propósito de caracterizar a interação secundária ($H_\alpha\cdots\pi$). Todavia, recentemente divulgamos por meio desta revista um estudo que mostra como a interação secundária ($H_\alpha\cdots\pi$) pode ser formada nos complexos $C_2H_4O\cdots C_2H_2$ e $C_2H_4S\cdots C_2H_2$ [15]. Nesse estudo, os dados FTMS disponíveis foram satisfatoriamente reproduzidos, mas, além disso, foram apresentados novos resultados que abordam a distorção sofrida pelo acetileno decorrente da formação do complexo heterocíclico. Foi debatido que de fato a formação da interação secundária ($H_\alpha\cdots\pi$) seria a causa pela perda de linearidade θ, tanto na ligação de hidrogênio (O···H—C) como também na própria molécula de acetileno. Entretanto, nessa análise foram utilizados critérios um tanto subjetivos, como por exemplo, as distâncias entre os átomos H_α e a ligação π do acetileno, e obviamente, a medida do ângulo de distorção θ. Nesse sentido, admitimos a necessidade de mais uma vez investigar e caracterizar tanto a

ligação de hidrogênio (O···H—C) como a interação secundária (H_{α}···π), mas aplicando teorias químico-quânticas mais específicas do que os tradicionais procedimentos *ab initio* e/ou teoria do funcional de densidade.

Teoria QTAIM: Subsistemas moleculares modelados como "átomos em moléculas"

Pela mecânica quântica, é bem estabelecido que a metodologia QTAIM (do inglês *Quantum Theory* of *Atoms in Molecules*) [16-17] desenvolvida por Richard Bader tem se mostrado como uma ferramenta clara e eficiente não apenas para identificar e caracterizar interações de natureza intra e/ou intermolecular, mas também no estudo atômico elementar de como os átomos se comportam quando ocorre a formação de ligações covalentes ou insaturadas [18-19]. Revivendo alguns conceitos, sabe-se que toda e qualquer informação relevante a um sistema é contida em uma função de estado observável ψ, pela qual o valor de uma propriedade física é obtido por intermédio da ação de um operador matemático, como, por exemplo, o Hermitiano linear ou o Hamiltoniano total. Segundo os conceitos mecânico-quânticos da metodologia QTAIM, as propriedades observáveis de um sistema químico estão contidas em sua densidade eletrônica molecular, $\rho_{(\mathbf{r})}$. Mesmo sendo uma das primeiras observáveis usadas na ciência, como por exemplo, na implementação da Teoria do Funcional de Densidade (DFT, do inglês *Density Functional Theory*) [20] por Hohenberg, Kohn e Sham [21-22], a densidade eletrônica é também considerada um parâmetro físico-químico bastante polêmico devido à inexistência de uma expressão analítica clara que a descreva e que possa ser usada na interpretação da concentração de carga. Trabalhando nesse sentido, alguns cientistas têm apresentado algumas propostas, como por exemplo, a baseada nos conceitos de Hirshfeld [23], conforme a equação (1).

$$\rho(\mathbf{r}) = \int \rho A(\mathbf{r}) \ln\left(\frac{\rho A(\mathbf{r})}{\rho A^{0}(\mathbf{r})}\right) + \int \rho B(\mathbf{r}) \ln\left(\frac{\rho B(\mathbf{r})}{\rho B^{0}(\mathbf{r})}\right) \qquad (1)$$

Considerando o contato entre os átomos A e B, a equação de Hirshfeld (1) mostra que a densidade eletrônica na ligação química ρ(r) pode ser estimada através da relação entre as densidades eletrônicas de A e B quando isolados ($\rho(r)A^{o}$ e $\rho(r)B^{o}$), e após a formação da molécula A—B (ρ(r)A e ρ(r)B). Em se tratando de conceitos da QTAIM [24], a densidade eletrônica é usada como observável mecânico-quântica para execução de integrações numéricas onde o vetor gradiente $\nabla\rho_{(\mathbf{r})}$ é a condição básica para se determinar a topologia molecular [25]. Considerando os átomos como sistemas de camada aberta (Ω) e restringindo condições de contorno na superfície molecular $S_{(\Omega,\mathbf{r})}$, Bader utilizou destes argumentos para mostrar que o fluxo de densidade de carga $\rho_{(\mathbf{r})}$ é nulo em qualquer ponto desta superfície [26]. Como conseqüências, o gradiente $\nabla\rho_{(\mathbf{r})}$ é

perpendicular a um vetor unitário (**n**) em cada ponto (r) da densidade eletrônica definida em $S_{(\Omega,\mathbf{r})}$, conforme mostrado pela equação (2):

$$\nabla\rho_{(\mathbf{r})}.\mathbf{n}_{(\mathbf{r})} = 0 \qquad (2)$$

Em uma seqüência de vetores gradientes da densidade eletrônica, têm-se, portanto, todas as suas trajetórias e por serem grandezas vetoriais, possuem direção e sentido, as quais podem ser ascendentes ou em declive [27]. Na prática, as trajetórias de $\nabla\rho_{(\mathbf{r})}$ são bem definidas por um ponto específico no espaço, denominado de atrator. Como o gradiente da densidade eletrônica é função de seus atratores, estes são propriamente os núcleos do sistema molecular. Considerando todos os atratores nucleares, o conjunto de trajetórias do gradiente forma uma base atômica ou o próprio sistema de camada aberta Ω. Em termos da teoria QTAIM, o termo Ω recebe uma definição químico-quântica traduzida simplesmente como "átomo" [28].

Não apenas no ambiente atômico, mas a abordagem QTAIM vai além e trata também alguns conceitos de ligação química. Conforme as trajetórias do gradiente da densidade eletrônica se moldam para descrever um sistema químico, estas trajetórias não se originam do infinito, mas de um ponto localizado entre dois atratores, os chamados Pontos Críticos de Ligação (BCP, do inglês *Bond Critical Point*) [29]. Quando duas trajetórias de $\nabla\rho_{(\Omega,\mathbf{r})}$ direcionadas aos núcleos são formadas a partir de um único BCP, estas são chamadas de Linhas Interatômicas (LI) ou Trajetórias de Ligação (BP, do inglês *Bond Path*) [30]. Em outras palavras, quando algum BP interliga dois atratores, admitimos que estes dois núcleos estão ligados formando uma ligação química. Resumidamente, QTAIM proporciona uma simples e eficiente descrição mecânico-quântica de como um átomo se localiza e se comporta em uma ligação química [31]. Conforme objetivo apontado neste trabalho, admitimos que os fundamentos e parâmetros QTAIM possam ser utilizados para caracterizar as ligações de hidrogênio (O···H—C) e (S···H—C), como também as interações secundárias (H_α···π) nos complexos $C_2H_4O\cdots C_2H_2$ e $C_2H_4S\cdots C_2H_2$.

Estratégia computacional

As geometrias otimizadas dos complexos $C_2H_4O\cdots C_2H_2$ e $C_2H_4S\cdots C_2H_2$ foram obtidas através de cálculos executados no programa GAUSSIAN 98W [32]. Para este estudo, foi utilizado o nível de teoria B3LYP/6-31G(d,p), tanto para determinar as geometrias de equilíbrio dos complexos, como para se efetuar os cálculos QTAIM, que foram realizados pelos programas GAUSSIAN 98W e AIM 2000 1.0 [33]. Para este último, foi necessário gerar a fonte WFN (*wave-function*) para que as integrações QTAIM fossem processadas.

Resultados e Discussão

Considerações teóricas

Conforme visto, os conceitos de átomo e ligação química se mostram viáveis de serem compreendidos pela teoria QTAIM [34-36]. Entretanto, as ligações químicas se relacionam com integrações topológicas da densidade eletrônica através da mecânica quântica conforme $\rho_{(\Omega,\mathbf{r})} = \psi\psi^*$ [37]. Como sabemos, para se obter a probabilidade eletrônica $\psi\psi^*$, tal sistema químico deve ter sua geometria modelada em um mínimo global de energia na superfície de energia potencial. Entretanto, alguns autores têm mostrado que a teoria QTAIM não se mostra eficiente para o cálculo de estruturas eletrônicas em condições fora do mínimo global de energia [38]. Por outro lado, outros trabalhos apresentam situações em que regiões de mínimos locais também podem gerar configurações e/ou conformações estruturais propícias para realização dos cálculos QTAIM [39]. Todavia, para os complexos $C_2H_4O\cdots C_2H_2$ (**I**) e $C_2H_4S\cdots C_2H_2$ (**II**) estudados neste trabalho, suas geometrias otimizadas ilustradas na Figura 1 foram obtidas em um mínimo global da superfície de energia potencial, em que os valores dos principais parâmetros estruturais para estes dois sistemas intermoleculares e de seus respectivos monômeros estão listados na Tabela 1.

Tabela 1. Parâmetros estruturais dos monômeros C_2H_2, C_2H_4O e C_2H_4S, e dos complexos $C_2H_4O\cdots C_2H_2$ e $C_2H_4S\cdots C_2H_2$. Todos os resultados foram obtidos a partir do cálculo B3LYP/6-31G(d,p).

Parâmetros	Sistemas moleculares e intermoleculares				
	C_2H_2	C_2H_4O	C_2H_4S	$C_2H_4O\cdots C_2H_2$	$C_2H_4S\cdots C_2H_2$
H–C*	1,066 (1,060)[a]	—	—	1,074	1,071
C≡C*	1,205	—	—	1,207	1,206
rC–C*	1,205	1,469 (1,464)[b]	1,482 (1,492)[c]	1,467	1,840
rC–Y*	—	1,430 (1,431)[b]	1,838 (1,81)[c]	1,436	1,480
rC–H^2*	—	1,089 (1,085)[b]	1,086 1,078)[c]	1,090	1,086
rC–H^1*	—	1,089 (1,085)[b]	1,086 (1,07)[c]	1,088	1,085
$R_{(H\cdots n)}$*	—	—	—	2,130 (2,40)[d]	2,801
$R_{(H^2\cdots C^3)}$*	—	—	—	3,108	2,948
$R_{(H^2\cdots C^4)}$*	—	—	—	3,931	3,535
θ**	—	—	—	25,08 (30)[d]	42,35
φ**	—	—	—	0,89	1,82
ϖ**	—	—	—	0,35	0,98

* Valores de r e R em angstroms;
** Valores de θ, φ e ϖ em graus. Y representa os átomos de oxigênio e enxofre nos complexos $C_2H_4O\cdots C_2H_2$ e $C_2H_4S\cdots C_2H_2$, respectivamente;

[a] = Ref. 40; [b] = Ref. 41; [c] = Ref. 42; [d] = Ref. 15; [e] = Ref. 43

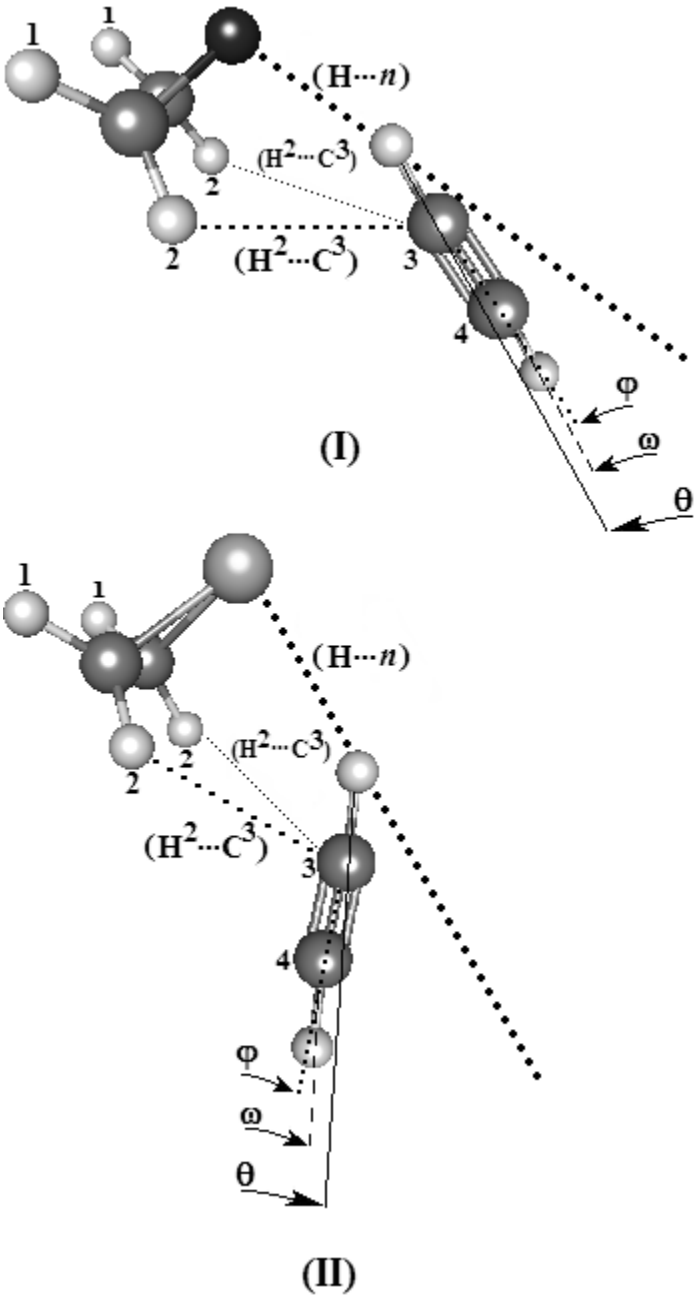

Figura 1. Geometrias otimizadas dos complexos $C_2H_4O\cdots C_2H_2$ (**I**) e $C_2H_4S\cdots C_2H_2$ (**II**) obtidas a partir da realização de cálculos B3LYP/6-31G(d,p).

Parâmetros da geometria otimizada

De acordo com resultados documentados em recentes trabalhos, as geometrias teóricas destes complexos foram discutidas em detalhes e, de acordo com a disponibilidade de dados experimentais, também foi feita uma comparação com dados das análises de microondas [40-43]. Podemos mais uma vez ressaltar que os resultados obtidos do cálculo B3LYP/6-31G(d,p) reproduziram com satisfatório sucesso os dados experimentais de distância das ligações H–C, C≡C, CC, C–H, e CY, ligação de hidrogênio $R_{(H\cdots n)}$; e desvio na linearidade da ligação de hidrogênio; θ. Sobre a molécula de acetileno, de fato este último será um dos principais focos neste estudo, principalmente na

caracterização por meio dos parâmetros QTAIM sobre a existência ou não da interação secundária. Previamente, podemos assumir que, de acordo com estudos semelhantes envolvendo complexos formados por interações π [7, 44], para os sistemas $C_2H_4O\cdots C_2H_2$ e $C_2H_4S\cdots C_2H_2$, a interação secundária entre os átomos de hidrogênio H^1 e a nuvem eletrônica π da ligação C≡C pode estruturalmente ser analisada pela distância entre H^1 e os carbonos C^3 e C^4 do acetileno.

A partir da análise dos resultados teóricos apresentados na Tabela 1, os valores das distâncias para as interações $R_{(H^2\cdots C^3)}$ e $R_{(H^2\cdots C^4)}$ são 3,108 Å e 2,948 Å, e 3,931 e 3,535 Å para os complexos $C_2H_4O\cdots C_2H_2$ e $C_2H_4S\cdots C_2H_2$, respectivamente. Se considerarmos os raios de van der Waals de 1,2 Å e 1,7 Å para os átomos de hidrogênio e carbono, temos que a soma de 2,9 Å para estes raios pode ser utilizada com critério estrutural para analisarmos as distâncias $R_{(H^2\cdots C^3)}$ e $R_{(H^2\cdots C^4)}$. É claramente perceptível que, o valor de 3,108 Å é 0,208 Å maior do que o valor padrão de 2,9 Å. Isso indica que, de acordo com a soma dos raios de van der Waals, não há contato entre as nuvens eletrônicas dos átomos de hidrogênio e carbono no complexo $C_2H_4O\cdots C_2H_2$. Conseqüentemente, a interação secundária entre oxirana e acetileno não existe. Por outro lado, temos que, no complexo $C_2H_4S\cdots C_2H_2$ as interações secundárias podem ser factíveis, pois a distância de 2,948 Å para $R_{(H^2\cdots C^3)}$ é muito próximo ao valor de 2,9 Å. Portanto, estamos em uma situação em que critérios geométricos padrões, tais como os raios de van der Waals, não são confiáveis para caracterizar a formação destas interações secundárias. Assim, se faz necessária à aplicação da teoria QTAIM, na qual por meio dos seus operadores moleculares de superfície, toda a estrutura eletrônica dos complexos $C_2H_4O\cdots C_2H_2$ e $C_2H_4S\cdots C_2H_2$ pode ser interpretada através da mecânica-quântica.

Contribuição da análise QTAIM

Pela definição da teoria QTAIM, a densidade eletrônica é obtida através de uma integração numérica, onde os três valores Hessianos (λ_1, λ_2 e λ_3) de $\rho_{(\mathbf{r})}$ possuem dois valores negativos (λ_1 e λ_2) e um positivo (λ_3).

$$\nabla^2\rho_{(r)} = \frac{\partial^2\rho_{(r)}}{\partial_x^2} + \frac{\partial^2\rho_{(r)}}{\partial_y^2} + \frac{\partial^2\rho_{(r)}}{\partial_z^2} = \lambda_1 + \lambda_2 + \lambda_3 \qquad (3)$$

Esta diagonalização da matrix Hessiana tem como justificativa o campo Laplaciano $\nabla^2\rho_{(\mathbf{r})}$ no ponto (r) e a elipicidade (ε), a qual é definida como $\varepsilon = \lambda_1/\lambda_2 - 1$, que é um valor positivo sempre que $\lambda_1 < \lambda_2 < 0$ e $\lambda_3 > 0$. A elipicidade é um parâmetro usado para descrever o caráter da ligação química, seja sigma ou insaturada. Analisando a Figura 2, temos que λ_1 e λ_2 estão orientados vetorialmente em um plano perpendicular ao eixo internuclear dos átomos A e B.

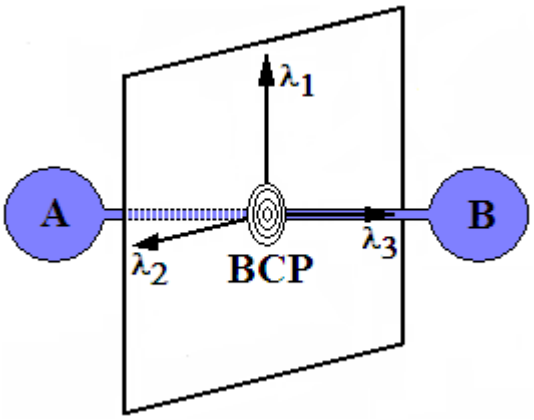

Figura 2. Ilustração esquemática do Ponto Crítico de Ligação (BCP) entre dois átomos A e B e a orientação tridimensional (x, y, z) das elipicidades λ_1, λ_2 e λ_3.

Considerando que o valor de λ_1 é muito alto, temos, portanto um caráter de ligação π, enquanto que $\lambda_1 = \lambda_2$ indica um formato cilíndrico no que se traduz em uma ligação sigma. Pela teoria QTAIM, este é um dos critérios usados para se determinar estabilidade molecular e ruptura de ligações químicas [45]. Todavia, os campos Laplacianos, ou as segundas derivadas da densidade eletrônica tridimensional trazem informações vitais para a compreensão do sistema químico. Em termos práticos, o Laplaciano $\nabla^2\rho_{(\mathbf{r})}$ tem a propriedade de descrever a concentração de densidade eletrônica em uma determinada zona de ligação. Por exemplo, se $\nabla^2\rho_{(\mathbf{r})} < 0$ temos que a densidade eletrônica se acumula nos BCP das ligações químicas, enquanto se $\nabla^2\rho_{(\mathbf{r})} > 0$ podemos afirmar que os núcleos atômicos suportam toda a concentração de carga. Conforme a equação (4), essa interpretação do Laplaciano é baseada em um teorema *virial* da densidade eletrônica total, o qual diz que, as energias cinéticas (K) e potenciais (U) se relacionam respectivamente com depressões e concentrações de densidade eletrônica [46], ou seja, $\nabla^2\rho_{(\mathbf{r})} > 0$ e $\nabla^2\rho_{(\mathbf{r})} < 0$ caracterizam interações intra ou intermoleculares (ligações de hidrogênio) e ligações σ ou π (hidrocarbonetos ou sistemas biológicos hiperconjugados, como DNA) [47].

$$\frac{1}{4}\ \nabla^2\rho_{(\mathbf{r})} = 2K + U \qquad (4)$$

A partir da densidade eletrônica $\rho_{(\mathbf{r})}$, do seu Laplaciano $\nabla^2\rho_{(\mathbf{r})}$, e por fim da elipicidade ε, muitos estudos tem sido desenvolvidos com o propósito de avaliar fenômenos de excelência básica na química, como por exemplo, a teoria ácido/base de Lewis [48]. Com relação aos monômeros C_2H_4O, C_2H_2 e C_2H_4S, e aos complexos heterocíclicos $C_2H_4O\cdots C_2H_2$ e $C_2H_4S\cdots C_2H_2$ estudados neste trabalho, os valores das densidades eletrônicas, Laplacianos e elipicidades das principais ligações químicas desses sistemas são apresentados nas Tabelas 2 e 3, respectivamente.

Tabela 2. Valores de densidade eletrônica $\rho_{(r)}$, Laplaciano $\nabla^2\rho_{(r)}$, e elipicidade ε das principais ligações químicas dos monômeros C_2H_2, C_2H_4O e C_2H_4S.

Monômeros	BCP	Parâmetros topológicos QTAIM		
		$\rho_{(r)}$	$\nabla^2\rho_{(r)}$	$\varepsilon = \lambda_1/\lambda_2 - 1$
C_2H_2	H–C	0,290	-1,140	0,000
	C≡C	0,401	-1,116	0,000
C_2H_4O	C–Y	0,250	-0,372	0,595
	$C–H^2$	0,255	-0,976	0,033
	$C–H^1$	0,255	-0,976	0,033
C_2H_4S	C–Y	0,158	-0,148	0,390
	$C–H^2$	0,285	-1,034	0,020
	$C–H^1$	0,285	-1,034	0,020

* Todos os valores apresentados são interpretados em unidades eletrônicas (u.e.).

Tabela 3. Valores de densidade eletrônica $\rho_{(r)}$, Laplaciano $\nabla^2\rho_{(r)}$, e elipicidade ε das principais ligações químicas dos complexos $C_2H_4O\cdots C_2H_2$ e $C_2H_4S\cdots C_2H_2$.

Complexos	BCP	Parâmetros topológicos QTAIM		
		$\rho_{(r)}$	$\nabla^2\rho_{(r)}$	$\varepsilon = \lambda_1/\lambda_2 - 1$
$C_2H_4O\cdots C_2H_2$	H–C	0,287	-1,159	0,000
	C≡C	0,402	-1,168	0,002
	C–C	0,259	-0,565	0,241
	C–Y	0,248	-0,380	0,670
	$C–H^2$	0,288	-1,056	0,036
	$C–H^1$	0,287	-1,052	0,0367
	(H···*n*)	0,019	0,052	0,015
	$(H^2\cdots C^3)$	—	—	—
	$(H^2\cdots C^4)$	—	—	—
$C_2H_4S\cdots C_2H_2$	H–C	0,288	-1,152	0,000
	C≡C	0,402	-1,165	0,003
	C–C	0,264	-0,608	0,168
	C–Y	0,157	-0,143	0,416
	$C–H^2$	0,287	-1,044	0,019
	$C–H^1$	0,286	-1,037	0,018
	(H···*n*)	0,009	0,027	0,028
	$(H^2\cdots C^3)$	0,004	0,015	0,832
	$(H^2\cdots C^4)$	—	—	—

* Todos os valores apresentados são interpretados em unidades eletrônicas (u.e.).

Como estamos estudando complexos de hidrogênio formados por interações intermoleculares, os cálculos QTAIM mostram que, de acordo com os valores das

densidades eletrônicas de 0,019 u.e. e 0,009 u.e. e os Laplacianos de 0,052 u.e. e 0,027 u.e. para as ligações de hidrogênio (H···*n*), os complexos $C_2H_4O\cdots C_2H_2$ (**I**) e $C_2H_4S\cdots C_2H_2$ (**II**) são considerados sistemas intermolecularmente ligados. Não apenas pela análise quântica de $\rho_{(r)}$ e $\nabla^2\rho_{(r)}$, mas podemos observar a formação da ligação de hidrogênio (H···*n*) de acordo com a visualização dos BCP apresentados na Figura 3. Conforme reportado em recentes trabalhos [11, 15], a formação de interações secundárias tem sido observada em sistemas heterocíclicos intermoleculares, mas para os complexos $C_2H_4O\cdots C_2H_2$ (**I**) e $C_2H_4S\cdots C_2H_2$ (**II**) os cálculos QTAIM revelam a existência da interação secundária em (**II**), cujos valores $\rho_{(r)}$ e $\nabla^2\rho_{(r)}$ são 0,004 u.e. e 0,015 u.e. Até então esta interação secundária era interpretada, seja teoricamente [15] ou experimentalmente [10], como sendo formada entre os átomos de hidrogênio H_α do grupos CH_2 e a densidade eletrônica da ligação π do acetileno.

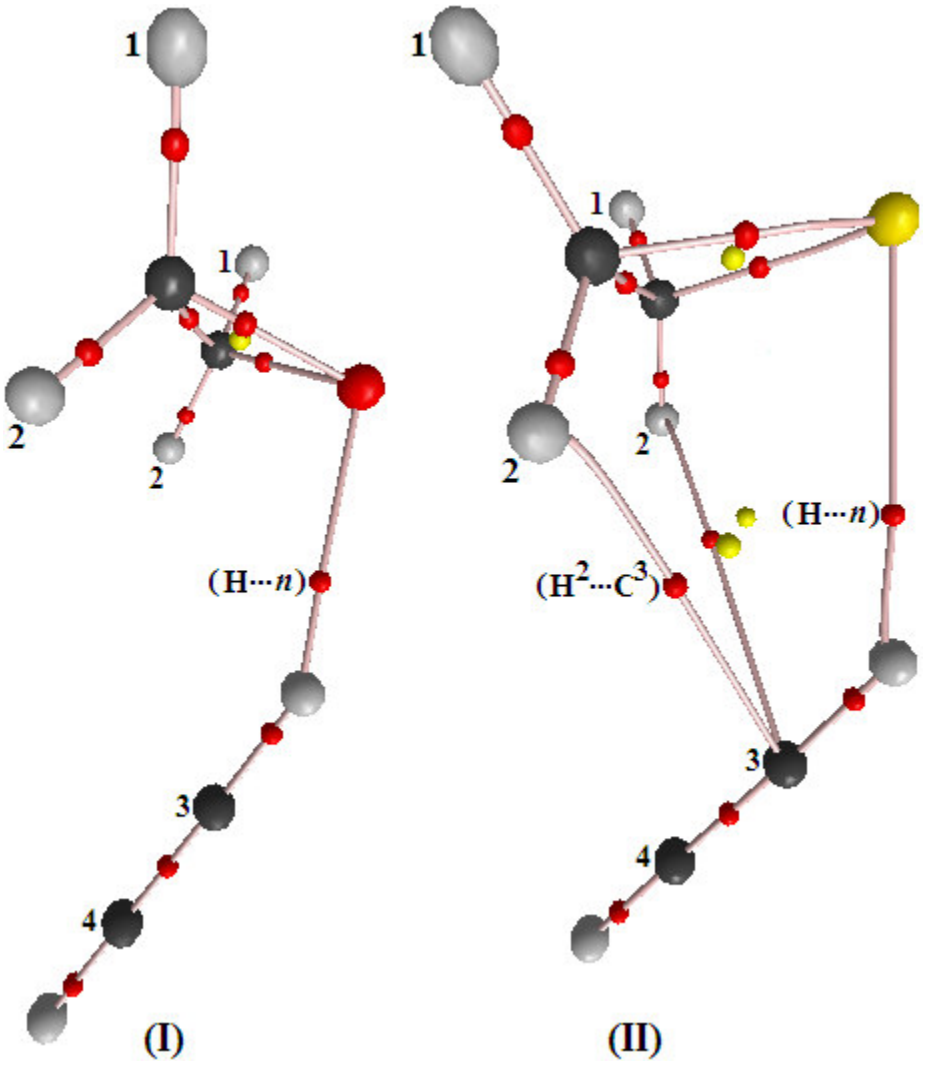

Figura 3. Pontos Críticos de Ligação (BCP) dos complexos $C_2H_4O\cdots C_2H_2$ (**I**) e

$C_2H_4S\cdots C_2H_2$ (**I**) obtidos através de integrações numéricas da densidade eletrônica QTAIM.

Todavia, estes novos resultados, debatidos neste trabalho, mostram uma interação direta entre H_α e o carbono C^3 do acetileno. Dessa maneira, o complexo (**II**) apresenta dois tipos de interações intermoleculares, ($H\cdots n$) e ($H^2\cdots C^3$), enquanto (**I**) apenas uma, ($H\cdots n$). Isso não significa dizer que o complexo (**II**) é mais fortemente ligado e mais estável que (**I**), mesmo porque as densidades eletrônicas intermoleculares de (**II**) são muito menores e as energias das ligações de hidrogênio (corrigida com BSSE e ZPE) desses sistemas são 6,42 kJ mol^{-1} e 4,15 kJ mol^{-1}, respectivamente [15]. Estruturalmente, mostramos que a formação da interação secundária no complexo (**II**) era mais propícia do que em (**I**), isso porque as distâncias entre H_α e C^3 eram compatíveis com a soma dos raios de van der Waals destes átomos. Além disso, deve-se também ressaltar que a estereoquímica da tiirana favorece a formação da interação secundária, como por exemplo, o ângulo de 180º entre os pares de elétrons desemparelhados do enxofre [49]. De acordo com a Figura 4, na qual está representada os mapas das linhas de contorno da densidade eletrônica dos complexos $C_2H_4O\cdots C_2H_2$ (**a**) e $C_2H_4S\cdots C_2H_2$ (**b**), respectivamente, estas linhas se originam no infinito e findam em um ponto crítico molecular, que em termos de teoria QTAIM, estes podem ser os núcleos (NA, do inglês *Nuclear Attractors*), anéis (RCP, do inglês *Ring Critical Point*), compartimento (CCP, do inglês *Cage Critical Point*) e as ligações, ou os já apresentados BCP [50].

No caso dos complexos $C_2H_4O\cdots C_2H_2$ e $C_2H_4S\cdots C_2H_2$, temos nas Figuras 4 e 5 as linhas que representam o gradiente da densidade eletrônica (veja equação 2), em que os critérios de elipicidade podem ser muito bem entendidos. Em termos da molécula de acetileno, a valor de 0,401 u.e. indica uma alta concentração de densidade eletrônica em sua ligação π C≡C. Entretanto, é bem conhecido que o caráter simétrico do acetileno provoca um valor praticamente nulo de elipicidade em C≡C (ε = 6,6 10^{-15}), sendo este um dos casos excepcionais em que $\rho_{(\mathbf{r})}$ e ε se mostram totalmente descorrelacionados [51-52]. Entretanto, de acordo com os resultados de elipicidade calculados para os complexos $C_2H_4O\cdots C_2H_2$ e $C_2H_4S\cdots C_2H_2$, temos que admitir a existência de um aumento nos valores de elipicidade na ligação π C≡C de 0,002 u.e. e 0,003 u.e., respectivamente. Nesse sentido, podemos considerar que a mudança na linearidade do eixo internuclear H-C-C-H do acetileno seja responsável por esse aumento de ε, conforme é conhecido que a elipicidade varia como concentração de carga na ligação C–C de 0,00, 0,23 e 0,45 para etano, benzeno e eteno, respectivamente [16]. Corroborando com este argumento, podemos perceber que a densidade eletrônica na ligação C≡C sofre uma pequena variação, de 0,401 u.e. no monômero C_2H_2 para 0,402 u.e. nos complexos $C_2H_4O\cdots C_2H_2$ e $C_2H_4S\cdots C_2H_2$, respectivamente.

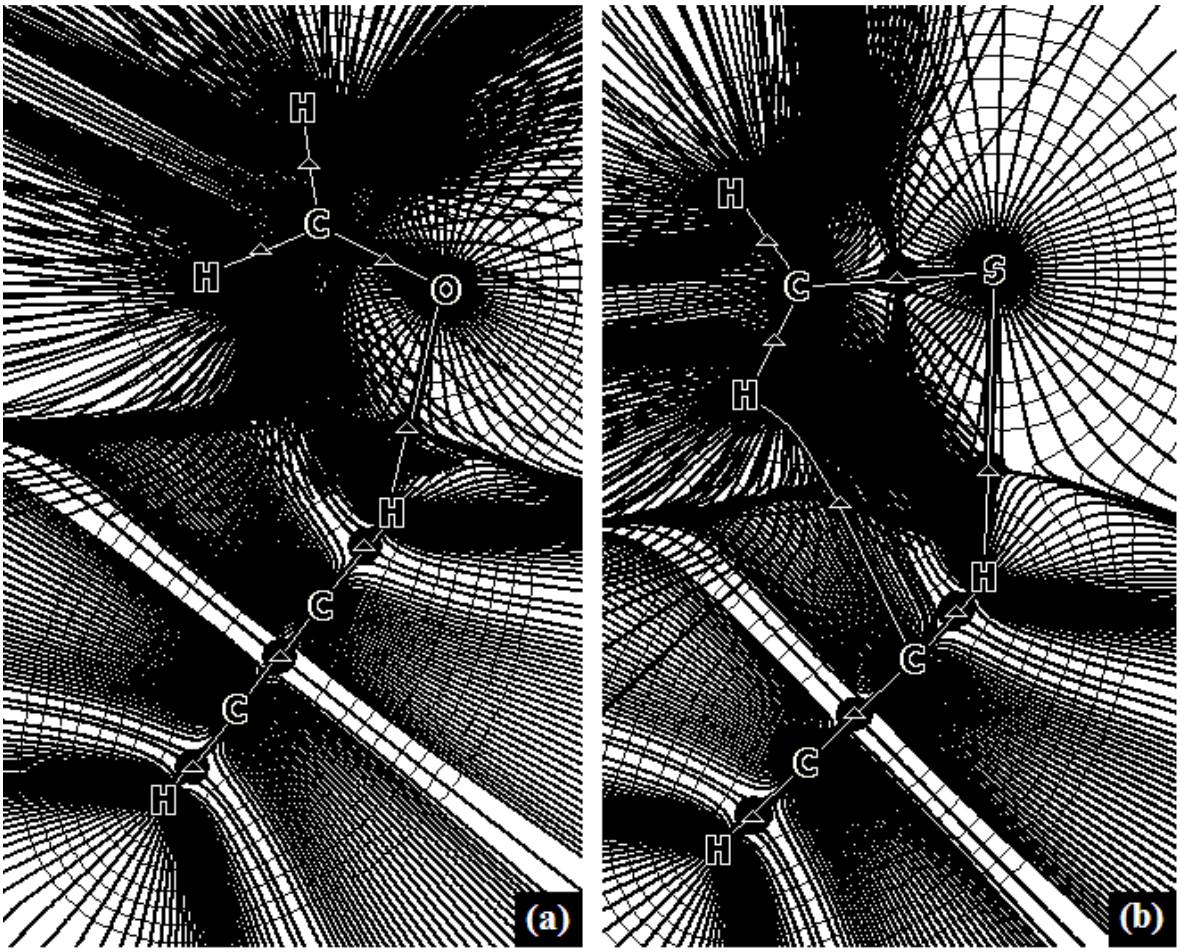

Figura 4. Mapas da superfície de densidade eletrônica indicando os caminhos de interação internuclear e os pontos críticos de ligação (BCP) nos complexos de hidrogênio $C_2H_4O\cdots C_2H_2$ (**a**) e $C_2H_4S\cdots C_2H_2$ (**b**).

Conclusões e Perspectivas

Neste trabalho teórico foi apresentado um estudo sobre a comprovação da existência de ligações de hidrogênio e interações secundárias nos complexos $C_2H_4O\cdots C_2H_2$ e $C_2H_4S\cdots C_2H_2$. Nesses sistemas, foi admitido que critérios estruturais como os valores tabelados das distâncias dos raios de van der Waals e os resultados calculados a partir do nível de teoria B3LYP/6-31G(d,p) estavam sendo utilizados para caracterizar a ligação de hidrogênio (H···*n*) e as interações secundárias ($H_\alpha\cdots\pi$). Entretanto, a partir da aplicação da teoria quântica de átomos em moléculas (QTAIM), tornaram-se possível a caracterização das ligações de hidrogênio (H···*n*), como também as interações secundárias ($H_\alpha\cdots\pi$). Inicialmente, o cálculo da densidade eletrônica $\rho_{(\mathbf{r})}$ e do seu Laplaciano $\nabla^2\rho_{(\mathbf{r})}$ mostra que a ligação de hidrogênio (H···*n*) é a interação preferencial na formação dos complexos $C_2H_4O\cdots C_2H_2$ e $C_2H_4S\cdots C_2H_2$. Entretanto, os cálculos QTAIM

revelaram que apenas o complexo $C_2H_4S\cdots C_2H_2$ possui interações secundárias ($H_\alpha\cdots\pi$). Este resultado concorda inteiramente com a análise estrutural, pois apenas o complexo $C_2H_4S\cdots C_2H_2$ possui uma conformação propícia para a formação da interação secundária, como por exemplo, a orientação dos pares de elétrons do enxofre que formam um ângulo de 180º [15]. Nossos resultados teóricos podem ser utilizados como um guia para os pesquisadores experimentais que utilizam a espectroscopia de Microondas e que investigam sistemas moleculares similares aos complexos $C_2H_4O\cdots C_2H_2$ e $C_2H_4S\cdots C_2H_2$. Em outras palavras, a identificação de interações secundárias tipo ($H_\alpha\cdots\pi$) é um fenômeno aceitável e pode ser utilizado para justificar a estabilidade desses complexos.

Outro importante aspecto teórico está na mudança da estrutura eletrônica do acetileno quando da formação dos complexos $C_2H_4O\cdots C_2H_2$ e $C_2H_4S\cdots C_2H_2$, em que a interação secundária ($H_\alpha\cdots\pi$) provoca uma distorção no eixo internuclear de C_2H_2, fato este que, através dos valores de elipicidade, observa-se um acumulo de concentração de densidade eletrônica na ligação C≡C. Este aumento de densidade eletrônica pode ser decorrente de uma transferência de carga dos pares de elétrons do oxigênio ou enxofre. Entretanto, devido à interação secundária no complexo $C_2H_4S\cdots C_2H_2$, devemos assumir a existência de uma outra transferência de carga, só que desta vez proveniente da ligação π C≡C do acetileno para os átomos de hidrogênio axiais H_α da tiirana [7]. Neste contexto, admitimos que esse fenômeno de transferência de carga mereça ser examinado, objetivo que será desempenhado em uma etapa posterior.

Agradecimentos

Os autores agradecem ao apoio das agências de fomento CAPES, CNPq e FACEPE.

ABSTRACT

A quantum-chemical validation about the formation of hydrogen bonds and secondary interactions in intermolecular heterocyclic systems

We have performed a detailed theoretical study in order to understand the charge density topology of the $C_2H_4O\cdots C_2H_2$ and $C_2H_4S\cdots C_2H_2$ heterocyclic hydrogen-bonded

complexes. Through the calculations derived from Quantum Theory of Atoms in Molecules (QTAIM), it was observed the formation of hydrogen bonds and secondary interactions. Such analysis was performed through the determination of optimized geometries at B3LYP/6-31G(d,p) level of theory, by which is that QTAIM topological operators were computed, such as the electronic density ρ(r), Laplacian $\nabla^2\rho(r)$, and ellipticity ε. The examination of the hydrogen bonds has been performed through the measurement of ρ(r), $\nabla^2\rho(r)$ and ε between (O···H—C and (S···H—C), whereas the secondary interaction between axial hydrogen atoms Hα and carbon of acetylene. In this insight, it was verified the existence of secondary interaction only in $C_2H_4S\cdots C_2H_2$ complex because its structure is propitious to form multiple interactions.

Key words: QTAIM, hydrogen bond, secondary interaction

Referências Bibliográficas

[1] Fuhrmann, C. N.; Daugherty, M. D.; Agard, D. A. *J. Am. Chem. Soc.* **2006**, *128*, 9086.

[2] Lewiński, J.; Zachara, J.; Justyniak, I.; Dranka, M. *Coord. Chem. Rev.* **2005**, *249*, 1184.

[3] Oliveira, B. G.; Araújo, R. C. M. U.; Chagas, F. F.; Carvalho, A. B.; Ramos, M. N.; *J. Mol. Model.* **2008**, *14*, 949.

[4] Grabowski, S. J.; Sokalski, W. A.; Leszczynski, J. *J. Phys. Chem. A* **2004**, *108*, 1806.

[5] Wojtulewski, S.; Grabowski, S. J. *Chem. Phys. Lett.* **2003**, *378*, 388.

[6] Armstrong, G. *Nature Chem.* doi: **10.1038/nchem.17**.

[7] Oliveira, B. G.; Araújo, R. C. M. U. *Quim. Nova* **2007**, *30*, 791.

[8] Oliveira, B. G.; Araújo, R. C. M. U.; Pereira, F. S.; Lima, E. F.; Silva, W. L. V.; Carvalho, A. B.; Ramos, M. N. *Quim. Nova* **2008**, 31, 1673.

[9] Oliveira, B. G.; Vasconcellos, M. L. A. A. *J. Mol. Struct. (THEOCHEM)* **2007**, *774*, 83.

[10] Legon, A. C. *Chem. Phys. Lett.* **1995**, *247*, 24.

[11] Oliveira, B. G.; Araújo, R. C. M. U.; Carvalho, A. B.; Ramos, M. N. *J. Theor. Comp. Chem.* **2007**, *6*, 647.

[12] Peebles, S. A.; Kuczkowski, R. L. *J. Phys. Chem. A* **1999**, *103*, 3884.

[13] Liu, Y.; Jäger, W. *J. Mol. Spectrosc.* **2001**, *205*, 177.

[14] Levine, I. N. *Molecular Spectroscopy*, John Wiley and Sons, New York, 1975.

[15] Oliveira, B. G.; Araújo, R. C. M. U.; Carvalho, A. B.; Ramos, M. N. *Quim. Nova* **2007**, *30*, 1167.

[16] Bader, R. F. W. *Chem. Rev.* **1991**, *91*, 893.

[17] Bader, R. F. W.; *Atoms in Molecules. A Quantum Theory*, Clarendon Press: Oxford, UK, 1991.

[18] Bader, R. F. W.; Hernández-Trujillo, J.; Cortés-Guzmán, F. *J. Comp. Chem.* **2007**, *28*, 4.

[19] Cortés-Guzmán, F.; Bader, R. F. W. *Coord. Chem. Rev.* **2005**, *249*, 633.

[20] Geerlings, P.; De Proft, F.; Langenaeker, W. *Chem. Rev.* **2003**, *103*, 1793.

[21] Hohenberg, P.; Kohn, W. *Phys. Rev. B* **1964**, *136*, 864.

[22] Kohn, W.; Sham, L. J. *Phys. Rev. A* **1965**, *140*, 1133.

[23] Parr, R. G.; Ayers, P. W.; Nalewajski, R. F. *J. Phys. Chem. A* **2005**, *109*, 3957.

[24] Matta, C. F.; Bader, R. F. W. *J. Phys. Chem. A* **2006**, *110*, 6365.

[25] Tal, Y.; Bader, R. F. W.; Nguyen-Dang, T. T.; Ojha, M.; Anderson, S. G. *J. Chem. Phys.* **1981**, *74*, 5162.

[26] Rodríguez, J. I.; Köster, A. M.; Ayers, P. W.; Santos-Valle, A.; Vela, A.; Merino, G. *J. Comp. Chem.* doi: **10.1002/jcc.21134**.

[27] Bader, R. F. W.; MacDougall, P. J.; Lau, C. D. *J. Am. Chem. Soc.* **1984**, *106*,1594.

[28] Bader, R. F. W. *J. Chem. Phys.* **1980**, *73*, 2871.

[29] Blanco, M. A.; Pendas, A. M.; Francisco, E. *J. Chem. Theory Comput.* **2005**, *1*, 1096.

[30] Runtz, G. R.; Bader, R. F. W.; Messer, R. R. *Can. J. Chem.* **1977**, *55*, 3040.

[31] Bader, R. F. W. *Acc. Chem. Res.* **1975**, *8*, 34

[32] Frisch, M. J.; Trucks, G. W.; Schlegel, H. B.; Scuseria, G. E.; Robb, M. A.; Cheeseman, J. R.; Zakrzewski, V. G.; Montgomery Jr., J. A.; Stratmann, R. E.; Burant, J. C.; Dapprich, S.; Millam, J. M.; Daniels, A. D.; Kudin, K. N.; Strain, M. C.; Farkas, O.; Tomasi, J.; Barone, V.; Cossi, M.; Cammi, R.; Mennucci, B.; Pomelli, C.; Adamo, C.; Clifford, S.; Ochterski, J.; Petersson, G. A.; Ayala, P. Y.; Cui, Q.; Morokuma, K.; Rega, N.; Salvador, P.; Dannenberg, J. J.; Malick, D. K.; Rabuck, A. D.; Raghavachari, K.; Foresman, J. B.; Cioslowski, J.; Ortiz, J.V.; Baboul, A. G.; Stefanov, B. B.; Liu, G.; Liashenko, A.; Piskorz, P.; Komaromi, I.; Gomperts, R.; Martin, R. L.; Fox, D. J.; Keith, T.; Al-Laham, M. A.; Peng, C. Y.; Nanayakkara, A.; Challacombe, M.; Gill, P. M. W.; Johnson, B.; Chen, W.; Wong, M.W.; Andres, J. L.; Gonzalez, C.; Head-Gordon, M.; Replogle, E. S.; Pople, J. A. Gaussian 98W, Revision A.1, Gaussian, Inc., Pittsburgh PA, **1998**.

[33] Pacote computacional AIM 2000 1.0 desenvolvido por Biegler-König, F. Universidade de Ciências Aplicadas, Bielefeld, Alemanha.

[34] Gomes, T.C.F.; Silva Jr., J.V.; Vidal, L.N.; Vazquez, P.A.M.; Bruns, R.E.; *Theor. Chem. Acc.* **2008**, *121*, 173.

[35] Silva Jr., J. V.; Faria, S. H. D. M.; Haiduke, R. L. A.; Bruns, R. E. *J. Phys. Chem. A* **2007**, *111*, 515.

[36] Silva Jr., J. V.; Haiduke, R. L. A.; Bruns, R. E. *J. Phys. Chem. A* **2006**, *110*, 4839.

[37] Bader, R. F. W. *Monatshefte füur Chemie* **2005**, *136*, 819.

[38] Hugas, D.; Simon , S.; Duran, M.; *Struct. Chem.* **2005**, *27*, 257.

[39] Roohi, H. *J. Phys. Org. Chem.* **2008**, *21*, 971.

[40] Hirose, C.; *Bull. Chem. Soc. Japan* **1974**, *47*, 976.

[41] Creswell, R. A.; Schwendeman, R. H. *Chem. Phys. Lett.* **1974**, *27*, 521.

[42] Cunningham Jr., G. L.; Boyd, A. W.; Myers, R. J.; Gwinn, W.D. *J. Chem. Phys.* **1951**, *19*, 676.

[43] Anttila, R.; Hietanen, J.; Kauppinen, J. *Mol. Phys*. **1979**, *37*, 925.

[44] Oliveira, B. G.; Araújo, R. C. M. U.; Carvalho, A. B.; Lima, E. F.; Silva, W. L. V.; Ramos, M. N.; Tavares, A. M. *J. Mol. Struct. (THEOCHEM)* **2006**, *775*, 39.

[45] Cremer, D.; Kraka, E.; Slee, T. S.; Bader, R. F. W.; Lau, C. D. H.; Nguyen-Dang, T. T.; MacDougall, P. J. *J. Am. Chem. Soc.* **1983**, *105*, 5069.

[46] Matta, C. F.; Boyd, R. J. *The Quantum Theory of Atoms in Molecules*, WILEY-VCH Verlag & Co. KgaA, Weinheim, **2007**.

[47] Popelier, P. L. A.; Aicken, F. M. *J. Am. Chem. Soc.* **2003**, *125*, 1284.

[48] Gillespie, R. J.; Popelier, P. L. A. *Chemical Bonding and Molecular Geometry: From Lewis to Electron Densities*, Oxford University Press, Oxford, 2001.

[49] Gillespie, R. J. *Molecular Geometry*, Van Nostrand-Reinhold, London, 1978

[50] Popelier, P. L. A. *Coord. Chem. Rev.* **2000**, *197*, 169.

[51] Wojtulewski, S.; Grabowski, S. J. *J. Mol. Struct.* **2002**, *605*, 235.

[52] Krygowski, T. M.; Grabowski, S. J. *Chem. Phys. Lett.* **2004**, *389*, 51.

ISSN 1984-6428
ONLINE
www.orbital.ufms.br

Orbital 2009, *1* (2), 183-192

Full Paper

Synthesis and antimicrobial activity of coumarin derivatives metal complexes: An in vitro evaluation

K. B. Vyas[a], K. S. Nimavat[a], G. R. Jani[b], M. V. Hathi[c]*

[a]Department of Chemistry, Govt. Science College, Gandhinagar, India.
[b]Department of Chemistry, M. N. College, Visnagar, India.
[c]R. R. Mehta Science College, Palanpur, India.

Received: 02 February 2009; revised: 04 March 2009; accepted: 14 March 2009. Available online: 14 May 2009

***ABSTRACT**: Complexes of 3-[{-(3',4'-di methoxy phenyl) }-prop-2-enoyl]-4-hydroxy-6-methyl-2H-chromene-2-one with Cu(II), Ni(II), Fe(II), Co(II) and Mn(II) have been synthesized and characterized using elemental analysis, IR spectra and conductivity measurements. These studies revealed that they are having octahedral geometry of the type $[ML_2(H_2O)_2]$. In vitro antimicrobial activity of all synthesized compounds and standard drugs have been evaluated against four strains of bacterial culture and one fungus, which includes two gram +ve bacterial culture and two gram -ve bacterial culture. The compounds show net enhancement in activity on coordination of metals with ligand but moderate activity as compared to standard drugs.*

***Keywords**: antimicrobial activity, coumarin, metal complexes, structural study*

**Corresponding author: kirankartik@yahoo.com*

Introduction

Coumarins contain the parent nucleus of benzo-α-pyrone and occur in plants of the families like Orchidaceae, Leguminaceae [1], Rutaceae, Umbellliferae and Labiatae. Some of the coumarins show distinct physiological photodynamic and bacteriostatic activities [2] and placed for many diverse uses [3]. Their chelating characteristics have long been observed and the bacteriostatic activity seems to be due to chelation.

The complexes of metallic salts are more potent and less toxic in many cases as compared to the parent drug [4] . These metal complexes are found to be interesting due to their biological applications like antifungal [5], antibacterial [6] and anti tumor [7] activity. Some chalcones derived from coumarin derivatives, possess significant antimicrobial activity [8]. Some 3-acetyl/acetoacetoacetyl-4-hydroxy benzopyran-2-ones have been reported as an anti-HIV agent [9]. Thus it was thought worthwhile to synthesize various novel metal complexes and to evaluate them for antimicrobial activity.

Chemistry

The growing potent literature of recent years reveals that chalcone a very active synthon and coumarin also show activity such as co agulant, bacterial and insecticidal prompted us to synthesize some new chalcone (III) by condensation of 3-acetyl 4-hydroxy-6-methyl- coumarin (2) with different aromatic aldehyde. These metal (II) complexes (4a-e) have been prepared by refluxing metal salt solution and the alcoholic solution of ligand (3) (Scheme 1).

Scheme 1

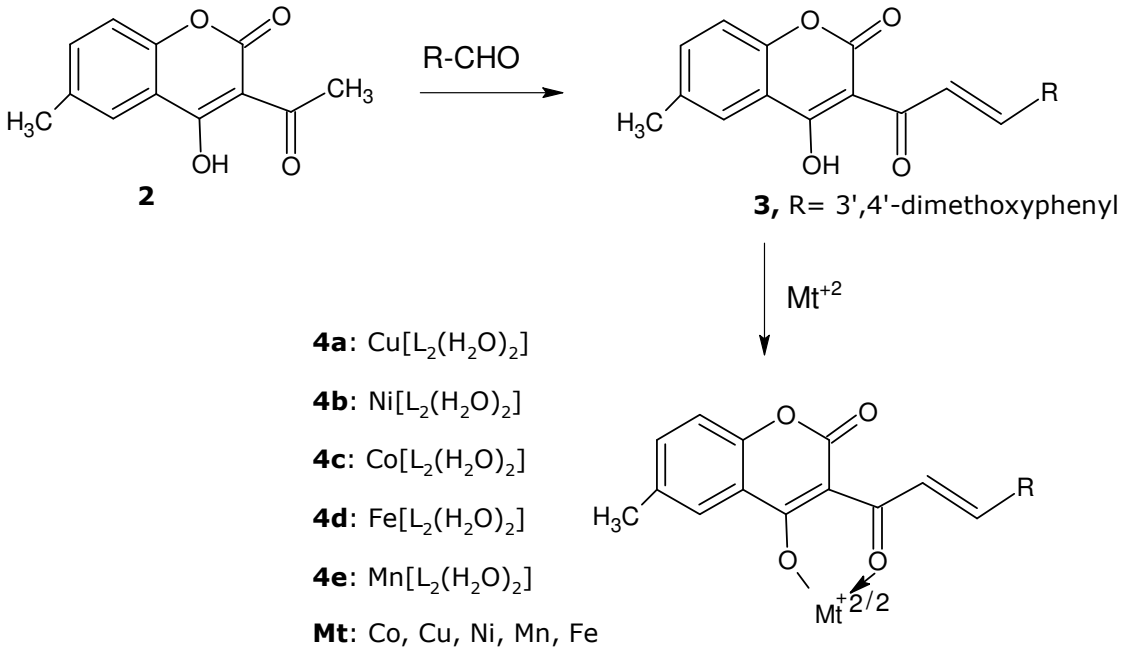

2

3, R= 3',4'-dimethoxyphenyl

4a: $Cu[L_2(H_2O)_2]$

4b: $Ni[L_2(H_2O)_2]$

4c: $Co[L_2(H_2O)_2]$

4d: $Fe[L_2(H_2O)_2]$

4e: $Mn[L_2(H_2O)_2]$

Mt: Co, Cu, Ni, Mn, Fe

Material and Methods

Chemistry

All the reagents were of AR grade. All the melting points were determined in open capillary tubes and are uncorrected. Infrared spectra (KBr) (νmax, cm^{-1}) were recorded on a Shimadzu 435 –IR Spectrophotometer. The metal and anions are estimated using standard procedure [10] .Elemental analyses are quite comparable with their structure. Elemental analyses of metal complexes indicates that the metal: ligand (M:L) ratio is 1:2 for all the divalent metal ions. The conductivity of metal complexes were determined using Thoshniwal Conductivity Bridge.

3-[{3-(3',4'-Di methoxy phenyl)}-prop-2-enoyl]-4-hydroxy-6 methyl-2H-chromen-2-one

3-[{3-(3',4'-Di methoxy phenyl)}-prop-2-enoyl]-4-hydroxy-6 methyl-2H-chromen-2-one were prepared according to the reported method (3) [11]. A mixture of 3-Acetyl-4- hydroxy-6-methyl-2-benzopyranone (2.52 mg, 0.01M); 3', 4'-di methoxy benzaldehyde (4.15 mL, 0.025 M) and piperidine (1 mL) were added into ethanol (50 mL). The reaction mixture was refluxed on water bath for 4 h, cooled and solid was separated. Then it was crystallized from ethanol, reddish yellow coloured compound was obtained. (m.w. 362 gm, 70%), M.P. 217°C. ^{1}H NMR($CDCl_3$) δ ppm : 2.41 (s, 3H, C<u>H</u>$_3$), 3.85 (s, 2 x 3H, OC<u>H</u>$_3$), 8.21(d, 1H, -C<u>H</u>=CH), 7.97 (d, 1H, -CH=C<u>H</u>), 3.92 (s, 1H, -O<u>H</u>), 6.66 to 7.82 (m, 6H, Ar-<u>H</u>). Elemental analysis; found: C, 68.85%, H, 4.91%,O,26.23% for $C_{21}H_{18}O_6$ required C, 68.80%, H, 4.85%, O, 26.15%. IR bands νmax (KBr cm^-): 1670 (C=O), 1578 (CH=CH), 1031 (C-O-C), 1708 (C=O of δ- lactone ring), 3429 (OH).

Bis [3-[{3-(3', 4'-Di methoxy phenyl)}prop-2-enoyl] 4-hydroxy-6- methyl-2H-chromen-2-one]copper(II)complex [Cu($C_{21}H_{17}O_6$)$_2$(H_2O)$_2$] (4a)

Copper chloride solution (10.0 mL, 0.1 M) diluted to 50 mL and excess of ammonium hydroxide was added to get the pH between 10.5-11.0. It was refluxed with excess of alcoholic solution of 3-[{3-(3', 4'-Di methoxy phenyl)} prop-2-enoyl] 4-hydroxy-6-methyl-2H-chromen-2-one (3) (3.62 mg, 0.1 M) on a water bath for half an hour when *light green* precipitates of copper complex were obtained. The precipitates were filtered, washed with distilled water and dried at 100^o C. The complex was crystallized from DMF. (m.w. 827.54 gm 62%). Elemental analysis: found C, 60.90%, H, 4.59%, Cu, 7.67 % for [Cu($C_{21}H_{17}O_6$)$_2$] required C, 60.80%, H, 4.45%, Cu, 7.50%. IR bands νmax (KBr, cm^-): 1619 (C=O), 1587 (CH=CH), 1072 (C-O-C), 1732 (C=O of δ-lactone ring), 590-500 (Cu-O).

Similarly other metal complexes were prepared. The complexes did not show clear melting point. They charred at temperature above 290^{O}C.

Conductivity

The conductivity of metal complexes was determined by using Thoshniwal Conductivity Bridge. It was dissolved in DMF and conductivity was measured.

Conductivity of the DMF was measured and solution of the complexes in DMF with different concentration was measured.

The molar conductivity was calculated using the formula:

$$\textbf{Molecular conductivity} = \frac{1000 \times K}{C}$$

Where, K=Conductivity of the sol. of the complexes in DMF. C = Concentration of the complexes (10^{-3} M). The conductivity data are in (Table 1) and the data indicate that the complexes are non- electrolyte in nature [12].

IR Spectral analyses

The Infrared spectra of the metal complexes were recorded on Shimadzu 435-IR Spectrophotometer between 4000-400 cm^{-1} (see Table 2).

The examination of the IR spectra of all the complexes reveals that:

(I) All the IR spectra have identical bands at their respective positions.

(II) Most of the bands appeared in the spectra of ligand are observed at the similar position in the IR spectra of metal complexes.

(III) The FT-IR spectra of all the complexes exhibited a broad peak around 3540 - 3320 cm^{-1} a sharp peak in the range 1623-1617 cm^{-1}. These peaks can be assigned to OH stretching and bending vibration, which indicate the presence of coordinated water molecule in the complexes. The peaks at 1623 and 1626 cm^{-1} corresponding to C=O have been shifted to +15-23 cm^{-1} the complexes, which indicate coordination through oxygen atom of the carbonyl group.

(IV) The peak at 1720 cm^{-1} is attributed to δ-lactone ring. In short, most of the bands appeared in the spectra of corresponding ligand are observed at the similar position in the IR spectra of metal complexes.

(V) In addition the IR spectra of complexes showed new bands between 590-500 cm^{-1} assigned to metal-ligand vibration (M-O).

^{1}H NMR Spectral analysis

^{1}H NMR Spectra of the Ni(II) complex was recorded. Unfortunately, however due

to the presence of a metal ion, proton resonance was not effected and one could observe only broad peaks indicating the formation of the complex.

Pharmacology

The antimicrobial activity was assayed by Cup plate agar diffusion method [13] by measuring inhibition zones in mm. *In vitro* antimicrobial activity of all synthesized compounds and standard drugs have been evaluated against four strains of bacteria which include two Gram +ve bacteria such as *Staphylococcus aureus, Bacillus megaterium* and two Gram-ve bacteria such as *Escherichia coli, Proteus vulgaris* and one fungi *Aspergillus nige*r.

The antibacterial activity was compared with standard drugs viz. Amoxycillin, Ampicillin, Ciprofloxacin, Erythromycin and antifungal activity was compared with standard drug viz. Griseofulvin.

Antibacterial activity

The purified products were screened for their antibacterial activity by using cup-plate agar diffusion method. The nutrient agar broth prepared by the usual method, was inoculated aseptically with 0.5 mL of 24 h old subculture of *S. aureus*, *B. megaterium, P. vulgaris*, and *E. coli* in separate conical flasks at 40-50 ^{O}C and mixed well by gentle shaking. About 25 mL of the contents of the flask were poured and evenly spread in petridish (90 mm in diameter) and allowed to set for two h. The cups (10 mm in diameter) were formed by the help of borer in agar medium and filled with 0.04 mL (40 µg/mL) solution of sample in DMF.

The plates were incubated at 37 ^{O}C for 24 h and the control was also maintained with 0.04 mL of DMF in similar manner and the zones of inhibition of the bacterial growth were measured in millimeter and recorded in Table 3.

Antifungal activity

A. niger was employed for testing antifungal activity by cup-plate agar diffusion method. The culture was maintained on Sub rouse dextrose agar slants. Sterilized Sub rouse dextrose agar medium was inoculated with 72 h old 0.5 mL suspension of fungal spores in a separate flask. About 25 mL of the inoculated medium was evenly spread in a sterilized petridish and allowed to set for 2 h. The cups (10 mm in diameter) were punched in petridish and loaded with 0.04 mL (40 µg/mL) of solution of sample in DMF. The plates were incubated at 30^{O}C for 48 h. After the completion of incubation period, the zones of inhibition of growth in the form of diameter in mm was measured. Along the test solution in each petridish one cup was filled up with solvent which acts as control. The zones of inhibition are recorded in Table 3.

Results and Discussion

Antimicrobial activity of the synthesized compounds and standard drugs is given Table 3. From the Table it is clear that the zones of inhibition area is much larger for the metal chelates than the ligand. The increase in antimicrobial activity is due to faster diffusion of metal complexes as a whole through the cell membrane or due to the combined activity of the metal and ligand [14].

The antimicrobial activity of tested compounds against different strains of bacteria and fungi is shown in Table 3. From Table 3 it can be concluded that all the compounds have displayed maximum activity against *P. vulgaris*. The compound 4b is highly active against *E. coli*. The compounds 4b and 4e also showed very good activity against *B. megaterium*, while compounds 4a and 4c showed good activity against *S. aureus*. From the data of anti fungal activity it is observed that almost all the compounds are highly active against *A. niger* except compound 3, which exhibits moderate activity.

As compared to standard drug Ciprofloxacin the compounds are less active, while other drugs have parallel activity.

The substitution of phenyl ring by $-OCH_3$ have much more effect on the bactericidal and fungicidal activity of complex.

It has been observed that Cu (II) complex have much toxicity. This is expected because the copper salts are mostly used as fungicides.

Such increased activity of the metal complexes can be explained on the basis of Overtone's concept [15] and Tweedy's chelation theory [16].

Most of the compounds inhibit the growth of the above organism, which cause decease in many plants. Hence such type of compounds may find as agricultural and garden bactericides and fungicides.

Acknowledgements

The authors express their gratitude to Dr. M. V. Hathi, the research guide for providing the necessary research facilities and research guidance.

Table 1. Elemental and metal analysis of metal (II) complexes

Sr.	Molecular formula	Molecular Weight	% OF CARBON		% OF HYDROGEN		% OF METAL		CONDUCTIVITY
			Calcd.	Found	Calcd.	Found	Calcd.	Found	
4a	$Cu[C_{21}H_{17}O_6]_2(H_2O)_2$	827.54	60.90	60.8	4.59	4.5	7.67	7.5	7.7
4b	$Ni[C_{21}H_{17}O_6]_2(H_2O)_2$	822.71	61.26	61.1	4.61	4.5	7.13	7.08	9.3
4c	$Co[C_{21}H_{17}O_6]_2(H_2O)_2$	822.93	61.24	61.0	4.61	4.4	7.16	7.0	9.8
4d	$Fe[C_{21}H_{17}O_6]_2(H_2O)_2$	821.85	61.32	61.2	5.11	5.0	6.79	6.7	11.1
4e	$Mn[C_{21}H_{17}O_6]_2(H_2O)_2$	818.93	61.54	61.3	4.64	4.5	6.70	6.5	10.9

Table 2. IR spectral data of metal (II) complexes

Sr.	Metal Complexes	Frequencies Cm^{-1}					
		Alkane	**Aromatic**	**Ketone**	**Alkene**	**M-O**	**Ether**
		$-CH_3$	**-CH**	**-C=O**	**CH=CH**	**Band**	**C-O-C**
4a	$Cu[C_{21}H_{17}O_6]_2(H_2O)_2$	2928	1511				
		2834	1249	1650	1609	590-500	1112
		1442	832	1710			
		1383					
4b	$Ni[C_{21}H_{17}O_6]_2(H_2O)_2$	2920	1562				
		2858	1296	1697	1612	590-500	1130
		1465	821	1715			
		1384					
4c	$Co[C_{21}H_{17}O_6]_2(H_2O)_2$	2922	1554				
		2853	1222	1689	1584	590-500	1138
		1460	833	1715			
		1375					
4d	$Fe[C_{21}H_{17}O_6]_2(H_2O)_2$	2920	1584				
		2850	1223	1669	1608	590-500	1137
		1418	819	1710			
		1376					
4e	$Mn[C_{21}H_{17}O_6]_2(H_2O)_2$	2933	1562				
		2858	1227	1610	1602	590-500	1072
		1464	821	1732			
		1383					

Table 3. Microbiological evaluation of compounds

Organism	Compounds						Standard drugs				
	3	**4a**	**4b**	**4c**	**4d**	**4e**	**Ampicillin**	**Amoxycillin**	**Ciprofloxacin**	**Erythromycin**	**Griseofulvin**
E. coli	18	22	24	18	19	23	16	17	26	22	0
P. vulgaris	19	21	27	19	20	22	24	21	28	18	0
B. mega	17	19	20	23	21	25	20	22	23	10	0
S. aureus	17	23	19	22	18	21	25	29	24	22	0
A. niger	19	20	24	18	22	21	0	0	0	0	21

References and Notes

[1] Spath, E. *Ber.* **1937***, 70A,* 83.
[2] Maggio, G. D. *Biochem. Appl.* **1958**, *5***,** 45.
[3] Glein, K. T. *U. S. Patent* 2740761. 1956. *Chem. Abstr.* **1956***, 50*, 1333788c.
[4] Singh, A.; Singh, P. *Indian J. Chem*. **2000**, *39A*, 874.
[5] Sharma, R. C.; Parashar, R. K. *J. inorg. biochem*. **1988**, *32*, 163.
[6] Abd el-waheb Z. H.; Mashaly, M. M.; Salman, A. A.; El-shetary, B. A.; Faheim A. A. *Spectrochimica Acta* **2004**, *60*, 2861.
[7] Jayasree S.; Arvindakshan, K. K., *Polyhedron* **1993**, *12*, 1187.
[8] Mulwad, V. V.; Bhagat, R. D.; *I. J. Heterocyclic Chem.* **1999***, 9*, 15.
[9] Manvar, D. C.; Karia D.; Shah. A. *Organic Chemistry: An Indian Journal* **2007***, 3*, 170.
[10] Vogel A. I. *A Textbook of Quantitative Chemical Analysis*, 5th edition , Longmans, London, 1991, p. 326.
[11] Hermes, S. A. *Chem. Abstr*. **1969**, *70*, 964224.
[12] Geary W. J. *Coord. Chem. Rec*. **1971**, 82.
[13] Barry, A. L. *Procedure and Theoretical Consideration for testing anti microbial agents in Agar media*, 5th edition William wilkins Baltimore, 1991.
[14] Harsfall, J. G. *Bot. Rev*. **1945**, *11*, 357.
[15] Rao, R. P. *Synth. React. Inorg. Met. Org. Chem*. **1993**, 16, 257.
[16] Malhotra R.; Kumar S.; Dhindsa, K. S. *Indian J. Chem*. **1993**, *32A*, 457.

ISSN 1984-6428
ONLINE
www.orbital.ufms.br

Orbital 2009, *1* (2), 193-202

Full Paper

Effect of fat chain length of sorbitan surfactant on the porosity of mesoporous silica

Marco Antonio Utrera Martines[a,b*], *Larissa Souza Mendes*[b], *Juliana Jorge*[b], *Gustavo Rocha de Castro*[b], *Nídia Maria Ribeiro Pastura*[c], *Cinthia Fraga Scofield*[d], *Wilma de Araújo Gonzalez*[c]

[a]Departamento de Química, Universidade Federal de Mato Grosso do Sul, CCET/UFMS, Av. Filinto Muller, 1555, Cidade Universitária, 79074-460, Campo Grande, MS, Brazil.
[b]Departamento de Física e Química, Faculdade de Engenharia de Ilha Solteira, UNESP, Av. Brasil, 56, Centro, 15385-000, Ilha Solteira, SP, Brazil.
[c]Instituto Militar de Engenharia, Praça General Tibúrcio, 80, 22290-270, Rio de Janeiro, RJ, Brazil.
[d]Departamento de Físico-Química, Centro de Tecnologia e Ciências, UERJ, Rua São Francisco Xavier, 524, Maracanã, 20550-013, Rio de Janeiro, RJ, Brazil.

Received: 13 December 2008; revised: 02 July 2009; accepted: 03 July 2009. Available online: 07 July 2009.

ABSTRACT: *The influence of the fat chain length of sorbitan surfactant was systematically explored, especially its influence on the material pore size. Then, mesoporous silica was synthesized according to a two-step process that provides intermediary stable hybrid micelles using ethoxylated derivative of fatty esters of sorbitan surfactants as the directing-structure agent and tetraethyl orthosilicate $Si(OEt)_4$ as the silica source. Finally, the materials' porosity could be controlled by adjusting the preparation parameters during the two steps synthesis of mesoporous silica.*

Keywords: *mesoporous silica, non-ionic surfactant, ethoxylation degree*

* *Corresponding author. E-mail: marco@nin.ufms.br*

Introduction

The intermediary region between the atomic and molecular physics and condensed matter physics can be defined as the region where mesometric-ordering materials can be obtained, this is located between the microscopic and macroscopic region. From a technologic point of view, understanding the problems related to catalysis, chemisorptions, aerosols, powder metallurgy, ferrofluid etc, is very important with regards to the study of matter system in this intermediate region. In addition, one expects that the next level of miniaturization of the photonic and microelectronic devices will depend on the systems of this intermediate region. From a basic point of view, the study of this state of matter, intermediary between molecule and solid, will be decisive and very important as it involves many chemical and physical principles that are usually dissimulated in infinitely sizable systems.

Since 1992, scientists working with zeolite syntheses and related materials such as catalyses and materials science [1], have been motivated with the discovery of mesoporous crystalline materials by the Mobil Research and Development Corporation research group [2, 3]. A large number of potential applications of these materials in the catalyses, separation [4] and advanced materials [5-8] areas have been developed in a short time. Microporous zeolites and molecular sieves have been expanded for the mesoporous region by mesoporous crystalline materials. Such findings created new opportunities, not only for catalysis, but also for areas involving applications of advanced materials. In the catalysis area, crystalline mesoporous materials are more efficient than conventional catalyser due to their high surface area and also because these materials present more accessible active sites [9]. The use of ordered silicates hosts for low dimensional quantum semiconductors was possible with the discovery of mesoporous materials [10]. The engineering of mesoporous materials with pore size between angstroms up to micrometer has been fruitful due to the use of organic molds to control inorganic solid structures [11]. The formation mechanism of mesoporous materials [12], from tetraethyl orthosilicate (TEOS), cethylmethylammonium bromide (CTAB) and water, involves a self assembly mechanism, where the electrostatic interactions between surfactants molecules and inorganic ions determine the mesophase obtained. In the presence of neutral surfactants, the hydrogen bonding in the place of electrostatic interactions becomes of crucial importance for the formation of organic-inorganic mesophase [13].

The pore size (or interlayer distance) of mesoporous materials is easily adjustable in the interval of 20 to 100 Å. In this context, the pore size can be adjusted by 3 different manners: (i) by changing the length of the chain alkyls group of surfactant

molecule; (ii) by adding the swelling agent (1,3,5-trimethylbenzene) that results in the expansion of micelle due to dissolution of the swelling agent into the hydrophobic region of micelle; or (iii) by aging the material prepared at low temperature (about 70 °C) into the mother liquid or high temperature (about 150 °C) for varying periods of time. Also, the pore size of silicates can be adjusted by silanization pos-synthesis. Materials with high surface area, frequently up to 1000 m^2/g, can be obtained by calcination of stable phases of silicate and self-structured surfactant molecules. Moreover, these materials can easily be modified by the different incorporation of cations, becoming acid or redox properties [3].

In this work we describe the influence of the fat chain length of sorbitan surfactant in the mesoporosity of silica prepared by two-step synthesis route using non-ionic surfactant as template.

Material and Methods

Mesoporous silica was synthesized with PEO (polyoxyethylene) surfactants with different ethoxylation degree: Tween 20 (PEO sorbitan monolaurate) (Fluka Chemicals), Tween 40 (PEO sorbitan monopalmitate) (Sigma Chemicals), Tween 60 (PEO sorbitan monostearate) (Sigma Chemicals), and Tween 80 (PEO sorbitan monoolate) (Sigma Chemicals). The silica source was tetraethyl orthosiliate (TEOS, $Si(OCH_2CH_3)_4$) (Merck). We used sodium fluoride as a silica condensation catalyst (Merck). All reagents were used as received.

Mesoporous silica was prepared according to the two-step synthesis [14]. A 0.02 $mol.L^{-1}$ aqueous solution of surfactant was prepared and the pH was adjusted at 2 by adding 2 mL of a hydrochloric acid solution. TEOS was added under magnetic stirring to reach a final TEOS/surfactant molar ratio of 8. After aging for 12 h at room temperature without stirring, this solution was heated to 40 °C in a thermostated-shaking bath. The final condensation step was induced by the addition of 4% of sodium fluoride (0.25 M) to the solution that was kept in the thermostated bath at 40 °C for 3 days, with slow shaking (40 rpm). A white powder is obtained with a yield close to 100%. Afterward, it was filtered, dried, and calcined at 620 °C for 6 h after step at 6 h at 200 °C.

All measurements were performed on calcined powders. They were characterized by scanning electron microscopy (SEM), transmission electron microscopy (TEM), X-ray diffractometry (XRD) and nitrogen adsorption/desorption. The TEM images were obtained with a Philips CM20 instrument operating at a 200 kV. The samples were ultrasonically dispersed in ethanol and dropped onto the carbon-coated copper grids prior to the measurements. The scanning electron microscopy work was performed with Jeol JSM-

5900 LV microscope of LME/LNLS, Campinas, operating at 20 kV. The samples were covered with Au to increase conductivity. XRD measurements were carried out with a Rigaku (Miniflex), with wavelength of the copper K-alpha line radiation (λ = 1.5418 Å). Most patterns exhibited a single diffraction peak that we assigned to pores length correlation [15]. This pore center to pore center correlation length will be named "d-spacing" to follow. Nitrogen absorption isotherms were measured at liquid-nitrogen temperature on a Micromeritics 2010 Sorptometer using standard continuous procedure. Surface areas were determined by the Brunnauer – Emmett – Teller (BET) method within a 0.05 – 0.02 relative pressure range. Pore size distributions were calculated only for sizes higher than 2.5 nm from the desorption branch by a polynomial correlation between relative pressure and pore diameter, deduced from the Broekhoff and Boer (BdB) model [16, 17]. To simplify comparison, we displayed the reduced adsorption curves (isotherms divided by the amount adsorbed at a relative pressure of 0.8) [18].

Results and Discussion

The synthesis of micelle-templated structures (MTS) is a multi-parameter process that includes structuralization of the surfactant at different pH values, pressure and temperature, as well as the nature and condensation of inorganic precursors. The interactions between organic templates and inorganic precursors remain a key factor that is applied at all times. The synthesis of mesoporous silica is based on the intermediate formation of hybrid micelles and is accomplished in two ways: the first one is the self-assemblage of hybrid micelles and hydrolyzed inorganic precursor, this step is thermally controlled, and the second one is silica condensation into the hydrophilic region of micelles that is kinetically governed.

The TEM, Figure 1 image evidences that the particles contain domains of perfectly ordered structure. However, the TEM images show only microscopic part of the spherical particle, the overall view of the structure ordering of a macroscopic amount of the sample obtained by means of XRD, Figure 2 indicates structural uniformity of the material for silica with surfactant removed.

The chain length influence is illustrated by the synthesis of mesoporous silica with the Tween family (20, 40, 60 and 80) at synthesis temperatures adjusted in the shaking bath at 40 °C. The scanning electron microscopy images displayed in Figure 2 exhibit micrometric spherical particles characteristic of MSU-1 and 2 types of mesoporous silica [19-21]. The material was named Michigan State University type material, or MSU-X silica (X refers to the nature of the surfactant: 1 for alkyl-PEO, 2 for alkylaryl-PEO, 3 for polypropyleneoxyde-PEO block copolymer, and 4 for Tween-type nonionic ethoxylated

sorbitan esters) is prepared under neutral [13, 15] or mild acidic conditions [14].

The morphologies of mesoporous silica particles obtained in the Tween family are spherically shaped with micrometric and sub-micrometric particles size. The final nanostructure and the morphology of MSU-X type material are highly dependent on the parameter of the reactional mean, such as a local interaction created by the lipophilic/hydrophilic equilibrium, the Brownian motion that destroys the network, the hydrolysis kinetic and polymerization of silica [22]. Synthesis of MSU-X type mesoporous silica based on hydrogen bonding illustrates perfectly the versatility of this approach, since the final material structure (pore diameter, particle size) can be readily modified by adjusting several synthesis parameters, with the same reaction medium.

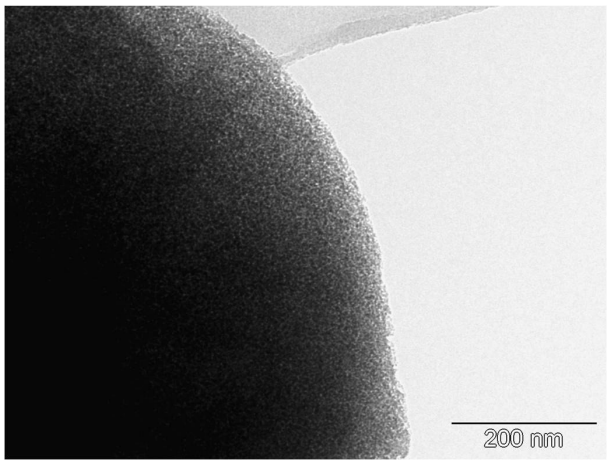

Figure 1. Transmission electron microscopy images of mesoporous silica prepared with Tween 60 as template.

MSU-4 type mesoporous silica samples have a highly ordered 3D wormhole mesostructure, as reveled by powder X-ray diffraction patterns, Figure 3. The overall quality of the structure can be estimated from the intensity of the diffraction line. The MSU-X silica X-ray pattern exhibits a single peak, characteristic of a single correlation length from pore center to pore center [15].

The mesoporous silica samples prepared in the presence of the Tween family exhibit a peaks on a specific degree, so, silica samples prepared with Tween 20, 40, 60 and 80 present a peaks at 46 Å, 48 Å, 50 Å and 52 Å, respectively. The samples' d-spacing increases with increasing chain length of the Tween family when we changed the ethoxylation degree during the mesoporous silica synthesis. The lengths of the hydrophobic chain of the Tween family are apparently marked by a parallel increase in the d-spacing, Figure 4. It is expected that the pore size changes the mesostructure with the length modification of the hydrophobic chain on the surfactant [2].

The nitrogen adsorption/dessorption isotherms, Figure 5, are characteristics of

mesoporous MTS-type materials. Therefore, all samples exhibit substantial framework-confined mesopores. The isotherm of the samples prepared with the Tween family does not exhibit any hysteresis, characteristic of pore necking, nor does the adsorption increase at high relative pressure, characteristic of a textural porosity. In addition, a parallel trend observed for the nitrogen adsorption/desorption isotherms with the adsorption jump shifted toward higher relative pressures is characteristic of an increasing pore size.

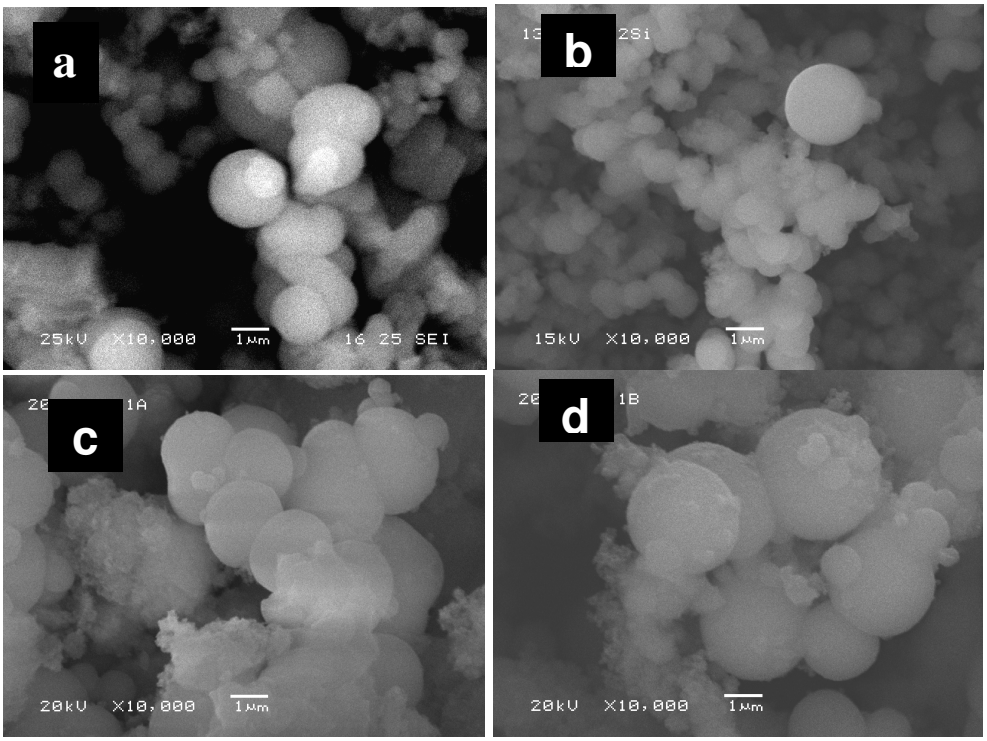

Figure 2. Scanning electron microscopy images of mesoporous silica prepared with Tween 20 (a), Tween 40 (b), Tween 60 (c) and Tween 80 as template.

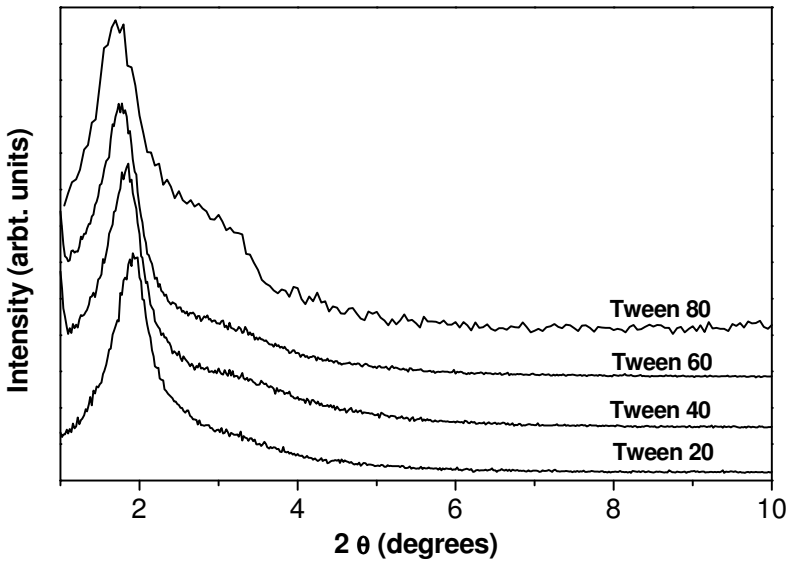

Figure 3. X-ray patterns of calcined mesoporous silica prepared at 40 °C as a function of Tween chain length: Tween 20 (a), Tween 40 (b), Tween 60 (c) and Tween 80 as template.

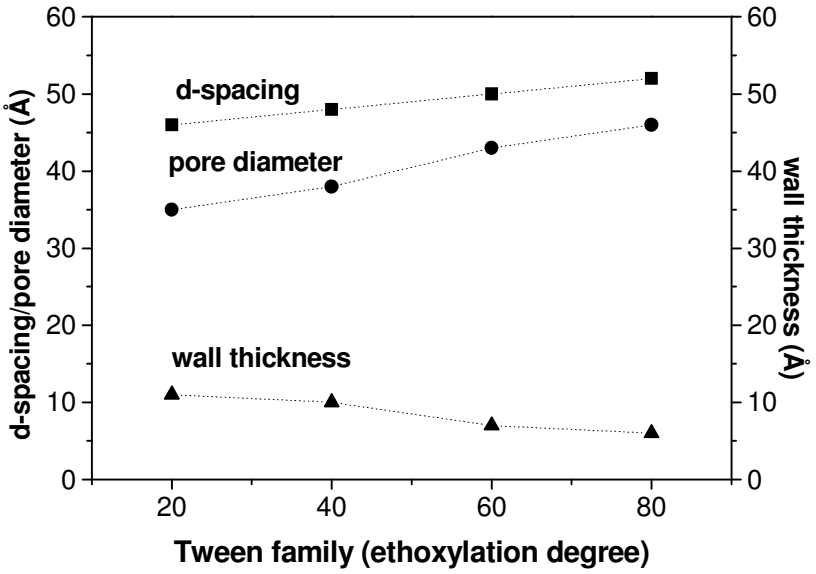

Figure 4. Evolution as a function of the chain length of Tween family of pore diameter of calcined mesoporous silica prepared at 40 °C with Tween X, when X (20, 40, 60 and 80) is the ethosylation degree.

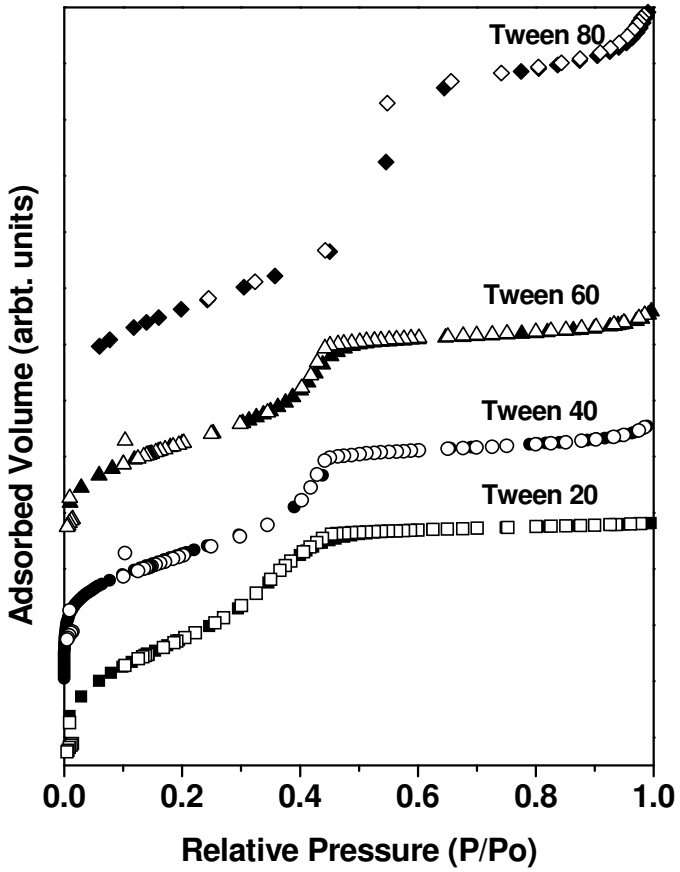

Figure 5. Reduced nitrogen adsorption (solid symbol)/desorption (open symbol) calcined mesoporous silica prepared at 40 °C as a function of Tween chain length: Tween 20 (a), Tween 40 (b), Tween 60 (c) and Tween 80 as template.

The pores size distributions for the samples are shown in Figure 6. The porosity of

mesoporous silica obtained in presence of the Tween family increases with increasing chain length of surfactant molecules used during the synthesis of mesoporous, thus, the pore size changed from 35 Å to 46 Å, when we changed the ethoxylation degree (Tween 20 to Tween 80) during the synthesis of mesoporous silica. Also, all samples presented pore size distributions, typical of mesoporous micelle-templated structures materials. The mesoporous silica, prepared in the presence of the Tween family as template, exhibit a high surface area. The surface area is 1016 m^2 g^{-1}, 780 m^2 g^{-1}, 868 m^2 g^{-1} and 961 m^2 g^{-1} for mesoporous silica prepared in the presence of Tween 20, 40, 60 and 80, respectively.

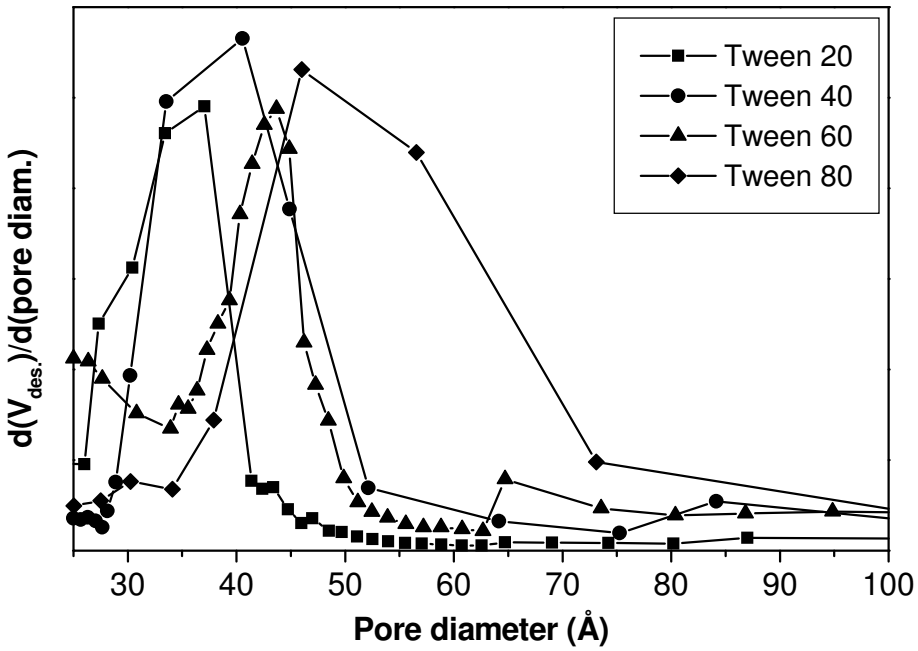

Figure 6. Evolution of pore diameter of calcined mesoporous silica prepared at 40 °C as a function of Tween chain length: Tween 20 (a), Tween 40 (b), Tween 60 (c) and Tween 80 as template.

In addition, the wall thickness (inorganic palisade) of mesoporous silica, calculated by the difference of the d-spacing and the pore size, decreased when it changed the ethoxylation degree (Tween 20 to Tween 80). This result is in agreement with XRD and pore size distribution, since the d-spacing and pore size increased with increasing chain length of surfactant molecules, Figure 4.

Conclusion

The mesoporosity of silica materials can be adjusted by the use of surfactants with different sizes of fat chains. The surface area is related with the average size of pores.

So, the use of surfactants with high ethoxylation degree produces materials with large pores that drive to a reduction of the specific area. Therefore, the mesoscopic characteristics of the silica material as its porosity, which can be controlled by adjusting its parameters.

Finally, the significant characteristic of these compounds is the considerable size of their pores, which makes them favorable candidates for posterior studies or applications; for example, mesoporous silica hierarchically organized is promising as materials standard for adsorption and catalyses studies for larges molecules.

Acknowledgments

The authors are grateful to FAPESP for grants and LME/LNLS for SEM measurements. M. M., L. M. and J. J. are grateful to FAPESP and CNPq for scholarships.

References and Notes

[1] Beck, J. S.; Vartuli, J. C.; *Curr. Opin. Solid State Mater. Sci.* **1996**, *1*, 76.
[2] Beck, J. S.; Vartuli, J. C.; Roth, W. J.; Leonowicz, M. E.; Kresge, C. T.; Schmitt, K. D.; Chu, C. T. W.; Olson, D. H.; Sheppard, E. W.; McCullen, S. B.; Higgins, J. B.; Schlenker, J. L. *J. Am. Chem. Soc.* **1992**, *114*, 10834.
[3] Kresge, C. T.; Leonowicz, M. E.; Roth, W. J.; Vartuli, J. C.; Beck, J. S. *Nature* **1992**, *359*, 710.
[4] Herbst, J. A.; Kresge, C. T.; Olson, D. H.; Schmitt, K. D.; Vartuli, J. C.; Wang, D. C. I.; US pat. 5, 378, 440, **1995**.
[5] Corma, A.; Fornés, V.; García, H.; Miranda, M. A.; Sabater, M. J. *J. Am. Chem. Soc.* **1994**, *116*, 9767.
[6] Leon, R.; Margolese, D.; Stucky, G. *Phys. Rev. B.* **1995**, *52*, 2285.
[7] Wu, C. G.; Bein, T. *Science* **1994**, *264*, 1757.
[8] Wu, C. G.; Bein, T. *Science* **1994**, *266*, 1013.
[9] Sayari, A. *Chem. Mater.* **1996**, *8*, 1840.
[10] Wu, C. G.; Bein, T. *Chem. Mater.* **1994**, *6*, 1109.
[11] Holland, B. T.; Blanford, C. F.; Stein, A. *Science* **1998**, *281*, 538.
[12] Firouzi, A.; Kumar, D.; Bull, L. M.; Besier, T.; Sieger, P.; Huo, Q.; Walker, S. A.; Zasadzinski, J. A.; Glinka, C.; Nicol, J.; Margolese, D.; Stucky, G. D.; Chmelka, B. F. *Science*, **1995**, *267*, 1138.
[13] Bagshaw, S. A.; Prouzet, E.; Pinnavaia, J. *Science* **1995**, *269*, 1242.
[14] Boissière, C.; van der Lee, A.; Mansouri, E.; Larbot, A.; Prouzet, E. *J. Chem. Soc., Chem. Commun.* **1999**, *20*, 2047.
[15] Prouzet, E.; Pinnavaia, T. J. *Angew. Chem. Int. Ed. Engl.* **1997**, *36*, 516.

[16] Broekhoff, J. C.; Deboer, J. H. *J. Catal.* **1968**, *10*, 377.
[17] Prouzet, E.; Cot, F.; Nabias, G.; Larbot, A.; Kooyman, P.; Pinnavaia, J. *Chem. Mater.* **1999**, *11*, 1498.
[18] Ryoo, R.; Ko, C. H.; Kruk, M.; Antochshuk, V.; Jaroniec, M. *J. Phys. Chem. B* **2000**, *104*, 11465.
[19] Boissière, C.; Larbot, A.; van der Lee, A.; Kooyman, P.; Prouzet, E. *Chem. Mater.* **2000**, *12*, 2902.
[20] Boissiere, C.; Martines, M. A. U.; Tokumoto, M.; Larbot, A.; Prouzet, E. *Chem. Mater.* **2003**, *15*, 509.
[21] Martines, M. A. U.; Yeong, E.; Persin, M.; Larbot, A.; Voorhout, W. F.; Kubel, C. K. U.; Kooyman, J. P.; Prouzet, E. *C. R. Chim.* **2005**, *8*, 627.
[22] Zhao, D.; Huo, Q.; Feng, J.; Chmelka, B.; Stucky, G. D. *J. Am. Chem. Soc.* **1998**, *120*, 6024.

ISSN 1984-6428
ONLINE
www.orbital.ufms.br

Orbital 2009, *1* (2), 203-214

Full Paper

DFT study of bridged oligo(bithiophene)s. Conformational analysis and opto-electronic properties

Si Mohamed Bouzzine[a], Mohamed Hamidi[a] and Mohammed Bouachrine[a,b*]*

[a]URMM/UCTA, Faculté des Sciences et Techniques, B. P. 509 Boutalamine, 5200, Errachidia, Morocco.
[b]UMIM, Faculté Polydisciplinaire de Taza, B. P. 1223/Taza Gare, Morrocco.

Received: 07 April 2009; revised: 14 July 2009; accepted: 29 July 2009. Available online: 02 August 2009.

***ABSTRACT**: In this paper, we have studied the conformational and opto-electronic properties of several oligomers of bridged oligo(bithiophene)s $(BTX)_n$, n=1 to 4 with (X: CH_2, SiH_2, C=O, C=S and $C=C(CN)_2$). The conformational analysis shows that the most stable conformation is anti-planar conformation. The opto-electronic properties of the octamer (OTX) lead us to suggest that this oligomer is a good model to reflect opto-electronic properties for the parent polymer.*

***Keywords**: oligothiophene, bridging effect, DFT, low band gap, donor acceptor polymer*

* *Corresponding author. E-mail: lrmm_fste@yahoo.fr*

Introduction

Polythiophene and its oligomers are almost the most intensively studied conducting polymers because of their good environmental stability [1, 2]. These materials have attracted much interest for potential application in opto-electronic devices due to their electronic and photonic properties [2]. Whereas polythiophenes obtained as highly amorphous, oligothiophenes are not amorphous and can be synthesized as well defined compounds. Moreover, these oligomers provide interesting models for understanding the structural and electronic peculiarities which control the charge transport and optical properties in parent polymers [3]. These materials are currently under intensive investigations for applications in film transistors [4], electroluminescent diodes [5], lasers [6], sensors [7] and photovoltaic cells [8].

One of the challenges when studying conducting polymers is to investigate new low band gap polymers. This even involves looking for polymers that are intrinsically conducting and thus do not require doping. Although various routes are presently followed for designing novel conducting polymers [9], a very exciting possibility in this direction is provided by the donor-acceptor polymers based on the approach suggested by Havinga et al. [10, 11]. Therefore, in the past decade, many efforts have been devoted to designing and synthesizing new polymer conducting materials, which have low band gap. Recently, a few low band gap polymers based on polyparaphenylene [12], polythiophene [13-15], were synthesized and studied intensively. Moreover, Lambert et al. [16, 17] have synthesized polydicyanomethylene-cyclopenta-dithiophene and poly-4H-cyclopenta-dithiophene-4-one with experimental band gap values of 0.8 and 1.2 eV, respectively.

In this regard, we investigated the geometric and electronic structures of some donor-acceptor polymers differing in their electron-donating and electron-accepting moieties. The electron-donating are derived from the bridging groups containing elements carbon C and silicon Si, where the electron-accepting groups are C=O, C=S and $C=C(CN)_2$.

The results of B3LYP/6-31G(d) studies of bridging effects of oligo(bithiophene)s with a variety of bridging groups (CH_2, SiH_2, C=O, C=S and $C=C(CN)_2$) (Scheme 1) showed that:

- The important reduction of the energy gap observed for the whole series of bridged compounds is explained on the basis of the orbital interaction analysis;

- The most relevant structural change is the decrease of the inter-rings bond between bridged thiophenes;

- The polymers with C=S and $C=C(CN)_2$ bridged groups are expected to exhibit the very low band gaps suggesting that these compounds can be used in the optoelectronic applications.

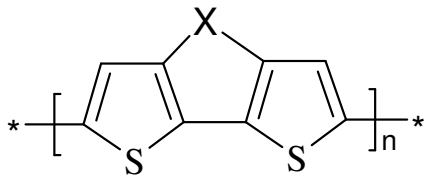

X: CH_2, SiH_2, C=O, C=S and $C=C(CN)_2$

Scheme 1: Studied oligo(bithiophene)s

Computational details

DFT method of three-parameter compound functional of Becke (B3LYP) [18] was used to study the bridged oligothiophenes. The 6-31G* basis set was used for all calculations [19–22]. The conformational analysis for the neutral structures was carried out by changing the torsional angle (θ, dihedral angle between central two thiophene rings, S—C—C—S) by 20 steps in the same direction between 0 (syn-planar) and 180° (anti-planar). For each conformation, θi were held fixed while the remaining variables were fully optimised, i.e., no rigid rotor approximation was adopted. The stable molecular geometries, corresponding to the energy minima on potential energy surface (PES), were separately obtained by releasing the constraints of the torsional angles, θi. To obtain the charged oligo(bithiophene)s structures, we started from the optimized structures of the neutral form. The geometric structures of charged structures were optimized independently from the neutral molecules prior to calculation of spin densities. Radical cations were treated as open shell systems by UB3LYP/6-31G* method. All calculations were carried out using the GAUSSIAN 03 program [23].

Results and Discussion

Conformational analysis

The results of the torsion potential of the oligo(bithiophene)s bridged by (X: CH_2, SiH_2, C=O, C=S and $C=C(CN)_2$) calculated at B3LYP/6-31G(d) level are presented in Fig. 1 and Fig. 2. The rotational profiles obtained are similar and both the existence of the syn–gauche conformer corresponding to average values of θ with 28.5° (see Table 1).

The region corresponding to anti-gauche conformer is very flat in both cases, for the both

computational level, the difference between the syn-gauche and the anti-gauche region is about 0.89 eV, the rotational barrier present five extrema, three maxima situated at 0°, 90° and 180° and two minima located at about 29° and 160° (see Table 1).

Table 1. Relative energy (Kcal/mol) and torsional angle of bridged quaterthiophene obtained at B3LYP/6-31G(d).

QTX	Syn	Syn-gauche	Perpendicular	Anti-gauche	Anti plane
4T	-	28.8/23.8(0.11)*	-	162.7 (0.00)	-
CH_2	1.23	28.8 (0.93)	3.46	162.0 (0.00)	0.06
SiH_2	1.04	28.1 (0.80)	3.28	166.6 (0.00)	0.01
C=O	1.00	29.9 (0.72)	2.94	159.7 (0.00)	0.07
C=S	1.04	30.8 (0.76)	2.57	161.3 (0.00)	0.04
$C=C(CN)_2$	1.18	34.5 (1.27)	2.97	160.9 (0.00)	0.09

* Relative energies of state

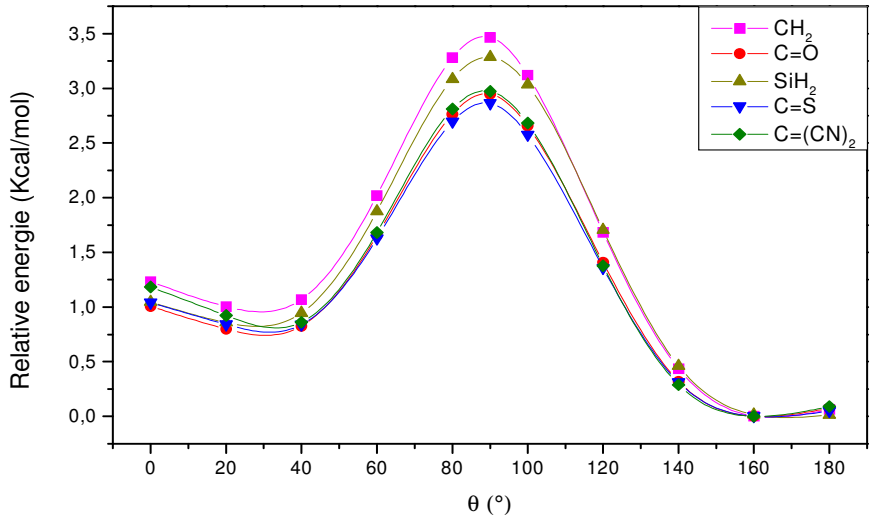

Figure 1: Torsion potential of oligo(bithiophene)s bridged by (X: CH_2, SiH_2, C=O, C=S and $C=C(CN)_2$) obtained by B3LYP/6-31G(d) level.

The torsional angles and barriers to internal rotation depend on the balance of two interactions: as a result of the π-electron conjugation between the thiophene rings, the molecules tend to remain planar, whereas the steric repulsion between hydrogens and groups (X: CH_2, SiH_2, C=O, C=S and $C=C(CN)_2$) causes the molecules to twist. The most significant result found with hybrid B3LYP functional is the presence of two minima. The first in the anti-gauche region corresponding to θ=160°, and the second in the syn-gauche conformer at θ=29° which is less stable than the anti-gauche conformer by about 0.87 Kcal/mol. A schematic representation of the syn- and anti-gauche conformer for all

bridged oligomers is given in Fig. 3. These representations were done by the animation option of the GaussView 3.0 graphical interface for Gaussian programs [23]. While the values of the most important geometrical parameters, for the most stable conformer (anti-gauche) structure are collected in Table 2.

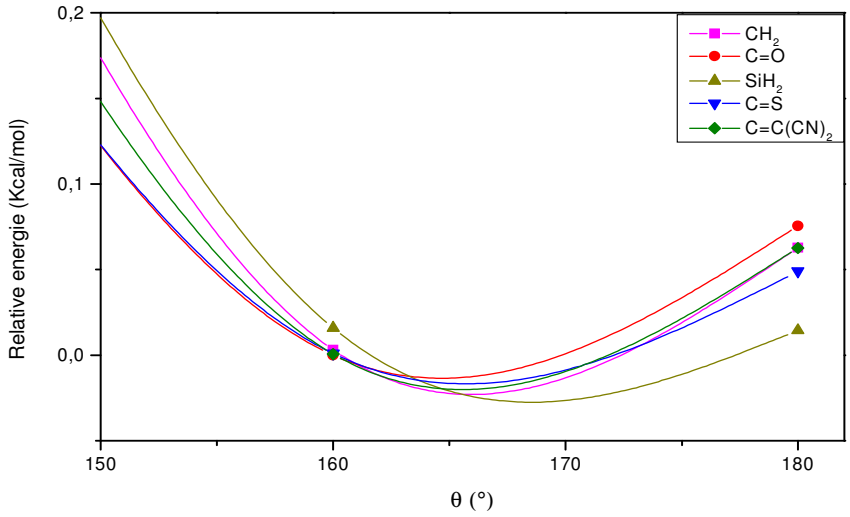

Figure 2: Torsion potential of oligo(bithiophene)s bridged by (X: CH_2, SiH_2, C=O, C=S and $C=C(CN)_2$) obtained by B3LYP/6-31G(d) level, for θ included between 150 and 180°.

The most relevant change observed in the comparison between the geometrical parameters, was more pronounced in the inner thiophene rings and in the terminal rings of the C—S and C=C bonds. This trend is in good agreement with theoretical calculations [24] and experimental results [25]. The structures of these oligomers present a shorting C—S and C=C bonds length in the terminal bonds of the thiophenes rings. In the comparison of the unbridged oligothiophene, the same evolution is noted by the C=C bond, but the bond C=C changes length while passing from the terminal to the inner of the chain. This variation of distance can be caused by the effect of insertion of the grouping X: CH_2, SiH_2, C=O, C=S and $C=C(CN)_2$ between the two thiophenes rings (see Fig. 3).

The variation of inter-ring bond C_1—$C_{1'}$ as well as the function of θ is showed in Fig. 4. All curves have similar look, and the shorter interring bond corresponds to conformation planar syn and anti, indicating that this conformation holds a larger conjugation between dienic structure what can be also evidenced by enlargement of interring bond between monomer (C_1—C_1') and a shortening of C—C single bond of the ring. As expected, the degree of conjugation changes with oligomers conformations being

minimal at θ=90° and maximal at planar conformations (anti-planar conformation) (see Fig. 4).

Table 2. Optimized structural parameters bond length (in Å), angle (in degree) of bridged quaterthiophene obtained at B3LYP/6-31G(d).

Parameters	$QTCH_2$	$QTSiH_2$	QTC=O	QTC=S	$QTC=C(CN)_2$	4T
C_1C_2	1.386	1.384	1.387	1.385	1.385	1.380
C_2C_3	1.411	1.416	1.408	1.411	1.413	1.419
C_3C_4	1.386	1.390	1.384	1.390	1.391	1.380
C_4C_5	1.440	1.451	1.456	1.451	1.446	1.441
C_5C_6	1.386	1.391	1.385	1.392	1.391	1.379
C_6C_7	1.419	1.424	1.416	1.419	1.420	1.422
C_7C_8	1.372	1.371	1.372	1.372	1.371	1.367
C_6C_{11}	1.516	1.879	1.504	1.419	1.480	-
C_3C_{11}	1.517	1.881	1.509	1.411	1.482	-
C_8S_9	1.750	1.743	1.751	1.754	1.752	1.786
C_5S_9	1.730	1.737	1.719	1.716	1.726	1.758
C_4S_{10}	1.730	1.736	1.719	1.717	1.726	1.757
C_1S_{10}	1.775	1.767	1.776	1.778	1.776	1.758
C_1C_1'	1.441	1.443	1.442	1.442	1.442	1.442
$C_1C_2C_3$	112.9	114.0	112.3	112.4	112.8	113.8
$C_2C_1S_{10}$	110.8	110.4	110.8	110.8	110.9	110.0
$C_2C_3C_4$	113.1	112.0	113.7	113.5	113.0	113.9
$C_1S_{10}C_4$	90.8	91.1	91.0	91.0	90.9	92.1
$C_3C_4S_{10}$	112.2	112.3	111.9	112.0	112.1	110.0
$C_3C_4C_5$	109.2	116.9	109.3	108.6	108.9	129.1
$C_4C_5C_6$	109.2	116.9	109.4	108.6	108.9	129.0
$C_4C_3C_{11}$	109.8	106.8	108.5	109.0	108.7	-
$C_5C_6C_{11}$	109.8	106.8	108.5	109.1	108.8	-
$C_3C_{11}C_6$	101.8	92.3	104.1	104.5	104.6	-
$C_5C_6C_7$	112.8	111.7	113.4	113.1	112.7	113.6
$C_6C_7C_8$	112.0	113.1	111.5	111.6	111.9	112.9
$C_7C_8C_9$	112.5	112.0	112.3	112.4	112.5	111.6
$C_8C_9C_5$	90.5	90.8	90.8	90.8	90.6	91.7
$C_9C_5C_6$	112.1	112.1	111.8	111.9	112.0	110.0

Calculation of band gap (Egap)

The band gap in conjugated oligomers is governed by their chemical structures. There are two theoretical approaches for evaluating the energy gap. One way is based on the ground-state properties, from which the band gap is estimated from the energy difference between the highest occupied molecular orbital (HOMO) and the lowest

unoccupied molecular orbital (LUMO) [24]. The TDDFT, which has been used to study systems of increasing complexity due to its relatively low computational cost and also to include in its formalism the electron correlation effects, this method gives a better account of the excitation energy and even oscillator strength but it is not perfect for determining the gap energy. Many paper in the literature showed that this method is not sufficient for this type of calculation in the case of conjugated molecules and it gives values of gap far from the values of the experience [24-29].

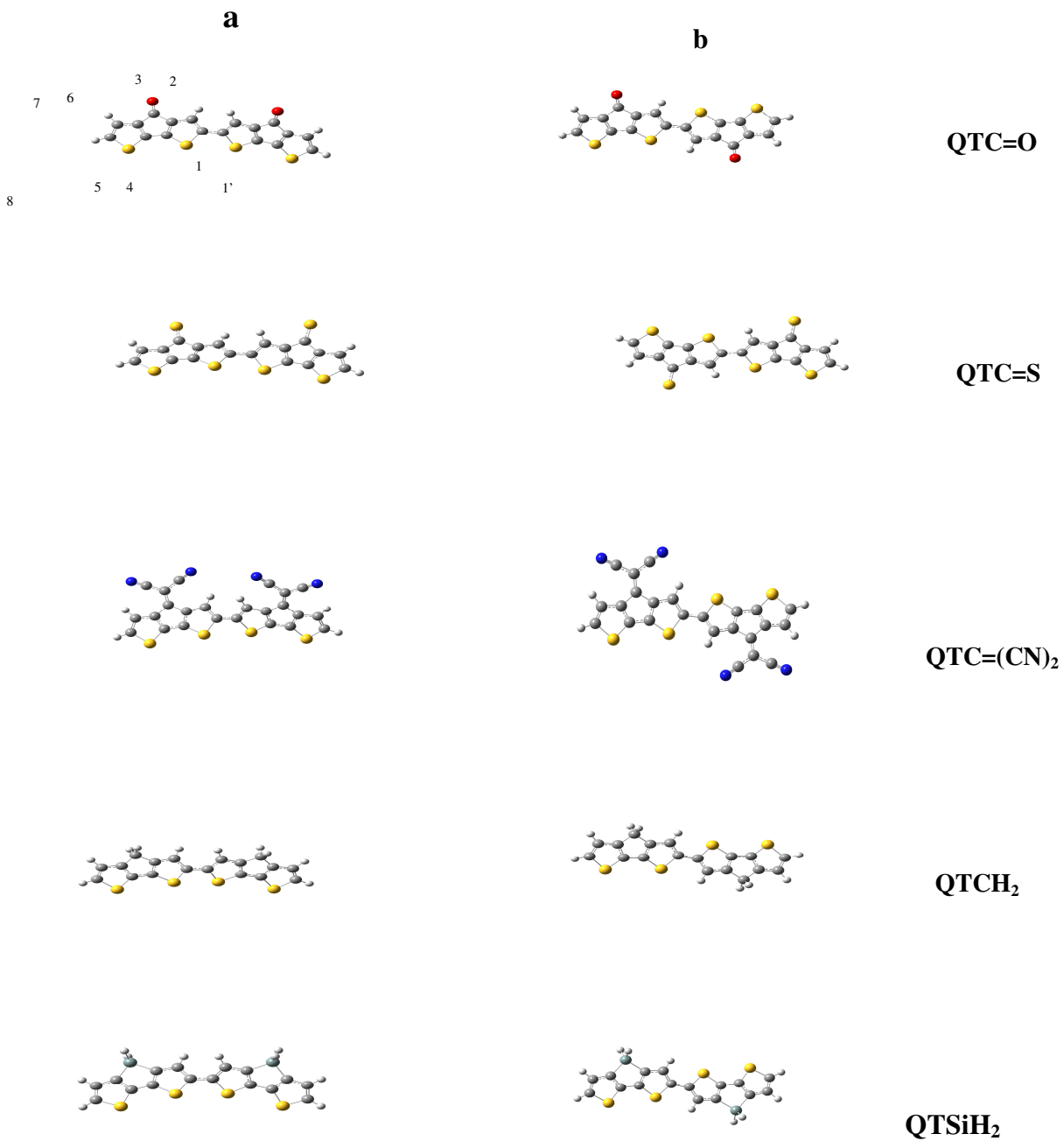

Figure 3: Geometries structural of bridged quaterthiophene: a) conformer syn-gauche b) conformer anti-gauche (stable conformation).

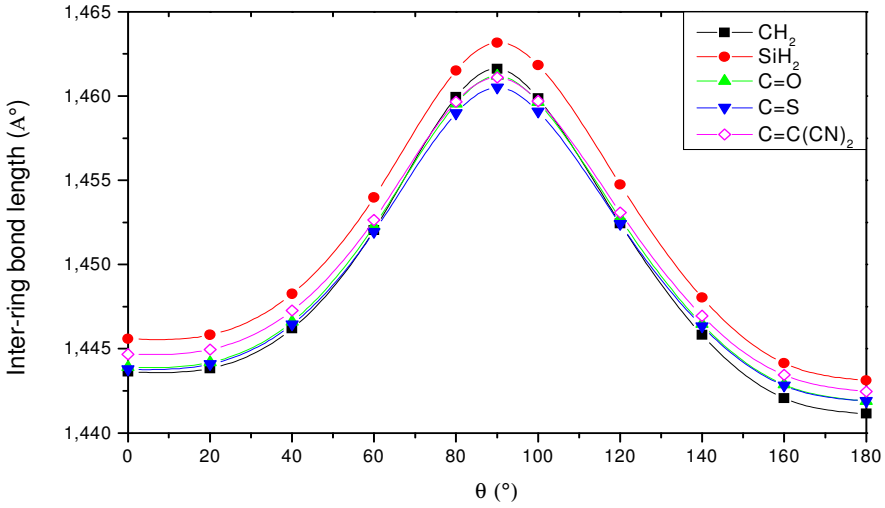

Figure 4: Inter-ring bond length as function of torsional angle θ for the bridged oligo(bithiophene)s QTX (X: CH_2, SiH_2, C=O, C=S and $C=C(CN)_2$).

For our work, we have used the method HOMO-LUMO because we have showed in preceding works that it is a best method which gives satisfactory results especially in the case of oligothiophenes and oligophenylenes [26].

Therefore, the detailed band gap theoretical calculations are carried out on the bridged oligomers structures. All values of band gaps were obtained by DFT(B3LYP/6-31G(d)). For comparison we have also presented in Table 3 the energy gaps calculated by TD/DFT method. The HOMO, LUMO and E_{gap}=HOMO-LUMO energies of the oligomers $(BTCH_2)_n$, $(BTSiH_2)_n$, $(BTC=O)_n$, $(BTC=S)_n$, $(BTC=C(CN)_2)_n$ with n=1 to 4, are presented in Table 3 and the relationships between the calculated energy gaps (E_{gap}) and the inverse chains length are plotted in Fig. 5. One can see that there is a good linear relation between the energy gap and the inverse chain length. Obviously, the E_{gap} presented in Table 3, yields a better agreement with the experimental data. However, we noted that calculations were performed in isolated state; they are still small variations of the calculated results and experimental values. The first factor responsible for deviations by both methods from experimental is that the predicted band gaps are for the isolated condensed phase chains, while the experimental band gaps are measured in the liquid phase, where the environmental influence may be involved. Additionally, the solid state effects have been neglected in the calculations. The theoretical band gaps calculated for isolated chains are expected to be about 0.2 eV larger than condensed phase values [27]. When taking into consideration this difference, the B3LYP/6-31G(d) method has the particularity to reproduce gap values similar to those of the experiment [28]. The band gaps obtained by DFT (B3LYP/6-31G(d)) is 2.41 eV for unbridged octathiophene (8T)

[29], which are higher than that $OTCH_2$ (2.23 eV),$OTSiH_2$ (2.27 eV), OTC=O (1.86 eV), OTC=S (1.43 eV) and $OTC=C(CN)_2$ (1.56 eV) indicating that the reduced band gap of bridged bithiophene oligomers are due to the effect of insertion of grouping (CH_2, SiH_2, C=O, C=S and $C=C(CN)_2$) between two thiophene rings. The measured values of OTX are very close to values measured experimentally [16, 17]. These results lead us to suggest that these oligomers are good models to reflect optoelectronic properties for corresponding parent polymer.

Table 3. Calculated values of HOMO, LUMO and Egap of bridged octathiophene (OT) derivatives (eV).

Polymers	E_{HOMO}	E_{LUMO}	**Egap**	**Egap** $_{exp}$
OT (unbridged)	-4.72	-2.31	2.41	2.3-2 [30]
$OTCH_2$	-4.32	-2.09	2.23	
$OTSiH_2$	-4.66	-2.39	2.27	
OTC=O	-4.98	-3.12	1.86	1.2 [16,17]
OTC=S	-4.95	-3.52	1.43	
$OTC=C(CN)_2$	-5.40	-3.84	1.56	0.8 [16,17]

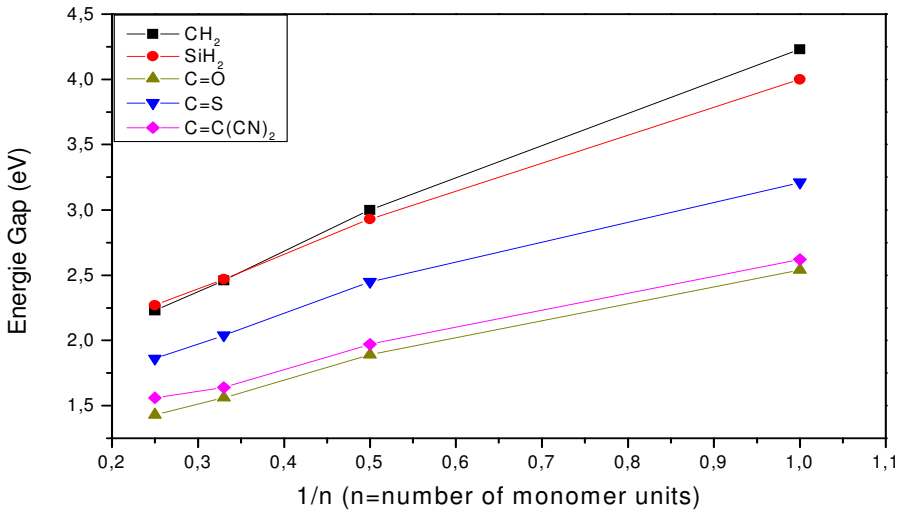

Figure 5: The band gap as a function of reciprocal chain length (n) in bridged oligo(bithiophene)s.

Conclusion

The calculation performed at the B3LYP/6-31G(d) level for bridged oligo(bithiophene)s gives torsional potentials. The most stable conformation is the anti-planar conformation. The calculated gap energy decreases with the chain length from the

dimer to the octamer, and when passing from the neutral to the doped form for each oligomer. The obtained energy band gap for the octamer is very close to those of polythiophene as measured experimentally. This octamer seems to be a useful model to understand electronic properties of the parent polymer. The calculation appears to be reliable for the estimation of the band gap of the conjugated polymers; the effects of bridging on the electronic properties of the octamer entities (OTX) have been examined. The insertion of CH_2, SiH_2, C=O, C=S and $C=C(CN)_2$ groups between two thiophene rings leads to a reduction of the energy gaps. Concerning the $C=C(CN)_2$ derivative the lowing of the HOMO-LUMO energy gap observed certainly indicates a possible reduction of the band gap in corresponding polymer.

Acknowledgments

This work has been supported by the convention CNRST/CNRS (Project chimie1009). We are grateful to the "Association Marocaine des Chimistes Théoriciens" (AMCT) for its pertinent help concerning the programs**.**

References and Notes

[1] Geiger, F.; Stoldt, M.; Schweizer, H.; Bauerle, P.; Umbach, E. *Adv. Mat.* **1993**, *5* 922.

[2] Garnier, F.; Horowitz, G.; Peng, X.; Fichou, D. *Adv. Mat.* **1990***, 2*, 592.

[3] Bäurele P. In: Electronic Materials: The Oligomer Approach. Müllen, K. and Wegner, G., eds. New York: Wiley-VCH, 1998, p. 105-197 (and the references therein).

[4] Horowitz, G.; Hajlaoui, M. E. *Adv. Mater.* **2000***, 12*, 1046; Meng, H.; Zheng, J.; Lovinger, A. J.; Wang, B. C.; Van Patten, P. G.; Bao, Z. *Chem. Mater*. **2003**, 1*5*, 1778; Mushrush, M.; Facchetti, A.; Lefenfeld, M.; Katz, H. E.; Marks T. J. *J. Am. Chem. Soc.* **2003***, 125*, 9414.

[5] Pasini, M.; Destri, S.; Porzio, W.; Botta, C.; Giovanella, U. *J. Mater. Chem*. **2003**, *13*, 807; Suzuki, M.; Fukuyama, M.; Hori, Y.; Hotta, S. *J. Appl. Phys*. **2002**, *91*, 5706.

[6] Pisignano, D.; Anni, M.; Gigli, G.; Cingolani, R.; Zavelani-Rossi, M.; Lanzani, G.; Barbarella, G.; Favaretto, L. *Appl. Phys. Lett*. **2002**, *81*, 3534.

[7] Torsi, L.; Lovinger, A. J.; Crone, B.; Someya, T.; Dodabalapur, A.; Katz H. E.; Gelperin, A. *J. Phys. Chem.* B **2002**, *106*, 12563; Roncali, J. *J. Mater. Chem.* **1999***, 9*, 1875.

[8] Noma, N.; Tsuzuki, T.; Shirota, Y. *Adv. Mater.* **1995**, *7*, 647; Videlot, C.; El Kassmi, A.; Fichou, D. *Solar Energy Mater. Solar Cells*. **2000**, *63*, 69; Hara, K.;

Kurashige, M.; Dan-Oh, Y.; Kasada, C.; Shinpo, A.; Suga, S.; Sayama, K.; Arakawa, H. *New J. Chem.* **2003**, *27*, 783; Ackermann, J.; Videlot, C.; El Kassmi, A.; Guglielmetti, R.; Fages, F. *Adv. Mater.* **2004**, *16*, 1709.

[9] Brédas, J. L.; *Adv. Mater.* **1995**, *7*, 263; Bakhshi, A. K. *Ann. Rep. R. Soc. Sect. C* **1992**, *89*, 147.

[10] Havinga, E. E.; ten Hooeve, W.; Wynberg, H. *Polymer Bull*. **1992**, *29*, 119.

[11] Havinga, E. E.; ten Hooeve, W.; Wynberg, H. *Synth. Met*. **1993**, *55*, 299.

[12] Colladet, K.; Nicolas, M.; Goris, L.; Lutsen, L.; Vanderzande, D. *Thin. Solid. Films* **2004***, 7*, 451; Thompson, B. C.; Kim, Y. G.; Reynolds, J. R. *Macromolecules* **2005**, *38*, 5359; Shahid, M.; Ashraf, R. S.; Klemm, E.; Sensfuss, S. *Macromolecules* **2006**, *39*, 7844.

[13] Bundgaard, E.; Krebs, F. C. *Macromolecules* **2006**, *39*, 2823.

[14] Van Duren, J. K. J.; Dhanabalan, A.; van Hal, P. A.; Janssen, R. A. J. *Synth. Met.* **2001**, *121*, 1587; Yoshino, K.; Nakajima, S.; Park, D.H. *Jpn. J. Appl. Phys. Part 2* **2008**, *27*, 716.

[15] Petersen, M. H.; Hagemann, O.; Nielsen, K. T.; Jørgensen, M.; Krebs, F. C. *Sol. Energy. Mater. Sol. Cells* **2007**, *91*, 996; Ashraf, R. S.; Klemm, E. J*. Polym. Sci. Part A* **2005**, *43*, 6445.

[16] Lambert, T.; Ferraris, J. P. *J. Chem. Soc. Chem. Commun*. **1991**,752.

[17] Ferraris, J. P.; Lambert, T. *J. Chem. Soc. Chem. Commun.* **1991**, 1268.

[18] Becke, A. D*. J. Chem. Phys*. **1993**, *98*, 5648.

[19] Ditchfield, R.; Hehre, W. J.; Pople, J. A. *J. Chem. Phys*. **1971**, *54*, 724.

[20] Hehre, W. J.; Ditchfiesld, R.; Pople, J. A. *J. Chem. Phys*. **1972**, *56*, 2257.

[21] Hariharan, P. C.; Pople, J. A. *Mol. Phys*. **1974**, *27*, 209.

[22] Gordon, M. S. Chem. Phys. Lett. 1980, 76, 163.

[23] Frisch, M. J.; Trucks, G. W.; Schlegel, H. B.; Scuseria, G. E.; Robb, M. A.; Cheeseman, J. R.; Montgomery, J. A.; Vreven, T.; Kudin-Jr, K. N.; Burant, J. C.; Millam, J. M.; Iyengar, S. S.; Tomasi, J.; Barone, V.; Mennucci, B.; Cossi, M.; Scalmani, G.; Rega, N.; Petersson, G. A.; Nakatsuji, H.; Hada, M.; Ehara, M.; Toyota, K.; Fukuda, R.; Hasegawa, J.; Ishida, M.; Nakajima, T.; Honda, Y.; Kitao, O.; Nakai, H.; Klene, M.; Li, X.; Knox, J. E.; Hratchian, H. P.; Cross, J .B.; Adamo, C.; Jaramillo, J.; Gomperts, R.; Stratmann, R. E.; Yazyev,O.; Austin, A. J.; Cammi, R.; Pomelli, C.; Ochterski, J. W.; Ayala, P. Y.; Morokuma, K.; Voth, G. A.; Salvador, S.; Dannenberg, J. J.; Zakrzewski, V. G.; Dapprich, S.; Daniels, A. D.; Strain, M. C.; Farkas, O.; Malick, D. K.; Rabuck, A. D.; Raghavachari, K.; Foresman, J. B.; Ortiz, J. V.; Cui, Q.; Baboul, A. G.; Clifford, S.; Cioslowski, J.; Stefanov, B. B.; Liu, G.; Liashenko, A.; Piskorz, P.; Komaromi, I.; Martin, R. L.; Fox, D. J.; Keith, T.; Al-Laham, M.A.; Peng, C. Y.; Nanayakkara, A.; Challacombe, M.; Gill, P. M. W.; Johnson, B.; Chen, W.; Wong, M. W.; Gonzalez, C.; Pople, J. A. GAUSSIAN 03, Revision B.04, Gaussian, Inc., Pittsburgh PA, **2003**.

[24] Cornil, J.; Beljonne, D.; Brédas, J. L. *J. Chem. Phys*. **1995**, *103*, 842; Alemán, C. Julia, L. *J. Phys. Chem*. **1996**, *100*, 14661; Moro, G.; Scalmani, G.; Cosentino, U.; Pitea, D. *Synth. Met.* **1998**, *92*, 69.

[25] Kozaki, M.; Yonezawa, Y.; Okada, K. *Org. Lett*. **2002**, *4*, 4535.

[26] Hay, P. J. *J. Phys Chem. A* **2002**, *106*, 1634; Curioni, A.; Andreoni, W.; Treusch, R.; Himpsel, F. J.; Haskal, E.; Seidler, P. *J. Appl. Phys Lett*. **1998**, *72*, 1575; Hong, S. Y.; Kim, D. Y.; Hoffman, R. *Macromolecules* **2001**, *34*, 6474.

[27] Salzner, U.; Lagowski, J. B.; Pickup, P. G.; Poirier, R. A. *Synth. Met.* **1998**, *96*, 177.

[28] Bouzakraoui, S.; Bouzzine, S. M.; Bouachrine, M.; Hamidi, M. *Solar Energy Materials Solar Cells* **2006**, *90*, 1393.

[29] Bouzzine, S. M.; Bouzakraoui, S.; Bouachrine, M.; Hamidi, M. *J. Mol. Struct. (Theochem)* **2005**, *726*, 271.

[30] Roncali, J. *Chem. Rev*. **1992**, *92*, 711; Hernandez, V.; Lopez Navarrete, J. T.; Marcos, J. L. *Synth. Met.* **1991**, *41*, 789; Tourillon, G.; Garnier, F. *J. Electroanal. Chem*. **1988**, *246*, 467.

ISSN 1984-6428
ONLINE
www.orbital.ufms.br

Orbital 2009, *1* (2), 215-227

Full Paper

A comparative study of polymer-dye interaction

Nandini R[a], Vishalakshi B[b]*

[a]Department of Chemistry, Mangalore Institute of Technology and Engineering (MITE), Moodabidri, 574 226, India.
[b]Department of Post-Graduate Studies and Research in Chemistry, Mangalore University, Mangalagangotri 574 199, India.

Received: 23 June 2009; revised: 31 July 2009; accepted: 04 August 2009. Available online: 21 August 2009.

ABSTRACT: *The interaction between an anionic dye Methyl Orange and two poly cations namely, Poly (N-vinyl-4-methylpyridiniumiodide), (PC1) & Poly (vinylbenzyltriphenylphosphoniumchloride), (PC2) has been investigated by spectrophotometric method. The polymers are observed to induce metachromasy in the dye as evidenced from the considerable blue shift in the absorption maximum of the dye. The interaction constant and thermodynamic parameters of interaction have been determined by absorbance measurements at the metachromatic band. The effect of additives such as ionic salts, alcohols, urea and polyelectrolytes on the reversal of metachromasy has been studied and used to determine the stability of the metachromatic complex and to understand the nature of binding.*

Keywords*: methyl orange, polycations, metachromasy, stoichiometry, thermodynamic parameters*

** Corresponding Author: E-mail: nandinifalnir@yahoo.com*

Introduction

The change in the absorption spectra of the dye when bound to a polyelectrolyte is termed as metachromasy. Metachromasia in the dye polymer interaction has been studied extensively since the discovery of this phenomenon in 1875 [1]. The concept of metachromasy suggests that a single individual compound is formed by the interaction of the dye and the chromotropic polymers. The investigations on the dye polymer complexation provide useful information about the nature and mechanism of binding process. Both polar and electrostatic interactions are involved in the binding of dye molecules on to the polymers [2-8]. Generally, a polyelectrolyte with relatively high charge density is found to be more efficient in inducing metachromasy. The interaction depends on the conformation of the dye and the polycations as well.

Methyl orange, an anionic dye has been used as a probe to study the mode and the extent of complex formation between small molecules, proteins and water-soluble polymers [9]. The binding of methyl orange and its homolog in aqueous solution has been studied by equilibrium dialysis method and the interaction constant and thermodynamic parameters of interaction has been evaluated and the significance of hydrophobic and electrostatic interaction accompanying the binding was also studied by Takagishi [10-12]. The interaction of methyl orange with dilute aqueous solution of ionone has also been reported [13]. The objective of the present study is to compare the binding affinities of methyl orange to the polycations mentioned in the previous studies and to determine the thermodynamic parameters of interaction. The stability of the metachromatic complex has been determined by studying the ease of reversal by using alcohols, namely methanol, ethanol and 2-Propanol as well by the addition of urea, sodium chloride, sodium lauryl sulphate and sodium carboxy methylcellulose.

Material and Methods

Materials

Methyl orange (MO), urea, sodium chloride, sodium lauryl sulphate, were purchased from Merck, and used without further purification. The solvents namely methanol, ethanol, 2-propanol (Merck) were distilled before use. The polycations poly(N-vinyl-4-methyl pyridiniumiodide) and poly(vinylbenzyltriphenylphosphoniumchloride) was a gift, the preparations of which are reported elsewhere [9]. The absorption spectra were recorded using a UV-2500 spectrophotometer.

Determination of stoichiometry of polymer-dye complex

Increasing amounts of polymer solution (0.0-9 mL, 1 x 10^{-3} mol.L^{-1}) were added to a fixed volume of dye solution (0.6 mL, 1 x 10^{-3} mol.L^{-1}) in different sets of experiments and the total volume was made up to 10 mL by adding distilled water in each case. The intensities were measured at 464 nm and at 378 nm in case of MO- PC1 and at 464 nm and 464 nm in case of MO-PC2 complex**.**

Study of reversal of metachromasy using polymer-dye complex

For measurements of the reversal of metachromasy, solutions containing polymer and dye in the ratio 1:2 in case of MO-PC1 and 1:3 in case of MO-PC2 were made containing different amount of alcohol. The total volume was maintained at 10mL in each case. The absorbances were measured at 378 nm and 464 nm in case of MO-PC1 complex and at 426 nm and 464 nm in the case of MO-PC2 complex.

Determination of thermodynamic parameters

The thermodynamic parameters were determined by measuring the absorbances of the pure dye solution at both 464 nm and at 378 nm in the case of MO-PC1 and at 464 nm and 426 nm in case of MO-PC2 in the temperature range (36-54 ^{0}C). The same experiment was repeated with solutions containing varying amounts of polymer at various polymer-dye ratios (2, 5, 10, and 20).

Results and Discussion

The absorption spectra of methyl orange at various concentrations are shown in Fig. 1**.** It shows a single band with absorption maximum at 464 nm indicating the presence of a monomeric dye species in the range of concentration studied. The spectral changes on the addition of increasing amount of PC1 and PC2 are shown in Fig. 2 and Fig. 3, respectively. The intensity of 464 nm decreases progressively upon addition of increasing amounts of polymer solution and the absorption maximum shifts to 378 nm in case of MO-PC1 and to 426 nm in case of MO-PC2. The blue shifted band is attributed to the stacking of the dye molecules on the polymer backbone this reflects high degree of co-operativity in binding [14].

Determination of stoichiometry

To determine the stoichiometry of the polymer-dye complex, a plot of $\mathbf{A_{378}/A_{464}}$ versus the polymer/dye ratio was made. A similar procedure was repeated for MO-PC2 complex also. On adding increasing amounts of PC1 &PC2 to MO it was found that the absorption at the monomeric band decreases gradually and a new band occurs at 378 nm in case of MO-PC1 and at 426 nm in case of MO-PC2 as shown in Fig. 4 and Fig. 5,

respectively. The stoichiometry of MO-PC1 complex was found to be 2:1 whilst that of MO-PC2 was found to be 1:1. A 1:1 stoichiometry indicates that one dye cation is bound to each potential anionic site resulting in stacking conformation. Whereas in the case of MO-PC1 the binding is 2:1 that indicates that the binding is at alternate anionic site this is due to lesser overcrowding and more aggregation of the bound dyes. Similar results were observed in case of binding of pincyanol chloride with poly(methacrylic acid) and poly(styrene sulfonate) [15].

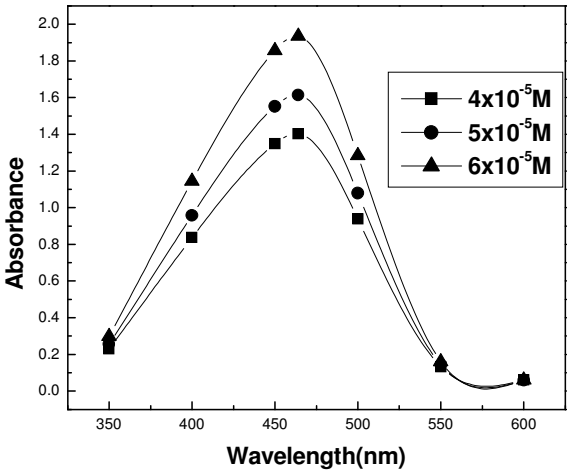

Figure 1. Absorption spectra of dye, MO.

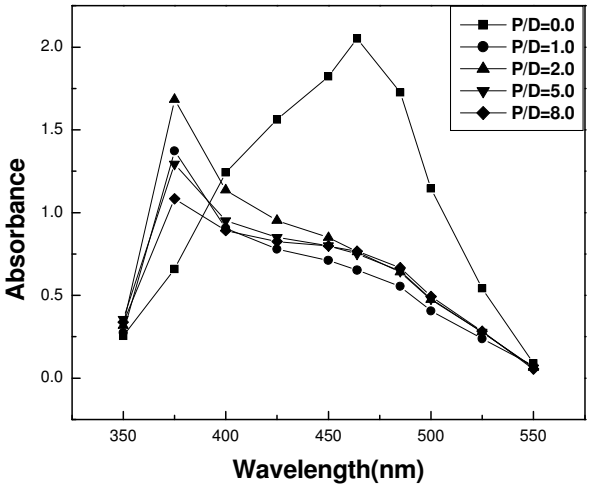

Figure 2. Absorption spectrum of MO-PC1 system at various P/D ratios.

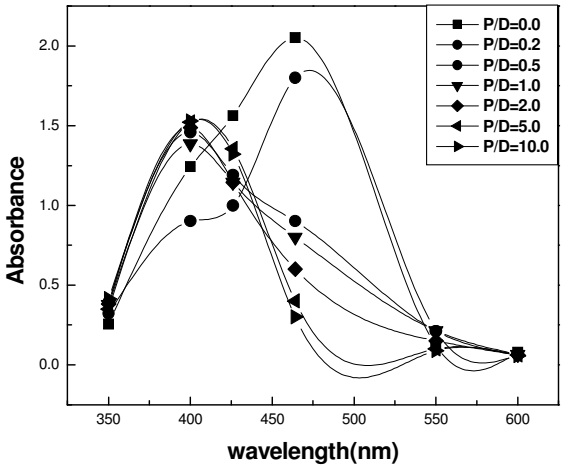

Figure 3. Absorption spectrum of MO-PC2 system at various P/D ratios.

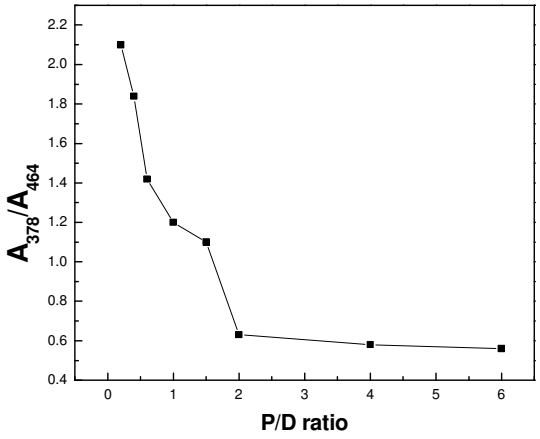

Figure 4. Stoichiometry of MO-PC1 complex.

Reversal of metachromasy

Effect of alcohols& urea

The metachromatic effect is presumably due to association of the dye molecules on binding with the polyanion, which may involve both electrostatic and hydrophobic interactions. The destruction of metachromatic effect may occur on addition of low molecular weight electrolytes and urea. The destruction of metachromasy by alcohol and urea is attributed to the involvement of hydrophobic bonding has already been established [16, 17]. The efficiency of alcohols in disrupting metachromasy were found to be in the order methanol < ethanol < 2-propanol, indicating that reversal becomes quicker with increasing hydrophobic character of the alcohols. The above facts are further

established in the present system. In case of MO-PC1, 60% methanol, 50% ethanol and 40% 2-Propanol were sufficient to reverse metachromasy. Whilst in the case of MO-PC2, 40% methanol, 30% ethanol, 25% 2-Propanol were sufficient to reverse metachromasy. This indicates stronger stacking of the bound dyes in case of PC1 than in the case of PC2. This may be well interpreted in terms of the conformation of polycations PC1 and PC2 respectively. Thus PC1 has a more flexible conformation due to the greater involvement of hydrophobic forces between the bound dye molecules. The results are shown in Fig. 6 and Fig. 7, respectively. Takagishi et al. [18] reported that, on binding of butyl orange by bovine serum albumin, urea reduces the structure of the aqueous environment of the dye and the polycation to participate in the formation of hydrophobic interaction. The molar concentrations of urea needed for reversal of metachromasy were found to be 5 $mol.L^{-1}$ in case of MO-PC1 complex and 4 $mol.L^{-1}$ in the case of MO-PC2 complex. The results are shown in Fig. 8 and Fig.9, respectively.

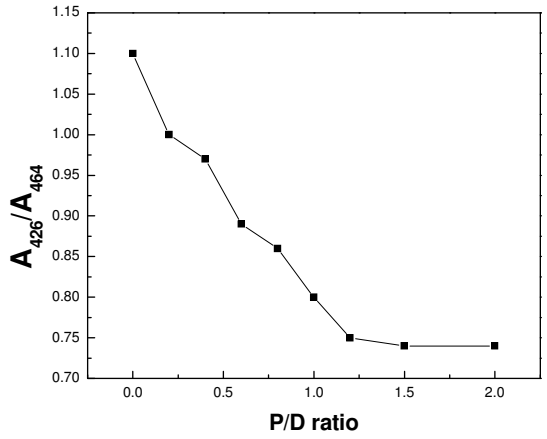

Figure 5 Stoichiometry of MO-PC2 complex.

Effect of ionic strength

Tan et al. [19] have reported the disruption of metachromatic band with the variation of ionic strength. Sodium chloride of varied ionic strength was added to MO-PC1 and MO-PC2, and the absorbances were measured in the range 350-700 nm. In case of PC1 the monomeric band reappears at higher ionic strength (1×10^{-3} $mol.L^{-1}$) than compared to that of PC2 ($1x10^{-4}$ $mol.L^{-1}$). In aqueous solutions the charged polymer molecule will be in the extended conformation due to the repulsion between the charged groups. On adding the dye the conformation of the polycation changes to a compact coil owing to dye binding, resulting from electrostatic interaction thus giving rise to metachromatic band. The concentration of sodium chloride required to reverse metachromasy was greater in case of MO-PC1 than in the case of MO-PC2. This indirectly

indicates that MO-PC1 complex is more stable than MO-PC2 complex. The results are shown in Fig. 10 and Fig. 11, respectively.

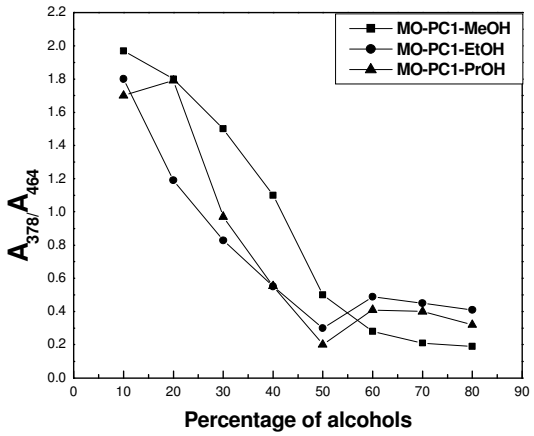

Figure 6. Effect of alcohols on reversal of metachromasy in MO-PC1 system.

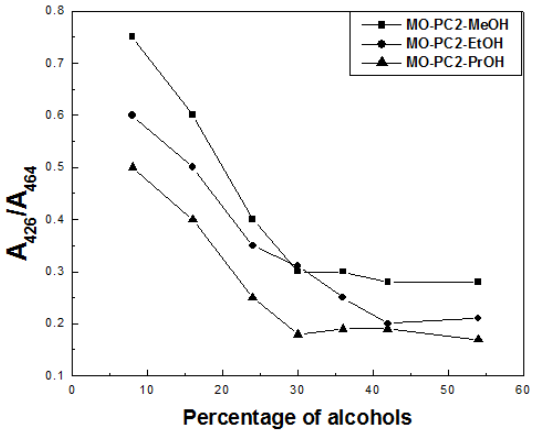

Figure 7. Effect of alcohols on reversal of metachromasy in MO-PC2 system.

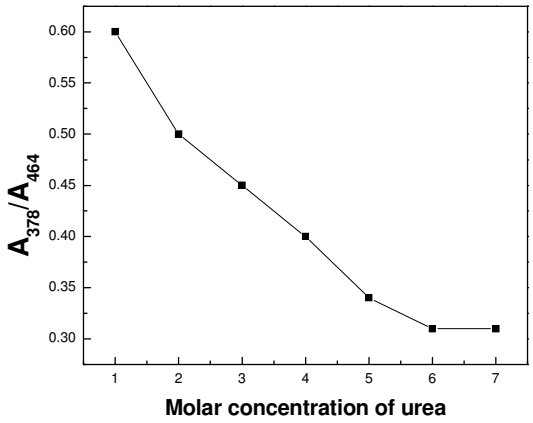

Figure 8. Effect of urea on reversal of metachromasy in MO-PC1system.

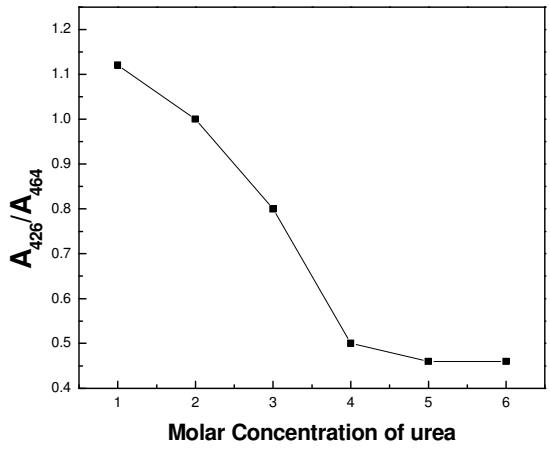

Figure 9. Effect of urea on reversal of metachromasy in MO-PC2 system.

Effect of surfactants

On adding increasing amounts of sodium lauryl sulphate to MO-PC1 and MO-PC2 complex it was found that the monomeric band gained intensity. The concentrations of sodium lauryl sulphate required to reverse metachromasy was found to be 1 x 10^{-4} mol.L^{-1} in the case of MO-PC1 and 1 x 10^{-5} mol.L^{-1} in the case of MO-PC2. This is due to the formation of micelles by the surfactants in aqueous solutions. The effects of surfactants have been reported in literature [20] .The results are shown in Fig. 12. The results match with those reported in the literature [21]. Similar results are obtained for reversal of metachromasy also using sodium carboxymethylcellulose.

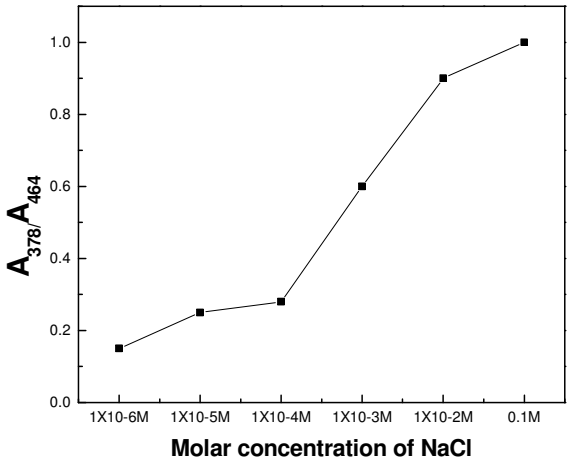

Figure 10. Effect of Sodium chloride on reversal of metachromasy in MO-PC1.

Effect of nature of the quarternising side chains:

In addition to coulombic forces, the non-ionic interactions between the dye molecules and the polymer side-chains contribute towards the binding mechanism. The effect of alkyl and aryl side chains on the dye binding characteristics of the quarternised poly-2-vinyl and poly-4-vinyl pyridine derivatives have already been reported [22]. This is further confirmed from interaction constants which are greater for the poly(*N*-vinyl-4-methyl pyridinium iodide), (PC1) than for poly(vinylbenzyltriphenylphosphonium chloride) (PC2) which could be due to the lesser steric hindrance offered by the methyl groups. A similar effect of an increase in the interaction energy between the dye and the polymer due to the intercalation of the dye and the polymer has been reported for methyl orange and poly(3-benzyl-1-vinylimidazolium bromide) [3].

Determination of interaction parameters

In order to determine the thermodynamic parameters of interaction between the dye and the polymer, absorbance (A) of the MO-PC1 complex was measured at 378 nm and that of MO-PC2 complex was measured at 426 nm using different sets of solutions containing varying amounts of polymer solution (C_S) in a fixed volume of dye solution (C_D). The plots of $C_D.C_S/ (A-A_O)$ against C_s for MO-PC1 and MO-PC2 systems at different temperatures are shown in Fig. 13 and Fig. 14, respectively. The absorbance measurements were carried out at four different temperatures. Absorbance results were treated using Rose-Drago eqn [23]: $C_D.Cs/(A-A_0) = 1/K_cL\ (\varepsilon_{ds}- \varepsilon_d) + Cs/L\ (\varepsilon_{ds}- \varepsilon_d)$. C_D refers to the initial molar concentration of the dye and C_S refers to the molar concentration of the polymer. The value of K_c was obtained from the slope and intercept of the plot of $C_DCs/ (A-A_0)$ against C_S. In each case the thermodynamic parameters of interaction such as ΔH shown in Fig. 15, ΔG and ΔS shown in Fig. 16 were also calculated. The thermodynamic parameters for MO-PC1 and MO-PC2 are given in Table.1.

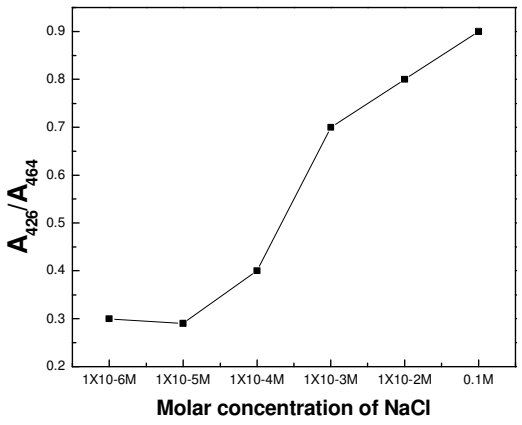

Figure 11. Effect of sodium chloride on reversal of metachromasy in MO-PC2 system.

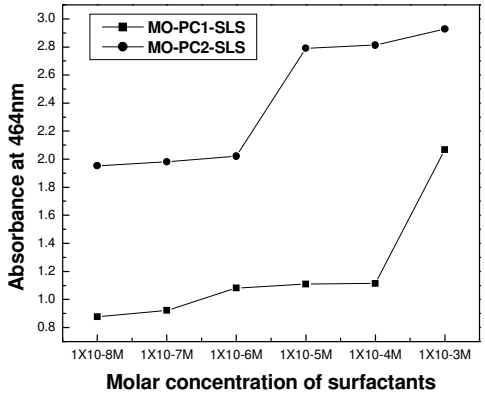

Figure 12. Effect of sodium lauryl sulphate on reversal of metachromasy MO-PC1 and MO-PC2 system.

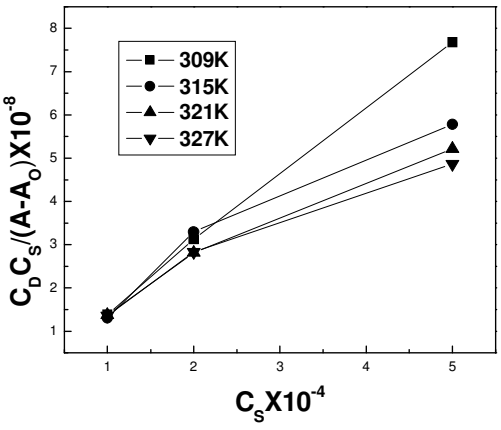

Figure 13. Plots of $C_D{\cdot}C_S/(A-A_O)$ against Cs for MO-PC1 system.

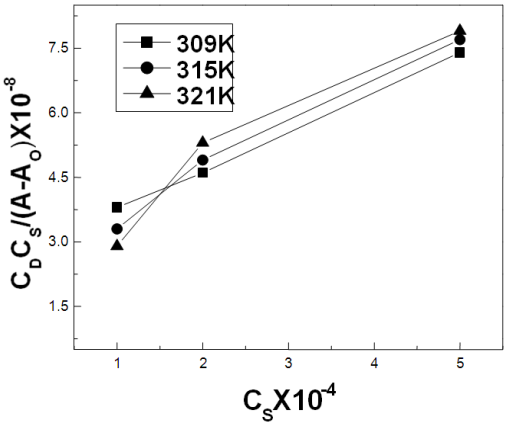

Figure 14. Plots of $C_D{\cdot}C_S/(A-A_O)$ against Cs for MO-PC2 system.

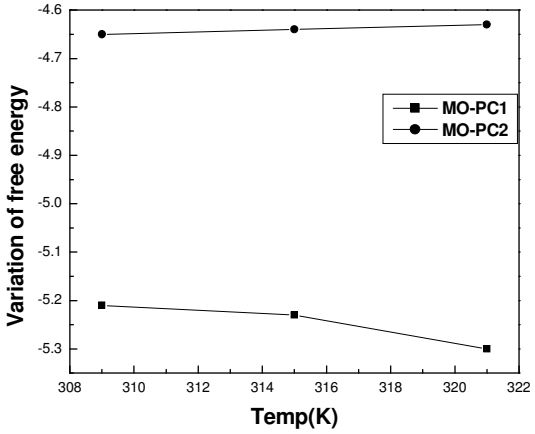

Figure 15. Variation of free energy for MO-PC1 and MO-PC2 systems.

Table 1. Thermodynamic Parameters for interaction of MO-PC1 and MO-PC2.

Temp (K)	Kcx10^{3}dm^3 mol^{-1a}		ΔGKcal. mol^{-1b}		ΔHKcal.mol$^{-1\ c}$		ΔS cal. mol^{-1}K$^{-1\ d}$	
	PC1	PC2	PC1	PC2	PC1	PC2	PC1	PC2
300	4.866	1.964	-5.532	-5.15	-2.306	-4.319	-4.827	-6.666
309	4.308	1.666	-5.33	-4.726				
315	4.266	1.58	-5.060	-4.423				
321	3.162	1.33	-4.948	-4.32				

a) Calculated from Fig. 13 and Fig. 14 according to Rose-Drago equation
b) Calculated from the thermodynamic equation ΔG = -RTln Kc.
c) Calculated graphically by plotting lnKc against 1/T according to van't Hoff equation, ln Kc = -Δ H/RT +C.
d) Calculated from the thermodynamic expression ΔG =Δ H - TΔS.

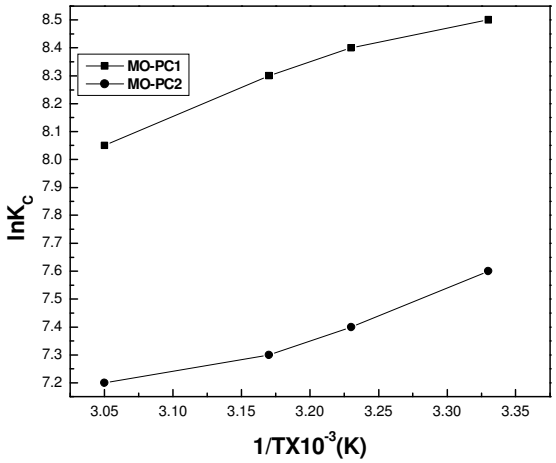

Figure 16. van't Hoff plot for MO-PC1 and MO-PC2 systems.

Conclusions

The polymers poly(*N*-vinyl-4-methylpyridiniumiodide) (PC1) and poly(vinylbenzyltriphenylphosphonium chloride) (PC2) induced metachromasy in the dye MO. The monomeric band occurs at 464 nm while the metachromatic band occurred at 378 nm in the case of MO-PC1 and at 426 nm in the case of MO-PC2. The spectral shifts in the case of MO-PC1 (86 nm) than in the case of MO-PC2 (36 nm) indicates that dye binding is stronger in the case of MO-PC1 than in the case of MO-PC2. These results are further confirmed by the reversal studies using alcohols, urea, sodium chloride and surfactants. The thermodynamic parameters further confirm the above fact. It is thus evident from the above studies that both electrostatic and non-ionic forces contribute towards the binding process and that the binding of PC1 with the dye ion is stronger than that between MO-PC2.Cooperativity in binding is observed to occur due to neighbor interactions among the bound dye molecules at lower P/D ratios leading to stacking. The stacking tendency is enhanced by the easy availability and close proximity of the charged sites.

References and Notes

[1] Takagishi, T.; Susimito, T.; Hayashi, A.; Kuroki, N. *J. Polym. Sci*, **1983**, *21*, 2311.
[2] Handel, T. M.; Cohen, H. L.; Tan, J .S. *Macromolecules* **1985**, *18*, 1200.
[3] Orchard, B. J.; Tan, J. S.; Finger, A. J. H. *Macromolecules* **1984**, *17***,** 169.
[4] Gummow, B. D.; Roberts, G. A. F. *Macromolecular Chem.* **1985**, *186*, 1239.
[5] Gummow, B. D.; Roberts, G. A. F. *Macromolecular Chem*. **1985**, *186*, 1245.
[6] Pal, M. K.; Schubert, M. *J. Am. Chem. Soc.* **1962**, *84*, 4384.
[7] Young, M. D.; Phillips, G. O.; Balazs, E. A. *Biochim. Biophys. Acta* **1967**, 141, 374.
[8] Quadrifoglio, E.; Crescenzi, V. *J. Colloid Interface Sci.* **1971**, *35*, 447.
[9] Vishalakshi, B.; Ghosh, S.; Kalpagam, V. *Polymer* **1993**, *34***,** 3270.
[10] Takagishi, T.; Kuroki, N. *J. Polym. Sci.* **1973**, *11*, 1889.
[11] Toru, R.; Takagishi, T.; Kozuka, H.; Kim, G. J. *J. Polym Sci. Polym. Chem. Ed.* **1982**, *20*, 2231.
[12] Takagishi, T.; Nakagami, K.; Imajo, K.; Kuroki, N. *J. Polym. Sci. Polym. Chem Ed.* **1976**, *12***,** 23.
[13] Hochberg G. C. *Colloid Polym Sci.* **1994**, *272*, 409.
[14] Barone, G.; Crescenzi, V.; Vitagliano, V. *Ric. Sci*. **1966**, *36*, 503.
[15] Pal, M. K.; Ghosh, B. K. *Macromol. Chem*. **1979**, *180***,** 959.
[16] Bank, O.; De Jong, B. *Protoplasma*, **1939**, 32**,** 489.
[17] Pal, M. K. *Histochemie* **1965**, *5***,** 24.
[18] Takagishi, T.; Takami, K.; Kuroki, N. *J. Polym. Sci*. **1975**, *13*, 437.

[19] Tan, J. S.; Schneider, R. L. *J. Phys. Chem* **1975**, *79*, 1380.
[20] Levine, A.; Schubert, M. *J .Am. Chem. Soc*. **1958**, *74***,** 5702.
[21] Singh, C.; Biswas, S.; Dasgupta, S. *J. Surface Sci. Technol.* **2008**, *24*, 21.
[22] Vishalakshi, B. *Journal of Polymer Science: Part A: Polymer Chemistry* **1995**, *33*, 365.
[23] Rose, N. J.; Drago, R. S. *J. Am. Chem. Soc.* **1959**, *81*, 6138.